The Riemann Mapping Theorem

Christopher J. Bishop

C.J. Bishop, Mathematics Department, SUNY at Stony Brook, Stony Brook, NY 11794-3651

E-mail address: bishop@math.sunysb.edu

1991 *Mathematics Subject Classification.* Primary: 30C35, Secondary: 30C85, 30C62

Key words and phrases. numerical conformal mappings, Schwarz-Christoffel formula, hyperbolic 3-manifolds, Sullivan's theorem, convex hulls, quasiconformal mappings, quasisymmetric mappings, medial axis, CRDT algorithm

The author is partially supported by NSF Grant DMS 04-05578.

Abstract. These are informal notes based on lectures I am giving in MAT 626 (Topics in Complex Analysis: the Riemann mapping theorem) during Fall 2008 at Stony Brook. We will start with brief introduction to conformal mapping focusing on the Schwarz-Christoffel formula and how to compute the unknown parameters. In later chapters we will fill in some of the details of results and proofs in geometric function theory and survey various numerical methods for computing conformal maps, including a method of my own using ideas from hyperbolic and computational geometry.

Contents

CHAPTER 1

Introduction to conformal mapping

In this chapter we introduce conformal maps with an emphasis on the Schwarz-Christoffel formula. We discuss several ideas including Möbius transformations, conformal invariants, crowding, domain decompositions and quasiconformal maps which will be explored in greater depth in later chapters.

1. Conformal and holomorphic maps

A conformal map between planar domains is a C^1, orientation preserving diffeomorphism which preserves angles. Write $f(x, y) = (u(x, y), v(x, y))$. We can compute it derivative matrix

$$Df = \begin{pmatrix} u_x & u_y \\ v_x & v_y \end{pmatrix}.$$

Since f preserves orientation and angles, the linear map represented by this matrix must be an orientation preserving Euclidean similarity. Thus it is a composition of a dilation and rotation and must have the form

$$\begin{pmatrix} a & b \\ -b & a \end{pmatrix} = \begin{pmatrix} r & 0 \\ 0 & r \end{pmatrix} \begin{pmatrix} \cos\theta & \sin\theta \\ -\sin\theta & \cos\theta \end{pmatrix},$$

which implies

$$u_x = v_y, \quad u_y = -v_x.$$

These are known as the Cauchy-Riemann equations. Thus f is conformal if it is C^1 diffeomorphism which satisfies the Cauchy-Riemann equations.

The simplest examples are the Euclidean similarities, and indeed, these are the only examples if we want maps $\mathbb{R}^2 \to \mathbb{R}^2$. However, if we consider subdomains of $\mathbb{R}^2$, then there are many more examples. The celebrated Riemann mapping theorem says that any two simply connected planar domains (other that the whole plane) can be mapped to each other by a conformal map. We will give a more precise statement of this later and will eventually give a proof of the result, but for the present we introduce some notation and a few more examples.

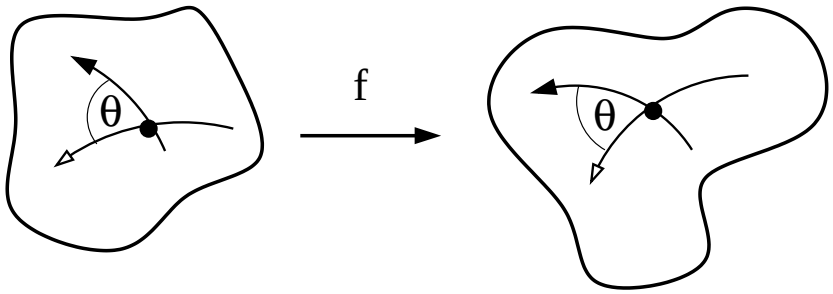

FIGURE 1. A conformal map preserves angles (and orientation).

After the linear maps, the next easiest conformal maps are quadratic polynomials. If we take

$$f(x,y) = (u(x,y), v(x,y)) = (x^2 - y^2, 2xy),$$

then we can easily check that

$$Df(x,y) = \begin{pmatrix} u_x & u_y \\ v_x & v_y \end{pmatrix} = \begin{pmatrix} 2x & -2y \\ 2y & 2x \end{pmatrix},$$

so the Cauchy-Riemann equations are satisfied. The map is not conformal on the plane since $f(-x,-y) = f(x,y)$ is 2-to-1 for $(x,y) \neq (0,0)$ and Df vanishes at the origin. However, it is a conformal map if we restrict it to a domain (an open, connected set) where it is 1-to-1, such as the open square $[0,1]^2$. The map sends this square conformally to a region in the upper half-plane. See Figure 5. Note that angles are doubled at the origin; we do not require that a conformal mapping of a domain preserve angles at boundary points and this map does not.

By this point, anyone who has had a course in complex analysis will have recognized the map f as complex squaring. We identity $\mathbb{R}^2$ with the complex numbers $\mathbb{C}$ by writing a real 2-vector (x,y) as a single complex number $z = x + iy$. The complex numbers form a field under the usual addition

$$z_1 + z_2 = (x_1 + iy_1) + (x_2 + iy_2) = (x_1 + x_2) + i(y_1 + y_2)$$

and multiplication defined using the relation $i^2 = -1$ as follows

$$\begin{aligned} z_1 z_2 &= (x_1 + iy_1)(x_2 + iy_2) \\ &= x_1 x_2 + i x_1 y_2 + i x_2 y_1 + i^2 y_1 y_2 \\ &= (x_1 x_2 - y_1 y_2) + i(x_1 y_2 + x_2 y_1). \end{aligned}$$

Complex squaring is then

$$z^2 = (x+iy)^2 = (x^2 - y^2) + i2xy,$$

which is the map described earlier.

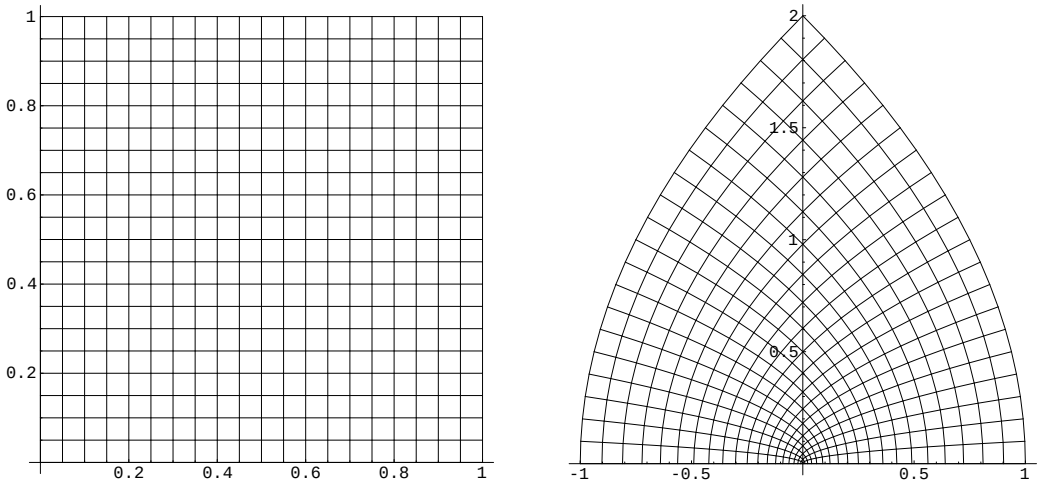

FIGURE 2. This illustrates the map $z \to z^2$ or $(x,y) \to (x^2-y^2, 2xy)$. The top left shows a grid in the square $[0,1]^2$. The top right shows the image under squaring map.

Complex multiplication is easier to understand in polar coordinates. Let $r = |z| = \sqrt{x^2+y^2}$ denote the distance from z to the origin and let $\theta = \arg(z)$ be the angle so that $x = r\cos\theta, y = r\sin\theta$. Note that if θ is a possible value of $\arg(z)$, then so is $\theta + 2\pi n$ for any integer n. In order to make $\arg(z)$ a function, we need to restrict to a single value, so we often choose $\theta \in (-\pi, \pi]$. This is the principal branch of arg and is denoted Arg(z). . Note that it has a jump discontinuity along the negative real axis. It is often convenient to choose other branches of arg which have discontinuities along a different ray, or possibly a curve connecting 0 to ∞. Given any simply connected domain $\Omega \subset \mathbb{C}$ which does not contain 0, we can always choose a continuous branch of $\arg(z)$ that is defined in Ω.

LEMMA 1. *Suppose Ω is a simply connected plane domain which does not contain the origin. Then there is a continous branch of* $\arg(z)$ *defined on Ω, i.e., there is a continuous function $f(z)$ so that* $\exp(\log|z| + if(z)) = z$.

PROOF. This "proof" is simply a reference to a standard result about topology. Consider $e^{it} : \mathbb{R} \to \mathbb{T}$ as a covering map. Note that $g(z) = e^{i \arg(z)}$ is a continuous map $\Omega \to \mathbb{T}$. Since Ω is simply connected, there is a lifting of g to a map $f : \Omega \to \mathbb{R}$, i.e., a map so that $g(z) = e^{if(z)}$. Thus f is the desired branch. See Appendix **??** for more about covering maps and some standard references. □

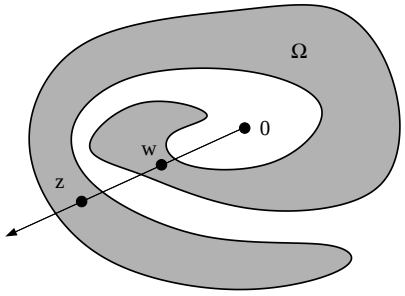

FIGURE 3. The points z and w lie on the same ray through the origin, but a continuous branch of arg on Ω will give z a value 2π larger than the value for w.

Define

$$e^z = e^{x+iy} = e^x(\cos y + i \sin y)$$

and

$$\log(z) = \log|z| + i \arg(z), \text{ if } z \neq 0.$$

The exponential functions satisfies the Cauchy-Riemann equations and the partials are never zero, so this function is conformal on any domain where it is 1-to-1. It is not 1-to-1 on the whole plane because $e^{z+2\pi i} = e^z$; each point except the origin has infinitely many preimages arranged along a vertical line. Each vertical line is mapped to a circle centered at the origin and teach horizontal line is mapped to a ray from 0 to ∞. See Figure 5. The logarithm is a branch of the inverse of this map; it sends rays to horizontal lines and circular arcs centered at the orgin to vertical lines.

A complex number z can be written as $z = re^{\imath\theta}$ where $r = |z|$ and $\theta = \arg(z)$. This is the polar coordinates form of a complex number. When we multiply two complex numbers the absolute values multiply and the arguments add, i.e.,

$$z_1 z_2 = (r_1 e^{i\theta_1})(r_2 e^{i\theta_2}) = r_1 r_2 e^{i(\theta_1+\theta_2)}.$$

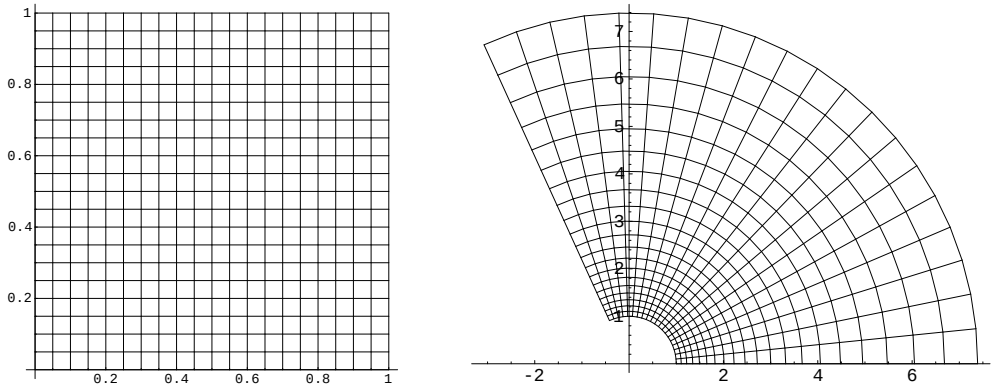

FIGURE 4. The same square grid of $[0, 2]^2$ and its image under e^z.

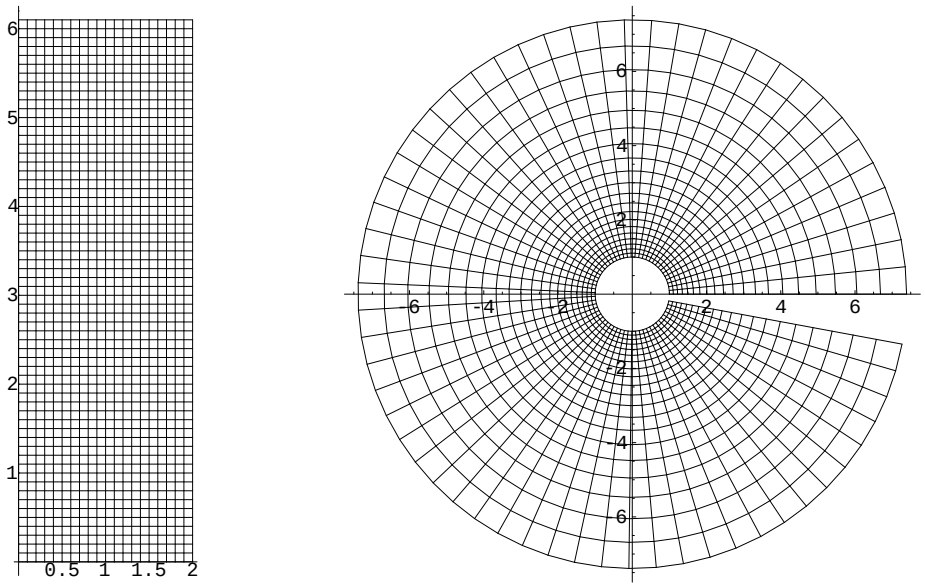

FIGURE 5. This illustrates the exponential map again. We take the image of $[0, 2] \times [0, 6]$. The line at height 2π will be mapped into the positive real axis. The top edge of the grid is just below this, so the image stops just before it reaches the axis.

This explains why the angle doubles at the origin in Figure 5. If we consider the maps z^3 and $z^{1/2}$, then angles at the origin will multiply by 3 and $\frac{1}{2}$ respectively, as

shown in Figure 5. In general we define

$$z^\alpha = e^{\alpha \log z} = e^{\alpha(\log|z| + i\arg(z))} e^{\alpha(\log|z| + i\mathrm{Arg}(z) + 2\pi i\mathbb{Z})}.$$

If α is an integer then this the various possible valuesof $\arg(\alpha)$ all give the same value of z^α. If $\alpha = p/q$ then there are q possible different values. Otherwise, z^α has infinitely many possible values. Moreover, some caution is needed when applying the rules of exponents. Consider

$$1 = \sqrt{1} = \sqrt{(-1)(-1)} = \sqrt{-1}\sqrt{-1} = i \cdot i = -1.$$

The problem is that $\sqrt{1}$ and $\sqrt{-1}$ each have two possible values and by choosing the wrong we can arrive at an apparent contradiction.

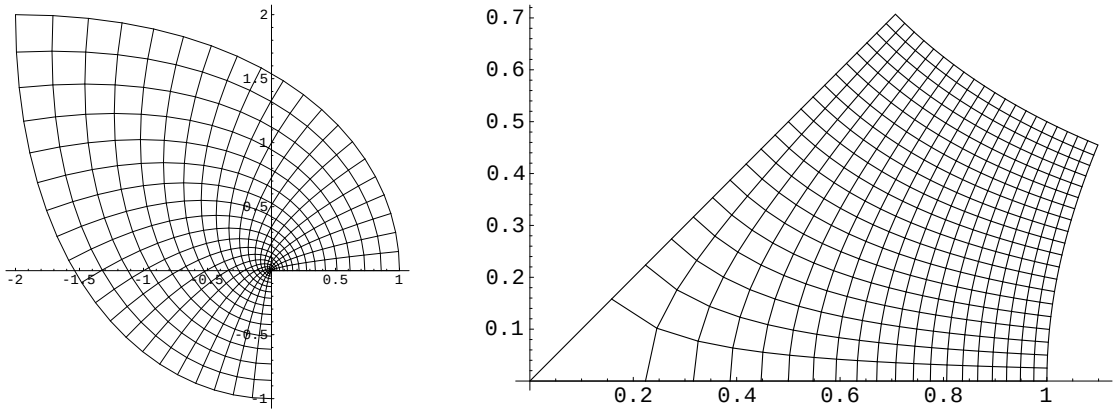

FIGURE 6. The images of $[0,1]^2$ under z^3 and $z^{1/2}$. These are all conformal maps of the square, but are not conformal at the origin (which is a boundary point).

A complex function of a complex variable is differentiable if

$$f'(z) = \lim_{h\to 0} \frac{f(z+h) - f(z)}{h},$$

exists. Here h can approach the origin in any way whatsoever. Two special ways of approaching are along the real or imaginary axes, which lead to the equations

$$f'(z) = \lim_{h\to 0} \frac{u(x+h,y) + iv(x+h,y) - u(x,y) - iv(x,y)}{h} = u_x + iv_x,$$

$$f'(z) = \lim_{h\to 0} \frac{u(x,y+h) + iv(x,y+h) - u(x,y) - iv(x,y)}{ih} = -iu_x + v_x.$$

Cauchy-Riemann equations. Conversely, is these partials exist, are continuous in a neighborhood of z and satisfy the Cauchy-Riemann equations, then f' exists and

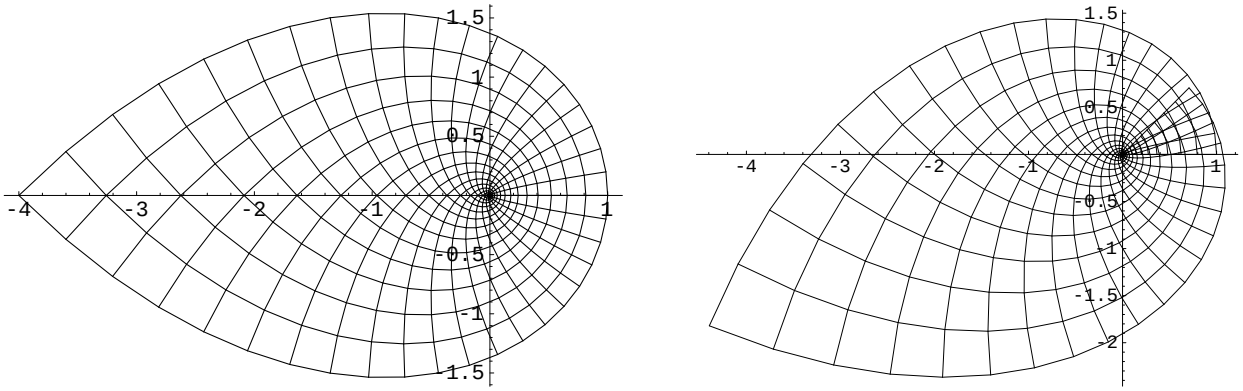

FIGURE 7. The images of $[0,1]^2$ under z^4 and $z^{4.5}$. In the first the segment $[0,16]$ is part of the boundary, not the interior of the dommain. For powers > 4, the map is no longer 1-to-1 and the image intersects itself.

equals $u_x + iv_x$. Continuity is required because examples like $xy/(x^2+y^2)$ show that a function can have partial derivatives at 0, but not even be continuous there. But if the partials exist and are continuous in neighborhood of a point, then results from calculus imply it is approximated by the linear map Df, i.e., if $h = s + it$, then

$$f(z+h) - f(z) = (u_x s + u_y t) + i(v_x s + v_y t) + o(|h|) = (u_x + iv_x)h + o(|h|), \tag{1}$$

which implies f is differentiable with derivative $u_x + iv_x$.

This is the first time we have used the "little-oh" notation, so perhaps we should explain it. The term $o(|h|)$ refers to term which is going to zero faster than $|h|$ as $|h| \to 0$. Equation (1) means that for every $\epsilon > 0$ there is a $\delta > 0$ so that if $|h| \le \delta$, then

$$|f(z+h) - f(z) - (u_x + iv_x) \cdot h| \le \epsilon h.$$

However, it is quicker and more convenient to write (1). Note that $o(1)$ stands for a term that tends to zero as the relevant parameter tends to its limit. Thus $o(h) = o(1) \cdot h$. The "big-Oh" notation $O(1)$ stands for a term that remains bounded as the relevant parametet tends to its limit. For example, $O(|x|)$ as $|x| \to \infty$ stands for a term that is bounded by $C|x|$ fore some fixed $C < \infty$ as $|x|$ grows.

The reader should now check that $(e^z)' = e^z$ and $(\log z)' = 1/z$ (on an region where log is defined and continuous). The usual rules of differentiation hold:

$$(f+g)' = f' + g', (fg)' = f'g + fg', (f/g)' = (f'g - fg')/g^2, (f \circ g)' = (f' \circ g)g'.$$

which implies the complex derivative exists. Therefore polynomials and rational functions are differentiable (at least at points where we don't divide by zero).

A power series is an infinite series of the form

$$\sum_{n=0}^{\infty} a_n(z-z_0)^n.$$

we say it converges at z if the sequence of partial sums has a finite limit, i.e.,

$$f(z) = \lim_{N\to\infty} \sum_{n=0}^{N} a_n(z-z_0)^n,$$

exists. Such a series obviously converges at $z = z_0$. More generally, there is a radius of convergence R ($R = 0, \infty$ are possible) where

$$\frac{1}{R} = \limsup_{n\to\infty} |a_n|^{1/n},$$

and the series converges inside $\{z : |z - z_0| < R\}$ and diverges in $\{z : |z - z_0| > R\}$. The series might or might not converge at various boundary points of the disk; this depends on the particular coefficients. When a power series converges, it defines a continuous function on the open disk of convergence and this function is complex differentiable. If it is also 1-1, then it is a conformal map of the disk. More surprisingly, if f is a conformal map of an open disk, then f has a power series converging to it in this disk. We will prove this in the next few pages, but first need to introduce complex integrals and the Cauchy integral theorem.

A curve is continuous map $\gamma : [a, b] \to \mathbb{C}$. We also call the compact set $\Gamma = \gamma([a, b])$ a curve, although technically this should be called the trace of γ. A curve γ is rectifiable if there is a $M < \infty$ so that

$$\sup_{\mathcal{P}} \sum_{k=1}^{n} |\gamma(x_{k-1}) - \gamma(x_k)| \le M,$$

for every finite ordered set $\mathcal{P} = \{a = x_1 < \cdots < x_{n+1} = b\} \subset [a, b]$. The smallest such upper bound is the length of γ, denoted $\ell(\gamma)$. $\mathcal{P}$ is called a parition of $[a, b]$ and $\|\mathcal{P}\| = \max_k |x_{k+1} - x_k|$ denotes the size of the largest gap between consequtive points.

Felix Klein was quoted in [] as saying "Everyone knows what a curve is, until he has studied enough mathematics to become confused through the countless number of possible exceptions." Figures 5 and 5 show two such possible exceptions.

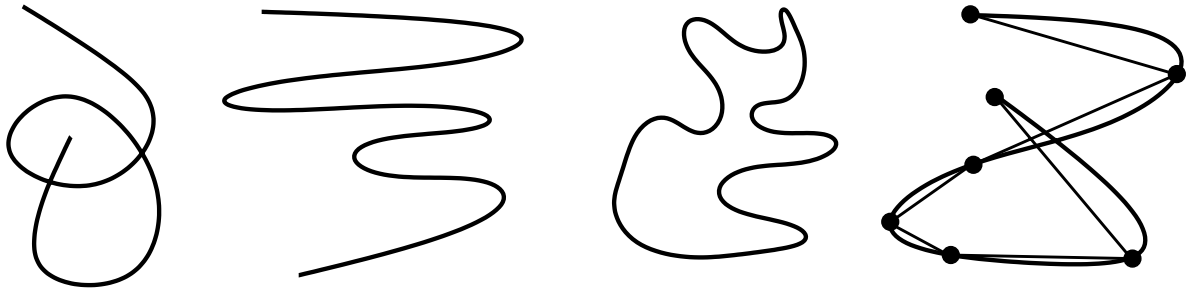

FIGURE 8. A curve is continuous image of a closed interval. A Jordan curve is a 1-to-1 image (no self-intersecting), and a closed Jordan curve has $\gamma(b) = \gamma(a)$. A rectifiable curve is one where inscribed polygons have uniformly bounded length.

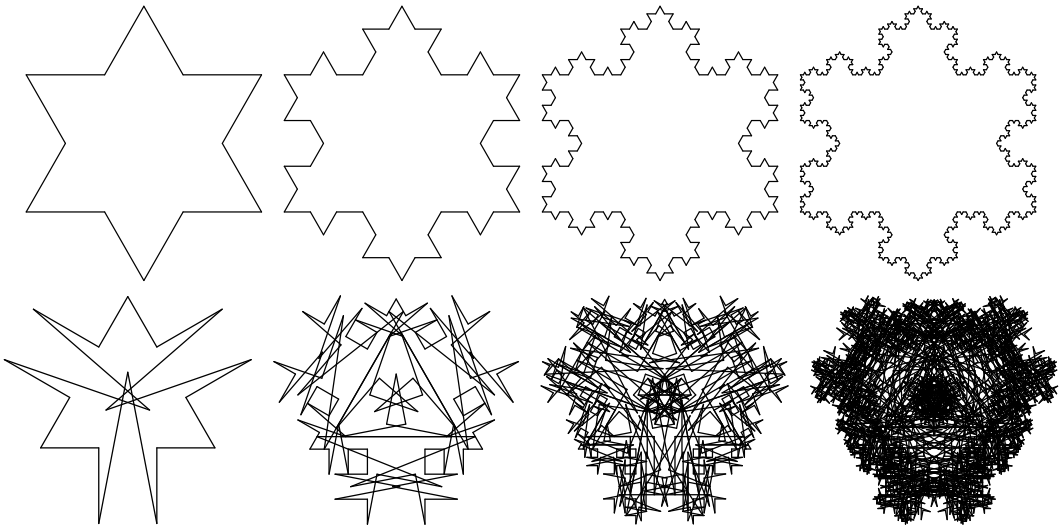

FIGURE 9. The top row shows four generations of the construction of the von Koch snowflake, a closed Jordan curve that is not rectifiable. The bottom row shows four generations of a variation of the snowflake. In this case the limiting curve covers an open set, i.e., is a type of Peano curve.

If γ maps into a domain Ω and f is a continuous function on Ω, we define the integral of f along γ as

$$\int_\gamma f(z)dz = \lim_{\|\mathcal{P}\|\to 0} \sum_{k=1}^{n} f(\gamma(x_k))(\gamma(x_{k+1}) - \gamma(x_k)),$$

where the limit is taken over paritions as the maximum gap tends to zero. If f is continuous and γ is rectifiable, then it is easy to see that this limit exists. If γ is

piecewise C^1, we sometimes write $\int_\Gamma f(z)dz$, instead of $\int_\gamma f(z)dz$. This is permissible since one can show that two different parameterizations of Γ (with the same starting and ending points) give the same integral. The following estimate is obvious, but very useful:

LEMMA 2. $\int_\gamma f(z)dz \leq \max_\gamma |f| \cdot \ell(\gamma)$.

If γ is differentiable, this definitions agrees with the idea of a line integral in calculus:

LEMMA 3. *If γ is a C^1 curve then*

$$\int_\gamma f(z)dz = \int_a^b f(\gamma(x))\gamma'(x)dx,$$

(where γ' is interpreted as a complex number instead of a 2-vector).

PROOF. The two integrals are limits of Riemann sums of the form

$$\sum f(z_k)(z_{k+1} - z_k), \quad \sum f(z_k)\gamma(x_k)(x_{k+1} - x_k),$$

and since $(z_{k+1} - z_k) = (x_{k+1} - x_k)\gamma'(x_k) + o(1)$, the result follows. □

An important consequence is the following equality: if $\gamma(t) = re^{it}$ maps $[0, 2\pi]$ onto a circle of radius r, then

$$\int_\gamma \frac{1}{z} dz = 2\pi i.$$

To see this, we simply compute the left hand side as

$$\int_0^{2\pi} \frac{1}{r} e^{-it} rie^{it} dt = i \int_0^{2\pi} dt = 2\pi i.$$

LEMMA 4. *Suppose f is continuous and $f = F'$ for some complex differentiable F on Ω. Then we claim that*

$$\int_\gamma f(z)dz = F(\gamma(b)) - F(\gamma(b)).$$

PROOF. To prove this consider a partition $\mathcal{P} = \{x_1 < \ldots x_{n+1}\}$ and let $z_k = \gamma(x_k)$. Since γ has compact image and f is continuous, it is uniformly continuous on $\Gamma = \gamma([a, b])$. Hence

$$|f(z) - f(w))| \leq o(1)$$

unifromly as $\|\mathcal{P}\| \to 0$ and thus

$$F(z) = F(w) + (z-w)f(w) + o(|z-w|),$$

for every $w \in \Gamma$. Since γ is uniformly continuous, if the gaps in our partition are small enough then $\gamma([x_{k+1}mx_k]) \subset D(z_k, r)$. Thus

$$\begin{aligned}\int_\gamma f(z)dz &= \sum_{k=1}^{n} f(\gamma(x_k))(z_{k+1}-z_k) + o(1)\\ &= \sum_{k=1}^{n}[F(z_{k+1})-F(z_k)] + o(\sum_k |z_{k+1}-z_k|) + o(1)\\ &= F(z_{n+1}) - F(z_1) + \o(\ell(\gamma)) + o(1),\end{aligned}$$

which gives the desired equality. In particular if γ is a closed curve, i.e., $\gamma(a) = \gamma(b)$, then $\int_\gamma f(z)dz = 0$. □

LEMMA 5. *If f is conformal on a domain Ω and γ is a closed rectifiable curve in $D(z,r) \subset \Omega$ then $\int_\gamma f(z)dz = o(r\ell(\gamma))$.*

PROOF. Since constants and linear functions of z are derivatives of other functions, the integral of one of these around a closed curve is zero. So if $\gamma \subset D(z_0, r)$ and

$$f(z) = f(z_0) + f'(z_0)(z-z_0) + o(|z-z_0|),$$

then

$$\begin{aligned}\int_\gamma f(z)dz &= f(z_0)\int_\gamma dz + f'(z_0)\int_\gamma (z-z_0)dz + \int_\gamma o(|z-z_0|)dz\\ &= 0 + 0 + o(r)\ell(\gamma).\end{aligned}$$

□

We say a domain Ω is decomposed in subdomians $\{\Omega\}$ if each $\Omega_k \subset \Omega$, they are pairwise disjoint and $\Omega = \cup_k \overline{\Omega_k} \cap \Omega$. Right now, we are only interested in decompositions of peicewise C^1 domains into finitely many piecewise C^1 subdomains, as illustrated in Figure 10. Note that if f is continuous on the closure of Ω, then

$$\int_{\partial\Omega} f(z)dz = \sum \int_{\partial\Omega_k} f(z)dz,$$

becuase each arc of $\partial\Omega_k$ which is interior to Ω is also a boundary arc of another domain, but with the opposit orientation. Thus these integrals cancel. The only

parts of the integrals on the right that don't cancel are the one on the boundary of Ω, and they sum to the integral on the left. Technically, we should write $\int_\gamma$ instead of $\int_{\partial\Omega}$ where γ is a parameterization of $\partial\Omega$, but the integral is independent of the particular parameteriation, so this abuse of notation is reasonable.

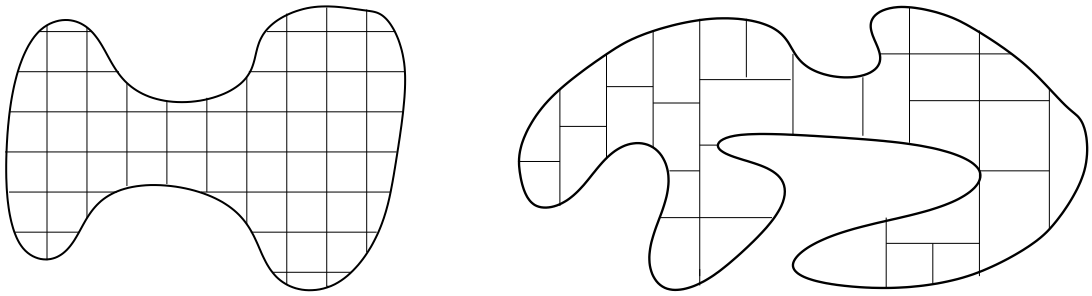

FIGURE 10. Decomposing a domain means breaking it into smaller domains. We will only be interested in decompositions of piecewise smooth domains into finitely many piecewise smooth domains with small diameter. For a piecewise C^1 curve this can be done by intersecting with a standard ϵ-grid, although more irregular decompositions are also allowed.

LEMMA 6. *Suppose $\gamma \subset \Omega$ is a closed Jordan curve which bounds a region which can be decomposed into $O(\epsilon^{-2})$ many regions each with boundary length $\leq \epsilon$. Suppose f has a continuous complex derivative on Ω. Then $\int_\gamma f(z)dz = 0$.*

PROOF. The integral around the boundary of each subpiece is $o(\epsilon^2)$ and there are $O(\epsilon^{-2})$. Thus the sum of these integrals tends to zero as $\epsilon \to 0$. The sum is always equal to $\int_\gamma f(z)dz$, so the lemma is proved. □

LEMMA 7. *Suppose f is holomorphic on a neighborhood of a closed disk $D = D(0,r)$ and $|z| < r$. Then*

$$f(z) = \frac{1}{2\pi i}\int_\gamma \frac{f(w)}{w-z}dw,$$

where $\gamma(t) = z_0 + re^{it}$ maps $[0, 2\pi]$ to the boundary of D

PROOF. Choose ϵ so $0 < \epsilon < (r - |z|)/2$ and let S be a line segment connecting the circles $C_\epsilon = \{w : |z-w| = \epsilon\}$ to $C_r = \{w : |w| = r\}$. Let γ be the curve consisting of four parts: traversing C_r one time in the counterclockwise direction, along S from

C_r to $C\epsilon$, around C_ϵ once clockwise and finally along S from C_ϵ to C_r. This curve bounds a slit annulus and can clear be decomposed as in Lemma 6, so the integral of f around γ is 0. The integrals over the two line segments cancel, so the integrals over the inner and outer circle also cancel. We rewrite the inner integral as

$$\int \frac{f(w)}{w-z}dw \int \frac{f(z)-f(0)}{w-z}dw + \int f(0)\frac{dw}{w-z}.$$

By an earlier computation the second integral on the right is $2\pi i f(0)$. The first is bounded by $\sup_{|w|=\epsilon} |f(w) - f(0)|$ which tends to zero as $\epsilon \to 0$. This proves the lemma. □

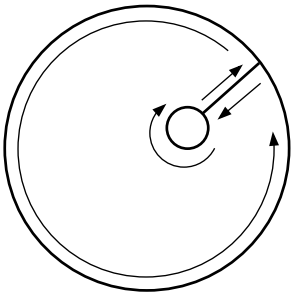

FIGURE 11. The curve used in the proof of Lemma 7.

Next we want to compute power series for holomorphic functions. The most important example is the geometric series

$$\sum_{n=0}^{\infty} z^n = 1 + z + z^2 + z^3 + \cdots = \frac{1}{1-z}.$$

The derivation is exactly the same as for real numbers in calculus. Suppose

$$1 + z + \cdots + z^n = S.$$

Then

$$z + z^2 + \ldots z^{n+1} = zS,$$

so subtracting gives

$$1 - z^{n+1} = S - zS = S(1-z),$$

$$S = \frac{1-z^{n+1}}{1-z},$$

$$1 + z + z^2 + \cdots + z^n = \frac{1-z^{n+1}}{1-z}. \tag{2}$$

For $|z| < 1$ we have $z^{n+1} \to 0$, which proves the result. Also note that if we differentiate (2) we get

$$0 + 1 + 2z + \cdots + nz^{n-1} = \frac{-(n+1)z^n(1-z) + (1-z^{n+1})}{(1-z)^2}. \tag{3}$$

For $|z| < 1$ the terms z^n and z^{n+1} tend to zero, so

$$\sum_{n=1}^{\infty} nz^{n-1} = 1 + 2z + 3z^2 + 4z^3 + \cdots = \frac{1}{(1-z)^2}.$$

The closely related function

$$\frac{z}{(1-z)^2} = z + 2z^2 + 3z^3 + \ldots,$$

is called the Koebe function and has an important place in the history of geometric function theory.

LEMMA 8. *If f is holomorphic on a neighborhood of the closure of $D = D(0,r)$ then f has a power series centered at 0 that converges in D.*

PROOF. Let γ be the curve that traverses ∂D once in the counterclockwise direction. Let $z \in D$. Then

$$\begin{aligned} f(z) &= \frac{1}{2\pi i}\int_\gamma \frac{f(w)}{w-z}dw \\ &= \frac{1}{2\pi i}\int_\gamma f(w)\frac{1}{w}[\sum_{n=0}^{\infty}(\frac{z}{w})^n]dw \\ &= \sum_{n=0}^{\infty}[\frac{1}{2\pi i}\int_\gamma \frac{f(w)}{w^{n+1}}dw]z^n \\ &= \sum_{n=0}^{\infty} a_n z^n. \end{aligned}$$

The infinite sum and integral can be exchanged because the sum is absolutely and unifromly convergent for $|z| < |w|$ (see Appendix D. Note that $|a_n| \le \max_\gamma |f| \cdot r^{-n-1}$, so the radius of convergence is $\ge r$. □

LEMMA 9. *If $f(z) = \sum_{n=0}^{\infty} a_n z^n$ is defined by a convergent power series in $D(0,r)$, then f is holomorphic and $f'(z) = \sum_{n=1}^{\infty} n a_n z^{n-1}$ in $D(,r)$*

PROOF. We compute the derivative by taking quotients

$$\begin{aligned} f'(z) &= \lim_{h\to 0}\frac{1}{h}[f(z+h)-f(z)] \\ &= \lim_{h\to 0}\frac{1}{2\pi i h}\int_\gamma \frac{f(w)}{w-z}-\frac{f(w)}{w-z-h}dw \\ &= \lim_{h\to 0}\frac{-1}{2\pi i}\int_\gamma \frac{f(w)}{(w-z)(w-z-h)}dw \\ &= \frac{-1}{2\pi i}\int_\gamma \frac{f(w)}{(w-z)^2}dw, \end{aligned}$$

where we have used uniform convergence to justify passing the limit through the integral. Next use (3).

$$\begin{aligned} f'(z) &= \frac{1}{2\pi i}\int_\gamma f(w)\frac{1}{w}[\sum_{n=1}^{\infty} n(\frac{z}{w})^{n-1}]dw \\ &= \sum_{n=1}^{\infty} n[\frac{1}{2\pi i}\int_\gamma \frac{f(w)}{w^{n+1}}dw]z^{n-1} \\ &= \sum_{n=1}^{\infty} n a_n z^{n-1}. \end{aligned}$$

□

From the power series formula one can derive $a_n = \frac{f^{(n)}(0)}{n}$, where $f^{(n)}$ denotes the nth derivative of f and $n = 1\cdot 2\cdot 3\cdots n$. Some important examples are

$$e^z = \sum_{n=1}^{\infty}\frac{1}{n}z^n,$$

$$(1+z)^\alpha = \sum_{n=0}^{\infty}\frac{\alpha(\alpha-1)\cdots(\alpha-n+1)}{n}z^n.$$

Thus every holomorphic function on the unit disk has a power series expansion and hence every conformal map does. While its easy to determine which power series correspond to holomorphic functions ($\limsup |a_n|^{1/2} \geq 1$) it is probably impossible to give a concise characterization of the series corresponding to 1-to-1 holomorphic functions (e.g., conformal maps). One of the most famous problems in complex analysis was the Beierbach conjecture that if f is 1-1 and holomorphic on $\mathbb{D}$ with $|f'(0)| = 1$, then

$$|a_n| \leq n.$$

Sharpness is shown by the Koebe function mentioned earlier. The conjecture was proven in 1984 by Louis deBrange in a technical tour-de-force, later simplified by other authors. Similar questions for related collection of maps still remain open.

2. Möbius transformations

A linear fractional transformation (or Möbius transformation) is a map of the form $z \to (az+b)/(cz+d)$. This is a 1-1, onto, holomorphic map of the Riemann sphere $\mathbb{S} = \mathbb{C} \cup \{\infty\}$ to itself. The non-identity Möbius transformations are divided into three classes. Parabolic transformations have a single fixed point on $\mathbb{S}$ and are conjugate to the translation map $z \to z+1$. Elliptic maps have two fixed points and are conjugate to the rotation $z \to e^{it}z$ for some $t \in \mathbb{R}$. The loxodromic transformations also have two fixed points and are conjugate to $z \to \lambda z$ for some $|\lambda| < 1$. If, in addition, λ is real, then the map is called hyperbolic.

Given two sets of three distinct points $\{z_1, z_2, z_3\}$ and $\{w_1, w_2, w_3\}$ there is a unique Möbius transformation that sends $w_k \to z_k$ for $k = 1, 2, 3$. This map is given by the formula

$$\tau(z) = \frac{w_1 - \zeta w_3}{1 - \zeta},$$

where

$$\zeta = \frac{(w_2 - w_1)}{(w_2 - w_3)} \frac{(z - z_1)(z_2 - z_3)}{(z - z_3)(z_2 - z_1)}.$$

A Möbius transformation sends the unit disk 1-1, onto itself iff it is if the form

$$z \to \lambda \frac{z - a}{1 - \bar{a}z},$$

for some $a \in \mathbb{D}$ and $|\lambda| = 1$. In this case, any loxodromic transformation must actually be hyperbolic.

Given four distinct points a, b, c, d in the plane we define their cross ratio as

$$\mathrm{cr}(a, b, c, d) = \frac{(d - a)(b - c)}{(c - d)(a - b)}.$$

Note that $\mathrm{cr}(a, b, c, z)$ is the unique Möbius transformation which sends a to 0, b to 1 and c to ∞. This makes it clear that cross ratios are invariant under Möbius transformations; that $\mathrm{cr}(a, b, c, d)$ is real valued iff the four points lie on a circle; and is negative iff in addition the points are labeled in counterclockwise order on the circle.

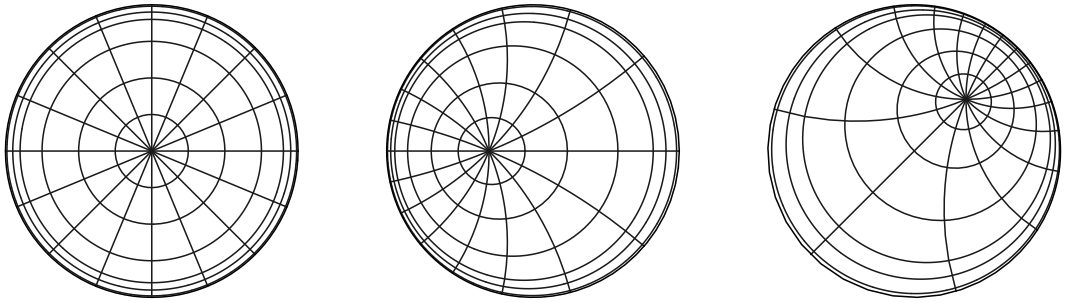

FIGURE 12. A polar grid in the disk and some images under Möbius transformations that preserve the unit disk.

Möbius transformations form a group under composition. If we identity the transformation $(az+b)/(cz+d)$ with the matrix

$$\begin{pmatrix} a & b \\ c & d \end{pmatrix}$$

then composition of maps is the same as matrix multiplication. For any non-zero λ, the translations $(\lambda az + \lambda b)/(\lambda cz + \lambda d)$ are all the same, but correspond to different matrices. We can choose one to represent the transformation, say the one with determinate 1, and this identifies the group of transformations the the group $\mathrm{SL}(2,\mathbb{C})$ of two by two matrices of determinate 1. (If $ad = bc$, then

$$\frac{az+b}{cz+d} = \frac{adz+bd}{cdz+d^2} = \frac{bcz+bd}{cdz+d^2} = \frac{b}{d}\frac{cz+d}{cz+d} = \frac{b}{d},$$

is constant and not a Möbius transformation.

The mapping

$$z \to \frac{az+b}{cz+d},$$

can be written as a composition of the maps

$$z \to cz + d,$$

$$z \to \frac{1}{z},$$

$$z \to \frac{a}{c} + \frac{bc-ad}{c}z,$$

which equivalent to claiming

$$\begin{pmatrix} a & b \\ c & d \end{pmatrix} = \begin{pmatrix} c & d \\ 0 & 1 \end{pmatrix} \begin{pmatrix} 0 & 1 \\ 1 & 0 \end{pmatrix} \begin{pmatrix} (bc-ad) & a \\ 0 & c \end{pmatrix}.$$

Either claim follows by a direct computation. The linear maps have the property that circles map to circles an lines map to lines. The inversion also has this property, although it may interchange the two types of sets. The equation

$$x^2 + y^2 + \alpha x + \beta y + \gamma = 0 \tag{4}$$

defines a circle in the plane, depending on the choice of α, β, γ. If we set $z = x+iy \neq 0$ and $\frac{1}{z} = u + iv$, then

$$u = \Re(\frac{x - iy}{x^2 + y^2}) = \frac{x}{x^2 + y^2},$$
$$v = \Im(\frac{x - iy}{x^2 + y^2}) = \frac{-y}{x^2 + y^2},$$
$$x = \frac{u}{u^2 + v^2},$$
$$y = \frac{-v}{u^2 + v^2},$$

so (4) becomes

$$\frac{u^2}{(u^2 + v^2)^2} + \frac{v^2}{(u^2 + v^2)^2} + \frac{\alpha u}{(u^2 + v^2)^2} + \frac{-\beta v}{(u^2 + v^2)^2} + \gamma = 0.$$

After simplifying this becomes

$$\frac{1}{(u^2 + v^2)^2} + \frac{\alpha u}{u^2 + v^2} + \frac{-\beta v}{u^2 + v^2} + \gamma = 0,$$

$$1 + \alpha u - \beta v + \gamma(u^2 + v^2) = 0,$$

which is the equation of a circle or line (depending on whether $\gamma \neq 0$ or $\gamma = 0$). Thus $z \to \frac{1}{/}z$ sends a circle not passing through the origin to a circle and a circle that does pass though 0 to a line (which is the same as a circle passing through ∞). Thus we have shown

LEMMA 10. *Möbius transformations map circles to circles, assuming the convention that lines are considered as circles through infinity.*

The reflection through a circle $|z - c| = r$ is defined by $\arg(w^* - c) = \arg(w - c)$ and $|w - c| \cdot |w^* - c| = r^2$. Möbius transformation preserve reflections, i.e., if τ is a linear fractional transformation that send circle (or line) C_1 to circle (or line) C_2 then pairs of symmetric points for C_1 are mapped by τ to symmetric points for C_2.

LEMMA 11. *Every Möbius transformation can be written as a even number of compositions of circle and line reflections.*

The proof is left to the reader.

In higher dimensions, reflections through planes and spheres still makes sense. In this case, Möbius transformations are defined as the group generated by any even number of compositions of such maps (even so that the result is orientation preserving).

Each reflection in a line can be extended to a reflection across a plane in 3-space that is perpendicular to $\mathbb{R}^2$. Similarly, any circle reflection in the plane can be extended to a reflection through a sphere in 3-space. From this it is possible to show that every Möbius transformation has a unique extension to a conformal map of $\mathbb{S}^2$ to itself.

The plane can be identified with a 2-sphere minus a point via stereographic projection. Möius transformations can be considered as mappings of the sphere to itself. To be more concrete, we consider the unit sphere $S^2 = \{(x, y, zz) : x^2 + y^2 + z^2 = 1\}$ in $\mathbb{R}^3$ and let $N = (0, 0, 1)$ denote the "north pole". Then $S^2 \setminus \{N\}$ is topolgocially a plane and the correspondence can be made explicit by joining each point of the (x, y)-plane to N by a straight line in $\mathbb{R}^3$. This line hits S^2 at some point $(u, v, t) \neq N$ and the map $(x, y) \to (u, v, t)$ is called the stereographic projection of the plane onto a sphere. We can easily compute formulas for this map. Set $r = \sqrt{x^2 + y^2}$ and $\rho = \sqrt{u^2 + v^2}$. Then we have $t^2 + \rho^2 = 1$ and $(r - \rho)/r = t$. Solving for t gives

$$t = \frac{r - 1}{r + 1},$$

which implies

$$u = \frac{x}{r\rho} = \frac{x}{r\sqrt{1 - t^2}},$$
$$v = \frac{y}{r\rho} = \frac{y}{r\sqrt{1 - t^2}}.$$

We leave it to the reader to check that circle or lines in the (x, y)-plane map to circles on S^2.

In 3 dimensions and higher, these are the only conformal maps. By a theorem of Liouville, any conformal map from a domain $\Omega \subset \mathbb{R}^3$ into $\Omega' \subset \mathbb{R}^2$ must the restriction of a Möbius transformation. This is not at all elementary. For one proof

(assuming the map is at least C^2, see "Inversion theory and conformal mappings" by [?]. The result is still true if we assume only C^1, but even harder to prove.

3. The Schwarz-Christoffel Formula

The Schwarz-Christoffel formula gives a formula for the Riemann map of the disk onto a polygonal region Ω: if the interior angles of P are $\alpha\pi = \{\alpha_1\pi, \ldots, \alpha_n\pi\}$, then

$$f(z) = A + C \int^z \prod_{k=1}^{n} (1 - \frac{w}{z_k})^{\alpha_k - 1} dw,$$

where $\{z_1, \ldots, z_n\}$ are the points that map to the vertices of the polygon (and will be called the prevertices or conformal prevertices or z-parameters). See e.g., [?], [?], [?]. The interior angles of an n-gon sum to $(n-2)\pi$, which implies $\sum_k \alpha_k = -2$.

On the half-plane the formula is

$$f(z) = A + C \int \prod_{k=1}^{n} (w - z_k)^{\alpha_k - 1} dw.$$

In the case of the half-plane, there is a special boundary point, namely ∞. We assume this point is mapped to the last vertex, v_n, of the polygon, then the Schwarz-Christoffel formula can be written as

$$f(z) = A + C \int \prod_{k=1}^{n-1} (w - z_k)^{\alpha_k - 1} dw.$$

The formula was discovered independently by Christoffel in 1867 [?] and Schwarz in 1869 [?], [?]. For other references and a brief history see Section 1.2 of [?]. It is also possible to formulate it with other base domains, such as an infinite strip (see [?]). See [?] for a version involving doubly connected polygonal regions. There are also versions for domains other than polygons, e.g., circular arc polygons as in [?], [?]. In this case, we get a simple formula for the Schwarzian derivative of the conformal map, but it involves unknown parameters with no obvious geometric interpretation.

LEMMA 12. *With notation as above* $\sum_{k=1}^{n} (\alpha_k - 1) = -2$.

PROOF. The interior angles of an n-gon sum to $(n-2)\pi$, so

$$\sum_{k=1}^{n} (\alpha_k - 1) = \frac{1}{\pi}(n-2)\pi - n = -2.$$

□

If we apply a Euclidean similarity to a polygon, the interior angles do not change. Thus the α parameters do not change. Such a mapping also leaves the z parameters unchanged. Thus the maps for different but similar polygons differ only by the constants A and C. Changing the first translates the image and the changing the second alters the size and orientation.

LEMMA 13. *The function $\prod_{k=1}^{n-1}(w-z_k)^{\alpha_k-1}$ is a non-vanishing holomorphic function on the upper half plane which extends continuously to each component of $\mathbb{R}\setminus\{z_k\}$ and has constant argument on each such component.*

PROOF. Suppose α and c are real numbers and consider $f(w) = (w-c)^\alpha$. If f is not an integer, then this is not a single valued holomorphic function on the whole plane. To make it holomorphic we need to remove a branch cut from c to ∞ and define a single valued branch on the remaining domain. For the Schwarz-Christoffel formula we want the integrand to be holomorphic in the upper half-plane, so we can choose any branch cut in the lower half-plane, and we choose a branch of $(w-c)^\alpha$ which is positive if w is real and $w > c$. If we do this then $\arg((w-c)^\alpha)$ piecewise constant on the real line with a jump discontinuity at c. It has value 0 to the right of c and value $\alpha\pi$ to the right of c.

When we multiply the various terms in the integrand of the SC formula, the arguments add. Thus the argument of the integrand is piecewise constant with jump at z_k parameter of size $\theta_k = \pi\alpha_k$, i.e.,

$$\arg(f') = \arg(C) + \sum_{k=1}^{n}(\alpha_k - 1)\arg(w - z_k).$$

The image of the segment $I_k = [z_k, z_{k+1}]$ thus has constant argument (i.e., it lies in a line segment) and the angle between the images of I_k and I_{k+1} is θ_k.

The first claim is obvious since it is a product of non-vanishing holomorphic functions. □

Since f' is bounded, except possibly at the z-parameters, its integral f is well defined and has a continuous extension to the boundary except at these points (in fact, it has a holomorphic extension across the complementary intervals). It will have a continuous extension to a z-parameters z_k if $|f'(z)| = O(|z-z_k|^\beta)$ for some $\beta > -1$, so that f' is integrable on the boundary in a neighborhood of z_k. This happens as long

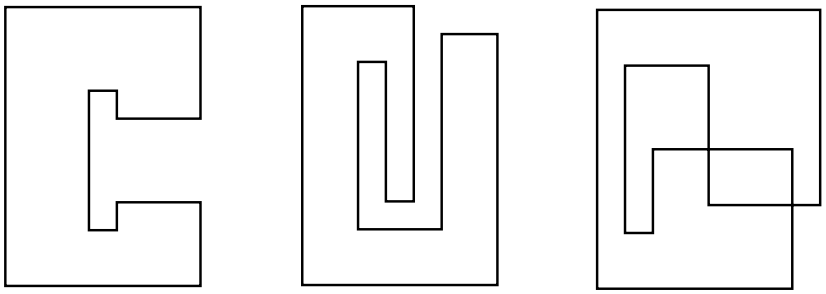

FIGURE 13. Different possible SC images using the same angles but different z-parameters.

as $\alpha_k > 0$ which happens iff $\theta_k > 0$. This is always the case for bounded polygons. It can happen that $\theta_k = 0$ for some unbounded polygons, e.g., an infinite strip can be considered as an unbounded polygon with two interior angles of size zero. In this case the Schwarz-Christoffel formula predicts that the map from the disk to the strip with prevertices $0, \infty$ should be given by

$$f(z) = A + C \int w^{-1} dw = A + C \log z,$$

which is correct. Moreover the maps fails to continuous exactly at the parameter value $z_1 = 0$ where the integrand has a pole of order -1.

In general, if we have two infinite edges which tend to infinity in directions $\theta_1 < \theta_2 \leq \theta_1 + 2\pi$ we define the corresponding interior angle at ∞ to be $\theta_1 - \theta_2$. This is in the interval $[-2\pi, 0]$ (including both endpoints, unlike the finite case). If we mapped the unbounded polygon by a Möbius transformation so that ∞ is mapped to the finite point (so the edges of the image are now circular arcs and not necessarily line segments), then this is the same as the negative of the interior angle at the image vertex. With this convention for the angle at ∞, the Schwarz-Christoffel formula can be extended to handle unbounded polygons (e.g., see []), but in these notes we will concentrate on the bounded case.

Our remarks so far prove the following.

LEMMA 14. *The SC formula for parameters $\{\alpha_k\}$ (with $\sum_{k=1}^n \alpha_k = -2$) and $z_1 < \ldots z_n$ defines a locally 1-1 holomorphic function which extends continuously to the boundary and maps each parameter interval 1-1 onto a line segment. If the map*

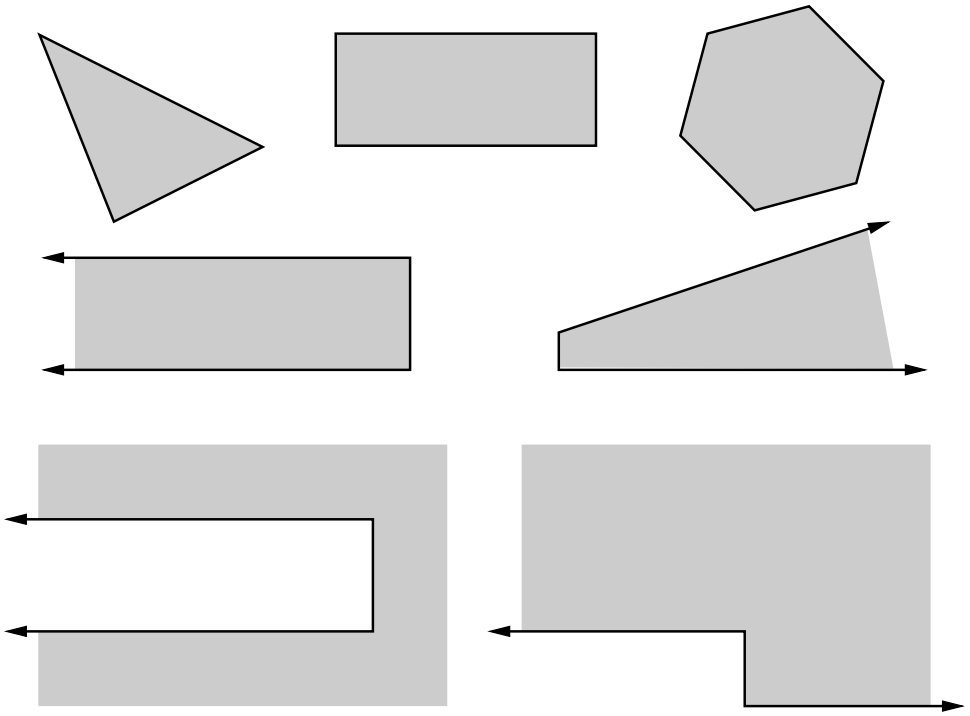

FIGURE 14. Some examples of regions for which the Schwarz-Christoffel formula gives explicit maps (i.e., we don't need to solve for the z-parameters). Triangles have only three prevertices which can be placed wherever we like. Similarly for the unbounded regions shown (assuming the angle at ∞ is is interpreted as discussed in the text). Because of the symmetries, prevertices for regular n-gons can be taken to be the roots of unity. Also because of symmetries the pervertices for a rectangle can be placed at $\pm\exp(\pm i\theta)$ where θ depends on the eccentricity e of the rectangle. This relationship is given by an explicit infinite product, which will be discussed in Section 5.

is globally 1-1 on the boundary then it defines a conformal map from the half-plane to a polygon with interior angles $\{\theta_k\}$

The last claim follows because this is a general property of holomorphic maps: if they are 1-1 on the boundary, they must be 1-1 on the interior.

The only remaining question is whether every bounded polygon can occur as the image of such a map, i.e., given the polygon, can we find parameter values so that the SC formula gives a map to the polygon? We shall see that this is the case later using the Riemann mapping theorem.

First, however, we want to check that the observations made above for the half-plane also apply to the Schwarz-Christoffel formula for the disk.

For the disk formula, there is a similar argument. The term

$$(1 - \frac{w}{z}) = \frac{z - w}{z} = -\frac{z - w}{0 - z},$$

has an argument that equals the angle between the vector $z - w$ and $0 - w$, which is the same as $(\pi - \psi)/2$ where ψ is the angle between z and w (see Figure 15. This means that as we move around the unit circle with $w = \exp(i\theta)$, the function $u(\theta) = \arg(1 - \frac{w}{z})$ has constant derivative $1/2$ except at the point z where the function jumps from $\pi/2$ to $-\pi/2$.

When raise this term to a power $(1 - w/z)^\alpha$, the argument changes with derivative $\alpha/2$ except for a jump of size $\alpha\pi$. When we take the product

$$\prod_{k=1}^{n} (1 - w/z_k)^{\alpha_k - 1},$$

the arguments sum, and so the argument of the product increases with derivative

$$\sum_{k=1}^{n} \frac{1}{2}(\alpha_k - 1) = \frac{1}{2}(-2) = -1,$$

except at the points $\{z_k\}$ where there are jumps of size $\pi(\alpha_k - 1)$ Thus the argument of

$$\prod_{k=1}^{n} (1 - w/z_k)^{\alpha_k - 1} dw,$$

is constant on the arcs between parameter values. Thus the Schwarz-Christoffel formula maps onto a polygonal region with the correct angles.

For maps onto a polygon there are three unknown SC-parameters, but a Möbius transformation of the disk can map three distinct points on the circle to any other three distinct points, so any triple will do. The only difference between the different choices is where the origin will map to. We are free to choose the harmonic measures of the three sides of the triangle any way we wish (as long as they sum to 1) and Schwarz-Christoffel formula gives the corresponding map. See Figure 16.

Quadrilaterals are the first case where we have a non-trivial parameter problem to solve. We have to find the correct 4-tuple on the unit circle and every 4-tuple is determined by its cross ratio $P \in (0, \infty)$ (up to Möbis equivalence). In the special case of rectangles, the domain is also determined by a single number, the eccentricty

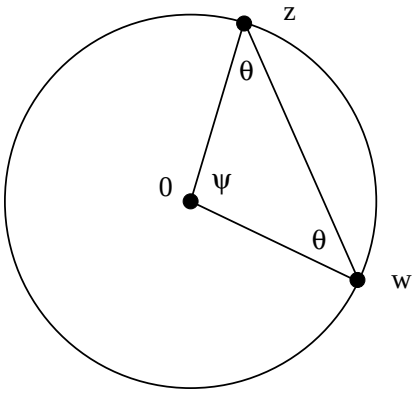

FIGURE 15. Since $0, w, z$ form an isosceles triangle, $\psi + 2\theta = \pi$, or equivalently, $\theta = (\pi - \psi)/2$.

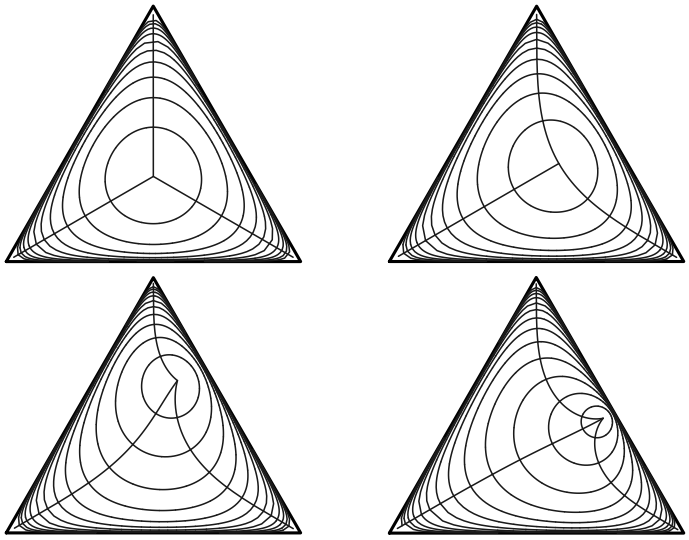

FIGURE 16. The Schwarz-Christoffel map onto a triangle has no parameters to solve for; any three distinct points give a map onto the triangle, but with the origin going to different points

R (up to Euclidean similarity). Thus there we expect a 1-1 correspondence between cross ratios of 4-tuple on $\mathbb{T}$ and eccentricities $0 < R < \infty$. Suppose Ω is a rectangle with vertices at $\{0, R, R+i, i\}$ and we have a conformal map of Ω to the upper half-plane that sends the vertices to $\{0, P, 1, \infty\}$. Alternatively, we might send the points to $\{Q, 0, 1, \infty\}$, $\{\infty, 0, M, 1\}$ or $\{0, 1, N, \infty\}$. It easy to see that

$$P(R) = M(\frac{1}{R}), Q(R) = \frac{P(R)}{P(R)-1}, N(R) = \frac{1}{P(R)},$$

so it is enough to calculate any one of these functions. For example $M(R)$ is given by

$$M = \exp(-\pi R)\frac{1}{16}\prod_{n=1}^{\infty}\left(\frac{1+\exp(-2n\pi R)}{1+\exp(-(2n-1)\pi R)}\right)^8. \tag{5}$$

We will give a proof of this later (see Chapter 5).

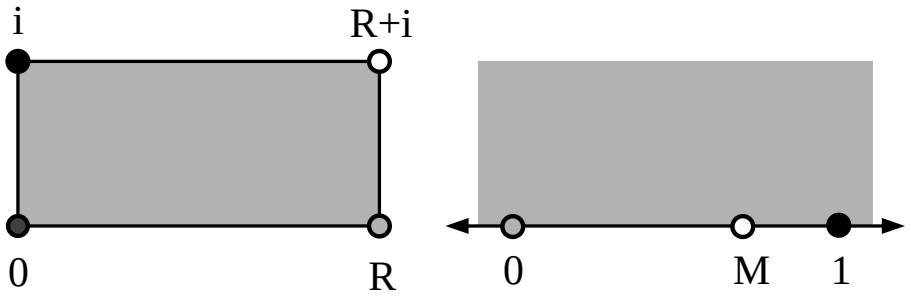

FIGURE 17. We assume f maps a rectangle to the upper half-plane with the vertices mapped as shown.

For $R > 0$ the infinite product converges and for R large (say $R \geq 1$) we have

$$\prod_{n=1}^{\infty}\left(\frac{1+\exp((1-2n)\pi R)}{1+\exp((-2n)\pi R)}\right)^8 = 1 + 8e^{-2\pi R} + O(e^{-4\pi R}).$$

Thus for $R \geq 1$, (equivalently $2 \geq 1$), we have

$$\log\left(\frac{1}{M}\right) = \pi R - \log 16 + 8e^{-\pi R} + O(e^{-2\pi R}),$$

which implies

$$M \simeq \exp(-\pi R).$$

If we take the 4-tuple to be $\{w, -\bar{w}, -w, \bar{w}\}$ where $w = e^{i\theta}$ is the first quadrant, then the cross ratio is easily computed to be

$$P = \tan^2(\theta),$$

or $\theta = \arctan(\sqrt{P})$. So if we want to compute the conformal map onto a $1 \times R$ rectangle, we compute M by (14), then compute θ as above and use the four points given. To find R given M, we can use a secant method for find a root of $M(R) = M_0$.

There is no simpler formula for the inverse of the Schwarz-Christoffel map but the inverse for a particular point can be computed either by using a Newton iteration

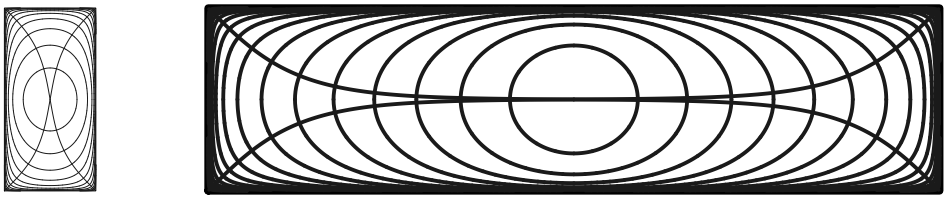

FIGURE 18. Rectangles plotted using the Schwarz-Christoffel formula and the relation between eccentricity and cross ration for $R = \frac{1}{2}$ and $R = 4$.

on the forward map, or numerical solution of the initial value problem

$$\frac{dz}{dw} = \frac{1}{f'(z)}, z(w_0) = z_0.$$

The Newton iteration is faster, but requires a good initial guess. Solving the IVP numerically is generally more reliable but slower, according to [**?**].

4. Crowding

Formula **??** also illustrates one of the main problems with numerical conformal mapping: crowding. The map of the disk onto a $1 \times R$ rectangle uses a 4-tuple on the circle with a cross ratio of $\approx \exp(-\pi R)$. If we take symmetric points $\{w, -\bar{w}, -w, \bar{w}\}$ with $w = e^{i\theta}$, for a moderate $R = 20$, this means

$$\theta \approx 5.1579 \times 10^{-28} = .00000000000000000000000000051579.$$

The separation between w and $\bar{w}$ is only about twice this size, which is smaller than machine precision on most computers. Thus, unless we take special care, a computer may think the parameters are $\{1, -1, -1, 1\}$ (which can be interpreted as the parameters for an infinite strip).

The connection between harmonic measure and Brownian motion gives us a good way to getting a "feel" for what the harmonic measure should look like. Consider the infinite strip in Figure 5 which has been divided into squares and start a a Brownian a the center of one of these squares. By symmetry it has an equal chance of first hitting any of the sides of the square and hence has a 1/2 probability of hitting the top or bottom of the strip before leaving the square. If it does it the left or right side of the square, then it has less than 1/4 chance of hitting a different dashed segment before running into the edge of the strip. Thus is has a less that 2^{-2n} chance of hitting n distinct dashed lines. Thus the harmonic decays exponentially as we travel down a

strip. A similar argument shows that in a $1 \times R$ rectangle, the harmonic measure of the short sides is at most $O(2^{-R})$ with respect to the center. Thus at least one side has harmonic measure this small, regardless of where we choose the Brownian motion to begin. This means that any conformal map of the rectangle to the disk must send two vertices to within distance 2^{-R} of each other. For polygons with long, narrow channels, this means that not all prevertices may be distinct in machine precision.

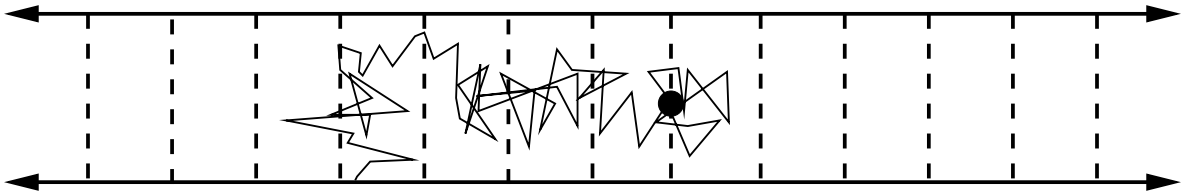

FIGURE 19. Brownian motion explains why harmonic measure decays exponentially fast in a strip. A motion starting on any of the dashed line has probability $\leq 1/4$ of hitting each of the adjacent dashed lines (with equality only if it starts at the midpoint).

In fact, the situation is a bit worse than indicated above, since the upper bound is not sharp. We can actually compute a conformal map from the disk to the strip $(0,1) \times (-\infty, \infty)$ as

$$z \to \frac{1}{\pi} \log(i \frac{z-1}{z+1}).$$

which shows that points with $|z-1| \approx \epsilon$ are mapped to points with $\Re(w) \approx \frac{1}{\pi} \log \frac{1}{\epsilon}$. Thus the short sides of a $1 \times R$ rectangle actually have harmonic measure $\approx \exp(-\pi R)$ with respect to the center. Even for $R = 10$, this is $\approx 2 \times 10^{-14}$. Thus we would have to start about a trillion random walks at the center of a 1×20 rectangle to expect to hit the short sides even once. Thus our method of estimating z-parameters using random walks is not practical in general.

The crowding phenomenon is the source of many of the difficulties in numerical conformal mapping. Roughly it says that conformal maps from a domain into a disk can undergo exponential compression, so that points that are well separated in the domain become identified in the disk (at least with finite precision). The inverse map from the disk to the domain is, in a loose sense, not even well defined numerically. The problem is that there is no choice of "center" for a polygon from which all the sides look about the same size (in the sense of harmonic measure) or even within

several orders of magnitude of the same size. we shall see later (e.g. Section 5) that one way around this is to compute conformal maps with respect to several different centers such that any small part of the domain "looks uncrowded" from some center point.

For the present we will simply avoid computing any examples where the separation of the SC-parameters is too small. Later we will present methods for dealing with such domains.

5. Power series of Schwarz-Christoffel maps

Note that using the general form of the binomial theorem,

$$(1+z)^p = \sum_{k=0}^{\infty} \frac{p(p-1)\cdots(p-k+1)}{k!} z^k,$$

we can easily compute power series for these functions in disks away from the singularities. For example, suppose we take $n = 4$, $\alpha = \{\frac{1}{2}, \frac{1}{2}, \frac{1}{2}, \frac{1}{2}\}$ and parameters $\mathbf{z} = \{1, i, -1, -i\}$. The Schwarz-Christoffel formula gives

$$\begin{aligned} f'(w) &= \prod_{k=1}^{n} (1 - \frac{w}{z_k})^{\alpha} \\ &= (1-w)^{-1/2}(1+iw)^{-1/2}(1+w)^{-1/2}(1-iw)^{-1/2} \\ &= (1-w^2)^{1/2}(1+w^2)^{-1/2} \\ &= (1-w^4)^{-1/2} \\ &= 1 + \frac{1}{2}w^4 + \frac{3}{8}w^8 + \frac{5}{16}w^{12} + \frac{35}{128}w^16 + \dots \end{aligned}$$

so

$$f(z) = z + \frac{1}{4}z^5 + \frac{1}{8}z^9 + \frac{5}{64}z^13 + \frac{7}{128}z^17 + \dots.$$

This series is plotted for various truncations in Figure **??**.

If we change the SC-parameters by a Möbius transformation, the image has the same shape, but the origin is mapped to a different point. Figure 21 illustrates this, In the first case, the Möbius transformation is symmetric with respect to the real axis so the four new parameters are as well, and hence the image domain is also symmetric. In the second example, the parameters are no longer symmetric, so we might not expect the image to be symmetric either (but since the angles are the same, it will still be a square), However, the figure is not rotated. This is becuase

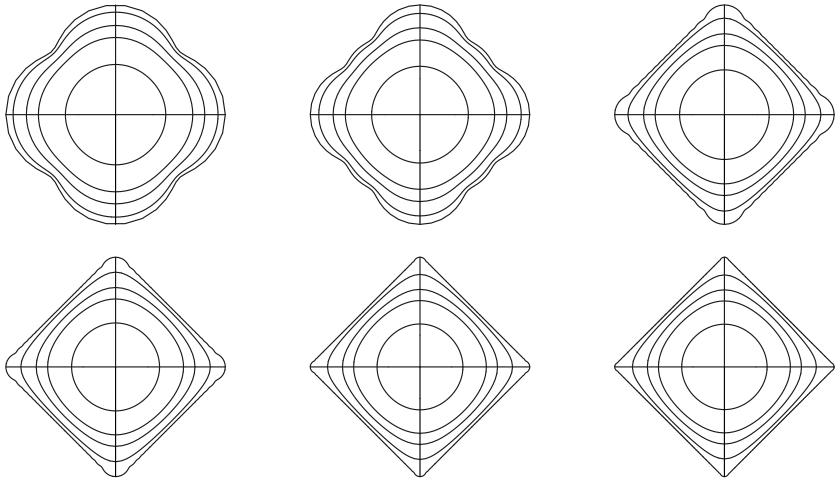

FIGURE 20. The image of the unit disk under different truncations of the power series for the conformal map onto a square. The truncations are at $n = 5, 10, 50, 100, 500, 1000$.

we choose our branches of $(1 - \frac{w}{z_k})^{\alpha_k - 1}$ to be real on the reals axis; thus the image edge containing the image of 1 will always be vertical (or have a fixed angle with the vertical if 1 is a SC-parameter).

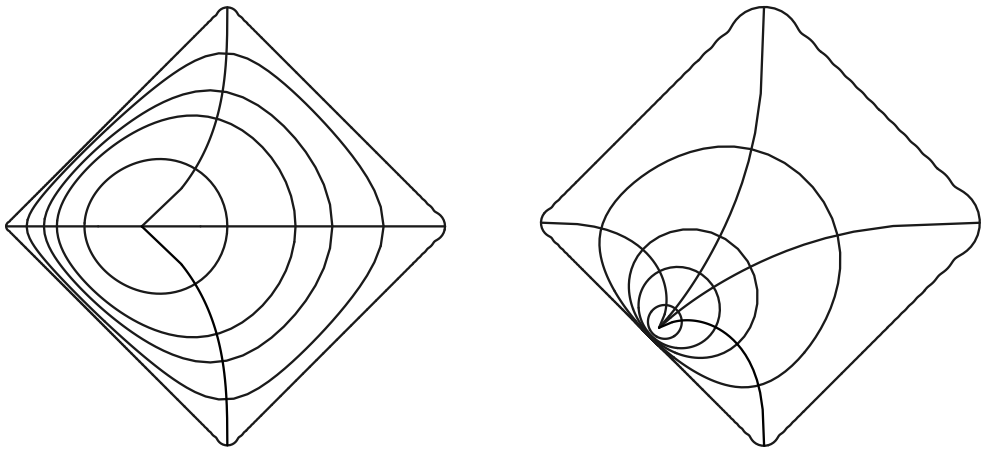

FIGURE 21. The same Schwarz-Christoffel map as in Figure 20, except that we have moved the SC-parametes by a Möbius transformation. In the first case we used $z \to (z - \alpha)/(1 - \bar{\alpha} z)$ with $\alpha = -1/2$ and in the second with $\alpha = -.9(1 + i)/\sqrt{2}$. Note, that this also effects the sharness of the corners, since some parameter values are now closer together.

The power series for more general Schwarz-Christoffel maps can be computed by finding the Taylor series for each term $(1+(\frac{-w}{z_k})^{\alpha_k-1}$ and then multiplying the series using the standard formula

$$(\sum_{n=0}^{\infty} a_n z^n)(\sum_{n=0}^{\infty} b_n z^n) = \sum_{n=0}^{\infty}(\sum_{k=0}^{n} a_k b_{n-k})z^n.$$

and then integrating term-by-term using

$$\int \sum_{n=0}^{\infty} c_n z^n = \sum_{n=0}^{\infty} \frac{c_n}{n+1} z^{n+1}.$$

For example, we we take

$$\alpha = \{\frac{1}{2}, \frac{3}{2}, \frac{1}{2}, \frac{1}{2}, \frac{1}{2}, \frac{3}{2}\frac{1}{2}, \frac{1}{2}\},$$

and eight equally spaced SC-parameters, we get

$$\begin{aligned} f(z) \;=\; & z + -0.333333iz^4 + 0.0555556z^{10} - 0.0454545iz^{12}0.0220588z^{18} \\ & -0.0197368iz^{20} + 0.0125z^{26} \\ & -0.0115741iz^{28} + 0.00828598z^{34} - 0.0078125iz^{36} \\ & +0.00600229z^{42}, 0, -0.00572311iz^{44} + \ldots. \end{aligned}$$

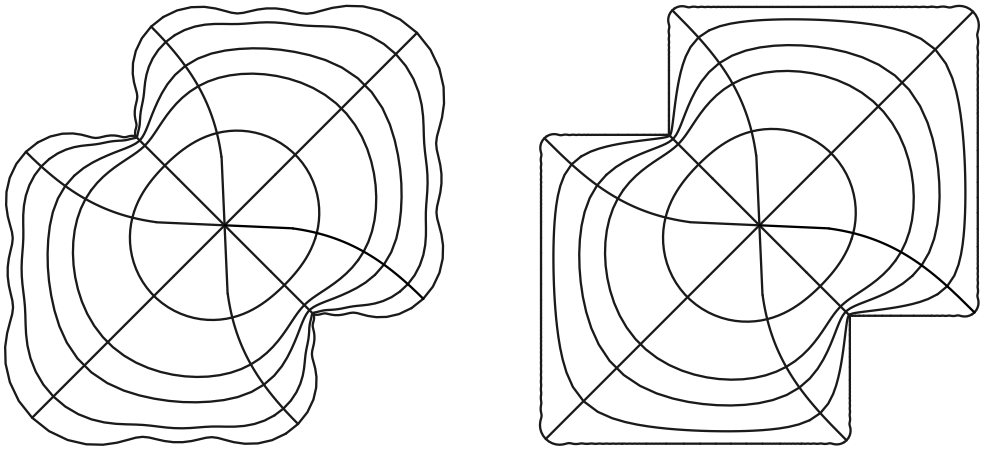

FIGURE 22. Truncations of a Schwarz-Christoffel map onto an 8-gon truncated at $n = 50$ and 500. Every edge has equal harmonic measure. Every edge has equal harmonic measure.

Even though every conformal map has a power series expansion in the disk, this expansion may not be a computationally effective way to represent the map. In the

following figures I show the image of the unit disk under truncations of the power series that represent conformal maps onto rectangles. These maps have the form

$$f(z) = \int_0^z \prod (1 - \frac{w}{e}^{-i\theta_k})^{-.5} dw,$$

where $\theta_k \in \{-\epsilon, \epsilon, \pi - \epsilon, \pi + \epsilon\}$. The form of this equation we be explained later, when we discuss the Schwarz-Christoffel formula. The parameter ϵ represents the probability that a random path started at the center of the rectangle will hit one of the two shorter sides before it hits one of the two longer sides. This determines the eccentricity of the rectangle, although the explicit relationship is a complicated infinite product and will be discussed later. The main point is that the smaller ϵ is, the longer the rectangle will be and the more terms will be needed to represent the map onto the rectangle accurately. In Figure 23, we take $\epsilon = 1$ and show truncations for $n = 5, 10, 50, 100, 500, 1000$. Even by $N = 100$ the the shape of the rectangle is clear. In Figure 24 we take $\epsilon = .001$ which corresponds to a much longer rectangle. In this case, we do not see the corners clearly even for 1000 terms of the power series. This example shows that the degree of approximation of a power series to a conformal map depends on the shape of the image domain. If there are thin corridors or "hard-to-reach" corners, then extremely high degree approximations may be needed. Later we will investigate ways to represent conformal maps that are accurate with much smaller storage.

The bad news is that this series converges rather slowly. In fact, for $\alpha \in (-1, 1) \setminus \{0\}$, the coefficients of the binomial series behave like

$$\frac{\alpha(\alpha - 1) \cdots (\alpha - k + 1)}{k!} \simeq k^{-\alpha},$$

which is not absolutely convergent. Integrating term-by-term, does give an absolutely convergent series, so we expect the power series for f to converge on the closed disk, but just barely on the boundary. In practice, these means that many, many terms may be needed to get reasonable accuracy.

If f is holomorphic on a disk $D = D(z_0, r)$, then f has a convergent power series

$$f(z) = \sum_{n=0}^{\infty} a_n (z - z_0)^n$$

on this disk. Since this series converges, the terms must tend to zero, hence they must be bounded and so

$$\limsup_n |a_n| t^n < \infty,$$

for every $t < r$. In fact, if f extends continuously to the boundary of the disk then we can apply Cauchy integral formula and do a little better

$$|a_n| = |\frac{|f^{(n)}(z_0)|}{N!} = |\frac{1}{2\pi} \int_{w:|w-z_0|=r} \frac{f(w)}{(w-z_0)^{n+1}} dw| \leq \frac{1}{2\pi r^n} \max_{\partial D} |f(z)|.$$

If f is a conformal map from the disk onto a polygon there is at least one boundary point where $|f'|$ blows up to infinity (because there is at least one vertex which has interior angle $< \pi$). Therefore the radius of convergence for the power series for both f and f' has radius exactly one and the convergence will be slow near the boundary. A single singularity on the boundary can cause the power series to converge slowly every on the boundary, even at points where the function itself has an analytic convergence across the boundary. The best known example of this is the geometric formula

$$\frac{1}{1-z} = 1 + z + z^2 + z^3 + \ldots,$$

which has only one singularity on the unit circle, is analytic elsewhere in the plane but the power series diverges everywhere on the unit circle.

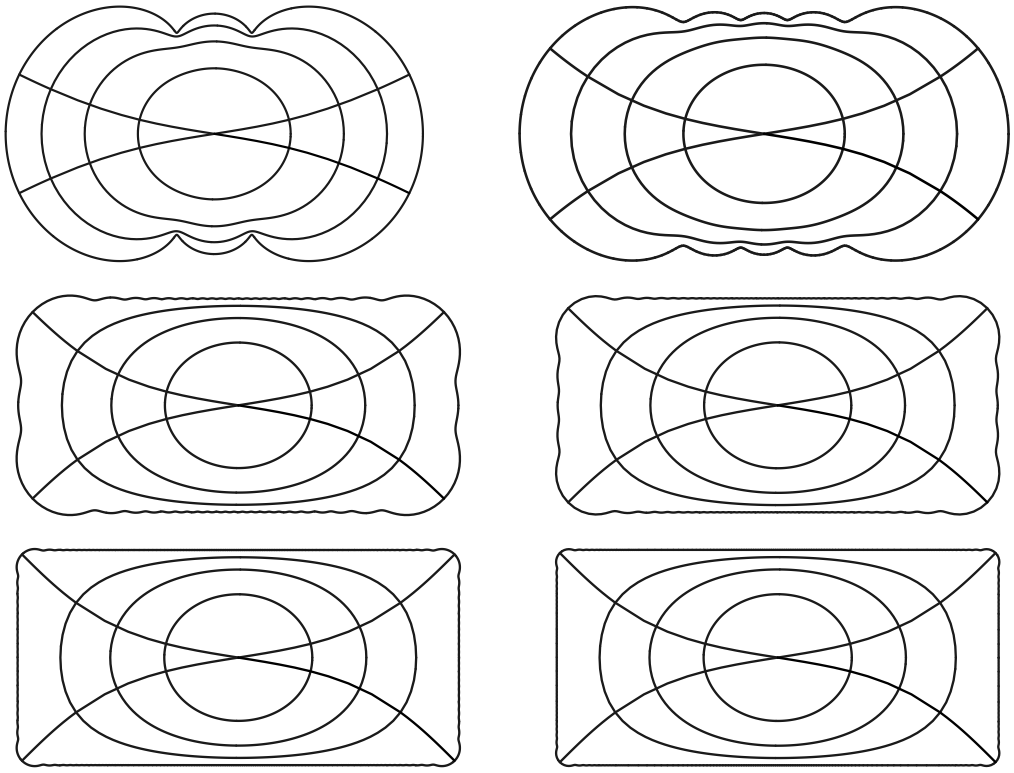

FIGURE 23. The image of the unit disk under different power series. Each one is a truncation of the infinite power series for the Schwarz-Christoffel map from the unit disk to a rectangle (chosen so the short edges have one tenth the harmonic measure of the longer sides). The truncations are at $n = 5, 10, 50, 100, 500, 1000$.

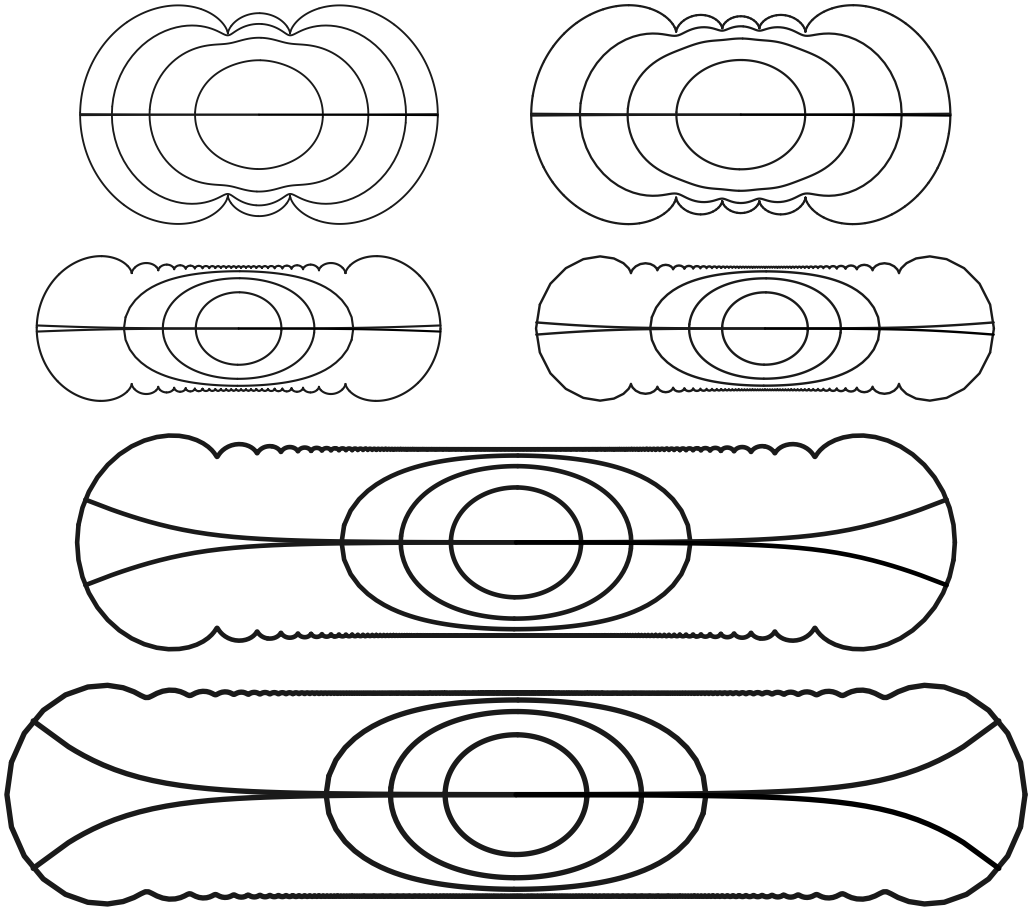

FIGURE 24. This is the same as the previous figure except that the target polygon has been changed so that the short sides have probability .001. The truncations are $n = 5, 10, 50, 100, 500, 1000$. This make the rectangle longer and requires a higher degree truncation to achieve the correct shape.

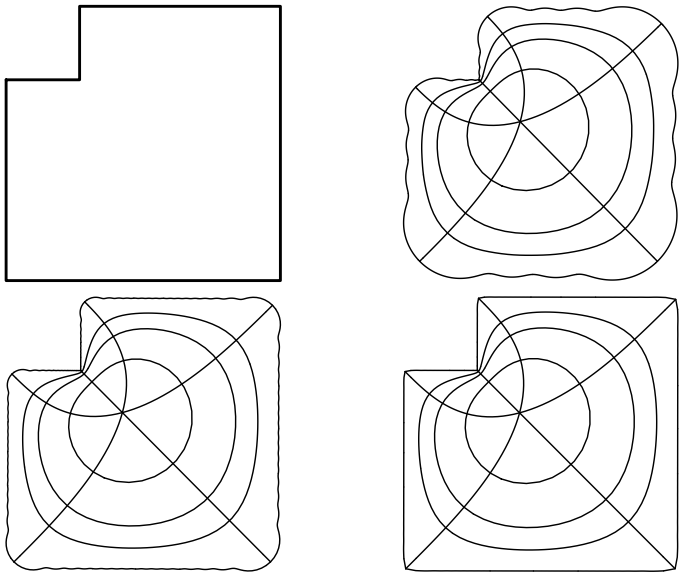

FIGURE 25. In the upper left is the target "L"-shaped polygon. The parameters for Schwarz-Christoffel are taken to be equidistributed in this example. The next three figures show the images of the disk under the power series for the map with truncations at order $20, 100, 1000$.

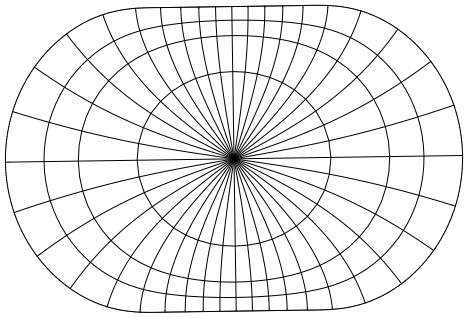

FIGURE 26. If the boundary is smooth then the power series is a better approximation. Here is a C^1 domain sampled at 40 boundary points to give a polygon. We then plotted the result using 20 terms of the power series. The domain is a square with half-disks attached to opposite sides.

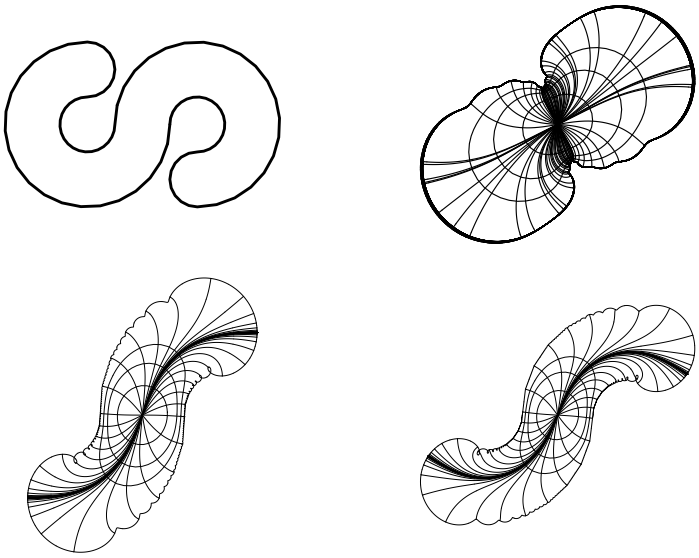

FIGURE 27. Even if the domain has a reasonable smooth boundary, crowding can still be a problem for power series. Here is an "S" shaped region and power series approximations with 100, 200 and 2500 terms.

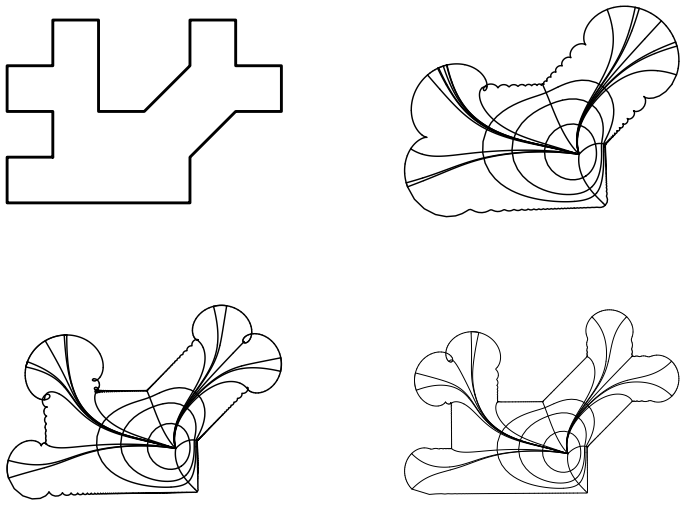

FIGURE 28. Again in the upper left is the target polygon. The next three figures show the images of the disk under the power series (centered at 0) for the Schwarz-Christoffel map with truncations of orders $100, 500, 2500$. In this example, the choice of SC-parameters is not obvious; the plots were made using parameters values found by Davis's method, which we will describe later.

6. Harmonic measure and Brownian motion

Suppose Ω is a simply connected domain. Choose a base point $z_0 \in \Omega$ and a conformal map $f : \mathbb{D}\Omega$. Assume for the moment that $\partial\Omega$ is a Jordan curve and that f has a 1-1, continuous extension to the boundary (see Caratheodory's theorem 5). Define the harmonic measure of $E \subset \partial\Omega$ with respect to the point z_0 as

$$\omega(z_0, E, \Omega) = \frac{1}{2\pi}|f^{-1}(E)|.$$

This does not depend on the particular choice of f since any two maps sending 0 to z_0 differ by a rotation of the disk.

If Ω is bounded by a polygon, then the harmonic measure of each side is determined by the spacing of the Schwarz-Christoffel parameters. Thus finding a set of parameters is equivalent to computing the harmonic measure of the sides of the polygon.

Brownian motion is the rigorous version of the idea of a "continuous random walk" in the plane. One can think of this as a limit of a random walk on an ϵ-grid as $\epsilon \to 0$. The important thing is that Brownian motion is conformally invariant; i.e., the image of Brownian motion under a conformal map is Brownian motion on the image domain. The harmonic measure $\omega(z, E, \Omega)$ is the probability that a Brownian motion started from z will first hit $\partial\Omega$ in the set E. On the disk, this is just normalized length measure on the boundary.

Brownian motion is a continuous version of a random walk. That is, it is a stochastic process $B(t)$, $t > 0$ such that

(1) Increments are independent: if $t_0 < t_1 < \ldots t_n$, then the random variables $B(t_0)$, $B(t_1) - B(t_0), \ldots B(t_n) - B(t_{n-1})$ are independent.
(2) Increments are normally distributed: if $s, t \geq 0$ then

$$\text{Prob}(B(s+t) - B(s) \in A) = \int_A (2\pi t)^{d/2} e^{-|x|^2/2t} dx.$$

(3) With probability one $B(t)$ is a continuous function of t.

We can also think of d-dimensional Brownian motion as a probability measure on the set of continuous paths in $\mathbb{R}^d$, i.e., functions from $[0, \infty)$ into $\mathbb{R}^d$. This is called Weiner measure and we shall denote it by Prob. For example, using this notation

property (3) would be written

$$\text{Prob}(B(t) \text{ is continuous }) = 1.$$

An event which happens with probability one with respect to Weiner measure will be said to happen almost surely.

Brownian motion was first described mathematically by Einstein in 1905, but was first proven to exist by Weiner in 1923. Brownian motion can be considered as the continuous limit of a random walk on a square grid, as shown in Figure 29. In fact, this grid structure is not really needed; one can take Brownian motion to be the limit of many different discrete walks (which must have mean value zero at each step). For example, in Figure 30, we show it as a limit of a walk in a triangular grid (at each time we may step unit distance in any of six directions) and in Figure 31 we show a walk in which at each time we step unit distance in any direction (chosen uniformly and at random). The fact that Brownian motion is the limit of this last process as the step size decreases to zero, gives a heuristic reason for its conformal invariance: since conformal maps send infinitesimal circles to infinitesimal circles the "random direction" process should be mapped to another such process, except with variable size circles depending on the size of the derivative of the conformal map.

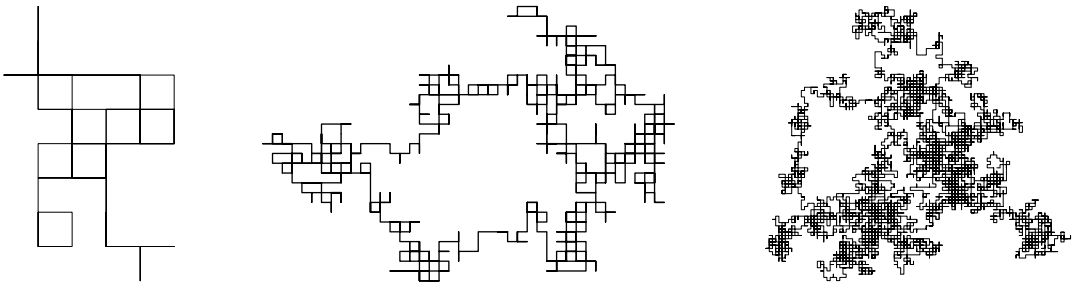

FIGURE 29. Random walks on a square grid with 100, 1000 and 10,000 steps.

Brownian motion itself is a rather technical process to deal with but there is a simpler process on Ω that has the same hitting distribution on the boundary and was introduced by Kakutani. Moreover, simulating a Brownian motion by a random walk on a very fine grid can take a long time, and Kakutani's process will speed this up. Starting at a point of $z\Omega$ choose a radius r so that $B(z,r) \subset \Omega$, e.g., take $r\lambda \text{dist}(z, \partial\Omega)$ for some fixed $0 < \lambda \leq 1$. If we start a Brownian motion at z and wait

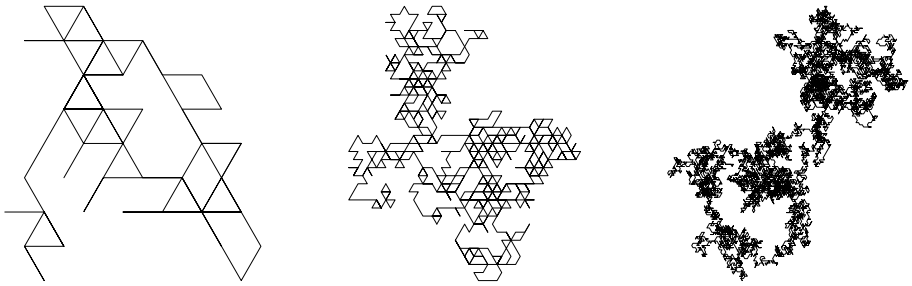

FIGURE 30. Random walks on a triangular grid with 100, 1000 and 10,000 steps.

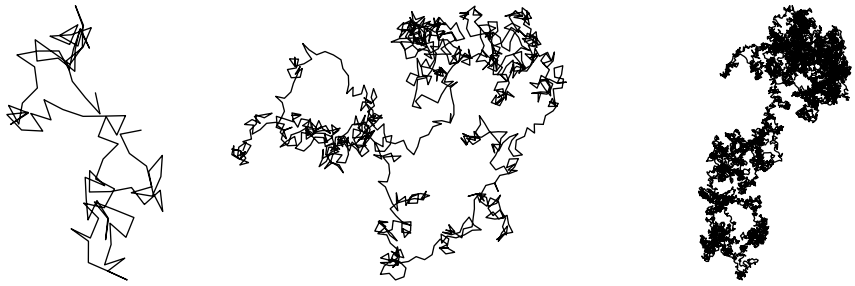

FIGURE 31. Random paths formed by stepping unit distance in a randomly chosen direction. The pictures show paths with 100, 1000 and 10,000 steps. Note that regardless of the discrete random walk, at large scales the results all look the same.

for the first contact with ∂B, this is the same as simply choosing a point at random on ∂B. Repeat this procedure to construct a sequence of points. This is the same as choosing a sequence along a single Brownian path with the selections becoming more frequent as the path approaches the boundary of the domain. With probability 1 the Brownian path hits the boundary of the domain and the sequence of points constructed must converge to the same boundary point. Thus the hitting probability of Kakutani's process is the same as for Brownian motion. See Figure **??**. Moreover, this process is faster to simulate. If we are simulating Brownian motion by a walk on an ϵ-grid, and the starting point is about unit distance from the boundary, then it takes about ϵ^{-2} steps to hit the boundary (or reach a grid point that is within ϵ on the boundary). On the other hand the Kakutani process will be within ϵ of the boundary in about $\log \frac{1}{\epsilon}$ steps. The main cost is to recompute the distance to the boundary each time (which is at worst an $O(n)$ computation in an n-gon and may

be faster if we are clever, e.g., precompute a Voronoi diagram and keep track of what cell we are in).

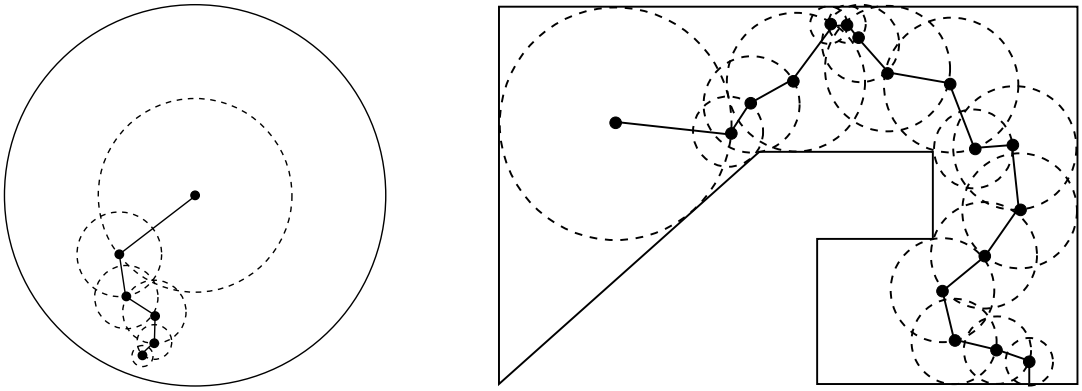

FIGURE 32. Examples of the paths in the Kakutani process with $\lambda = 1/2$ in the disk and $\lambda = 1$ in a polygon.

Therefore one way to approximate the z-parameters for a polygon is to choose a basepoint for the interior and simulate many Brownian paths starting from this point and keep a count of how many hit each edge. This count (divided by the total number of paths) gives the approximate harmonic measure of each edge and hence the approximate separation between the corresponding prevertices. The trouble with this method is that it is slow, very slow. In the best case, the number of sides of the polygon is small and all sides have comparable harmonic measure, i.e., they are all about equally likely to be hit. The bad news is that the hitting frequencies of random paths will converge to the actual harmonic measures with error that tends to zero like $n^{-1/2}$, e.g., about a million random walks are required to get three decimals of accuracy. The really bad news is that usually the sides do not all have large harmonic measure and if some sides have very small measure then we have to wait even longer for them to get hit frequently enough to estimate their measure. For example, consider the "L"-shaped polygon in Figure **??**. The vertices are $\{0, 2, 2 + 31, 1 + 3i, 1 + i, i\}$ and the starting point is $1.5 + i$. The left picture shows 10 sample paths of the Kakutani process, the center shows 100 paths and the right shows 1000 paths. Even after a 1000 sample paths, only one has managed to reach the top horizontal edge, and this polygon is by no means extreme.

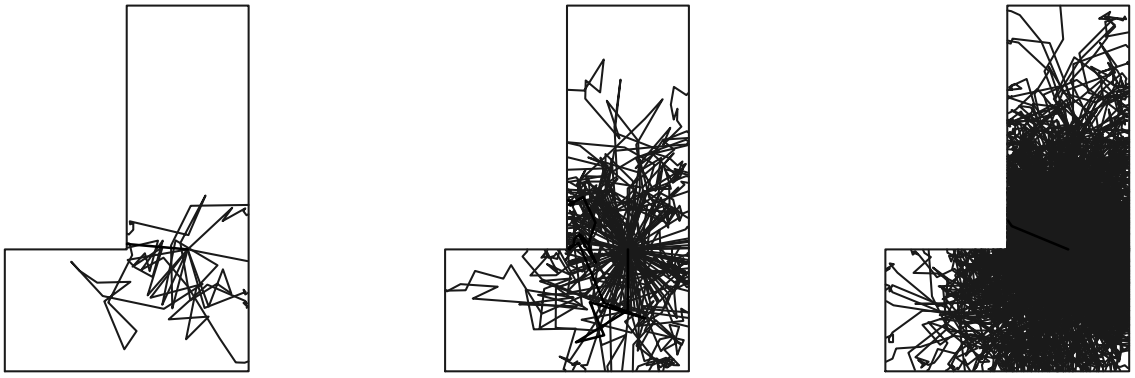

FIGURE 33. These show the polygon with 10, 100, and 1000 random walks. Note how hard it is for the remote edges to get hit. After 1000 attempts the top edge still has not been hit. If the smallest harmonic measure of any edge is ϵ the we expect to need $1/\epsilon$ to get even one hit on that edge.

Table 1 shows the number of hits per side for two experiments; one with 1,000 random paths and one with 10,000 random paths. In Figure 34, we show the images of the Schwarz-Christoffel maps when we use the parameters given by these experiments. The left picture is the target polygon, the center is uses the parameters from the 1,000 path experiment and the right uses 10,000 paths. The latter looks noticeable better, and we shall see later that it is indeed about 10 times better, according to a certain precise measure of the closeness of polygons. In Section 5 we shall discuss an improvement of this method, but using random walks to estimate harmonic measure should not be considered a really practical approach. We have introduced it because it is pretty, easy to understand and is guaranteed to produce the correct answer (eventually). Moreover, the intuition provided by thinking of harmonic measure (and hence the z-parameters) as the hitting probability of Brownian motion is invaluable and frequently leads us to quickly to the right answer (even if we later replace this intuition by a calculation or proof based on techniques such as extremal length, hyperbolic geometry or potential theory). We shall see one such case in the next section.

1	131	0.823097	0
2	516	3.24212	0.823097
3	1	0.00628319	4.06522
4	271	1.70274	4.0715
5	76	0.477522	5.77425
6	5	0.0314159	6.25177

1	1143	0.718168	0
2	4952	3.11143	0.718168
3	27	0.0169646	3.8296
4	2833	1.78003	3.84657
5	961	0.603814	5.62659
6	84	0.0527788	6.23041

TABLE 1. The left table was generated using 1,000 random walks and the right by 10,000 random walks. in each table the columns give, respectively, the side number, the number of hits on that side, the corresponding spacing between parameters and a choice of the parameters themselves. The vertices are $\{0, 2, 2+31, 1+3i, 1+i, i\}$ and the center point is $z = 1.5 + i$. In our numbering scheme the first edge is the horizontal edge on the bottom.

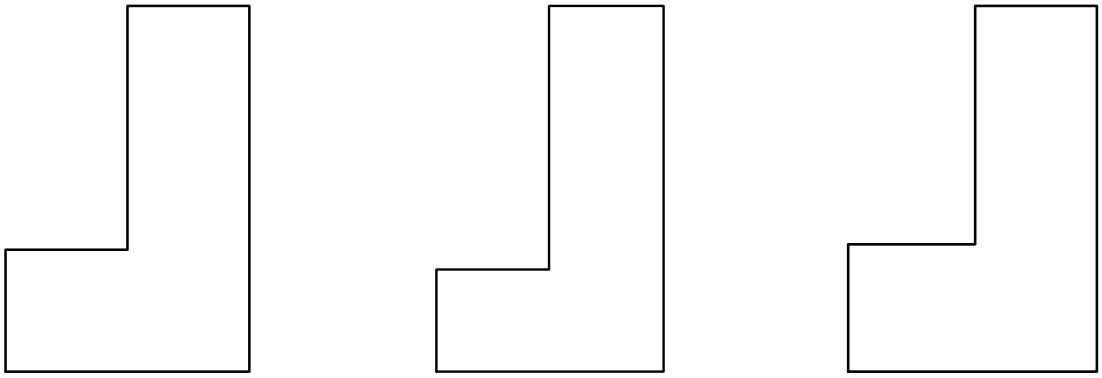

FIGURE 34. On the left is the target polygon, in the center the SC image derived from 1,000 random walks and on the right is the SC image using parameters derived from 10,000 random walks inside the polygon. The values of the parameters are given in Table 1.

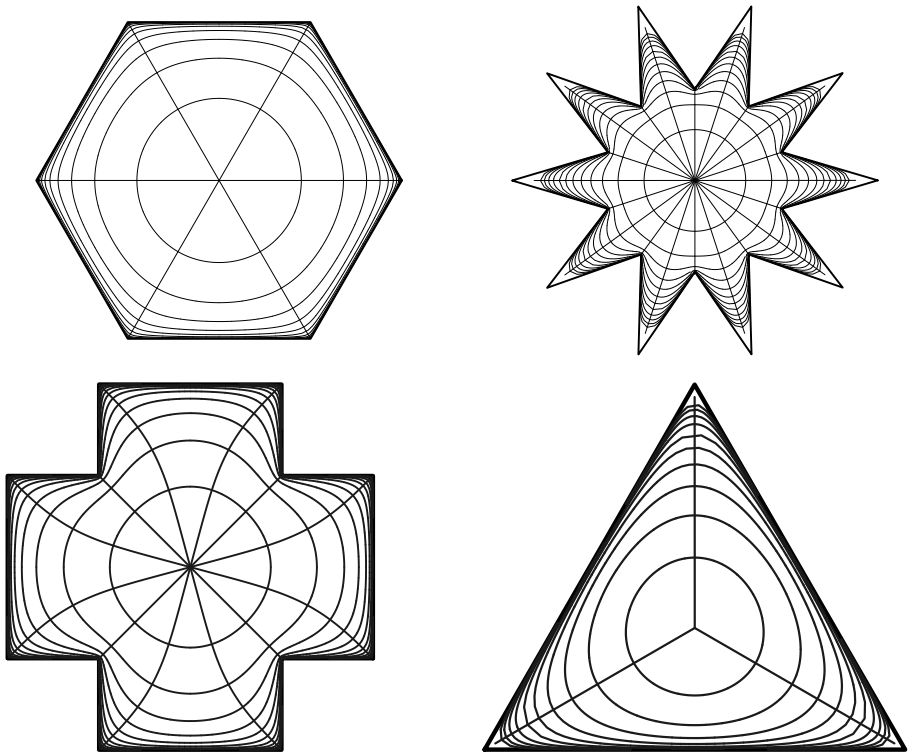

FIGURE 35. Polygons for which every edge has the same harmonic measure.

If a domain has a symmetry, then the conformal map should have a corresponding symmetry. For example, if the domain Ω is symmetric with respect to the real line, and we choose the conformal map $f : \mathbb{D} \to \Omega$ with $f(0)$ real and $f'(0) > 0$, then f will also be symmetric with respect to the real line, i.e., $f(\bar{z}) = \overline{f(z)}$. When a polygon has symmetries, then certain edges must have harmonic measures which agree (at least with respect to properly chosen base points) and this reduces the number of independent parameters we must solve for in the Schwarz-Christoffel formula.

For example, the domains in figure 5 have rotational and reflection symmetries that map any edge to any other edge, so every edge must have the same harmonic measure. Thus the parameters must be evenly distributed around the circle.

Even if the domain is not so symmetric that every edge has the same harmonic measure with respect to some point, there may still be able to group the edges into subcollections, so that each edge in a subcollection has the same harmonic measure. For example, the domain in Figure **??** is the second generation in the construction

of the von Koch snowflake and has 48 sides. However, the symmetries of the domain divide the edges into 4 classes of twelve sides each and the harmonic measure is the same for any two edges of the same class. Thus the problem of determining the z parameters is reduced from a 48-dimensional problem to 4 dimensions. To obtain Figure **??** we ran a random walk from the origin and recorded the class of the edge it stopped on. From this we estimated the harmonic measure of each class and gave each edge from a given class the same harmonic measure. Compare these results with Figure 36, where we used many more random walks to try to estimate the harmonic measure of each individual side.

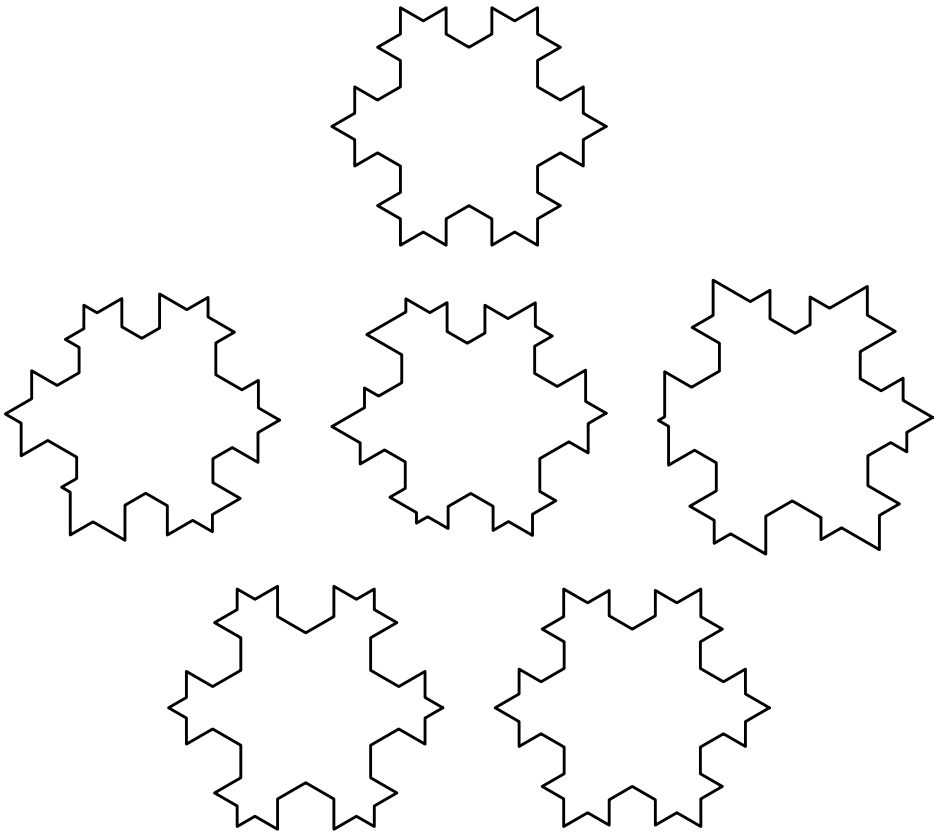

FIGURE 36. The top shows the target polygon: a second generation von Koch snowflake. The middle row shows three attempts to find the SC parameters using 1000 random walks where each of the 48 edges was considered separately. The bottom row uses the 12 fold symmetry of the polygon. The 48 edges are grouped into 4 collections; the number of hits in each collection is counted and divided by 12 to give the harmonic measure of each side. The left shows the result after 100 random walks and the right after 1000 random walks.

7. The quasiconformal distance between polygons

When computing approximations for the z-parameters it would be nice to have a way of measuring how close our approximations are to correct parameters, assuming we can do this without actually knowing the correct parameters. Moreover, we should remember that there is more than one choice of "correct" answer, so that simply want

A standard way to measure the distance between sets is with the Hausdorff distance, which is defined as

$$d(E, F) = \inf\{\epsilon : E \subset F^\epsilon \text{ and } F \subset E^\epsilon\},$$

where $E^\epsilon = \{x : \text{dist}(x, E) < \epsilon\}$ is an ϵ neighborhood of E. However, for our purposes, we will often want to consider two regions that correspond under Euclidean similarities to be the same, so using the Hausdorff distance would be difficult to compute, even for polygons.

For polygons, the most obvious thing to do is compute the vector of sidelengths normalized by total length

$$\{\frac{|v_{k+1} - v_k|}{\sum_k |v_{k+1} - v_k|}\}$$

and compute the distance to the corresponding vector for the target polygon with respect to some norm on $\mathbb{R}^n$ (e.g., ℓ^1, ℓ^2, ℓ^∞).

The difficulty with this method is that when there are sides with many different length scales, the longer sides contribute much more to the distance than the short sides, e.g., see Figure **??**. Moreover, it is not clear that comparing the sides of the polygon in this way has a simple interpretation in terms of the geometry of the z-parameters.

We would like to have a distance based on comparing shapes of polygons, so that small distance means that the shapes are similar at all scales. Moreover, the distance should have a reasonable interpretation in terms of the z-parameters. The distance we will consider is based on the class of quasiconformal maps. Conformal maps have derivative maps that are Euclidean similarities. In particular the derivative maps send circle to circles. A K-quasiconformal map has a derivative which sends circles to ellipses of eccentricity at most K.

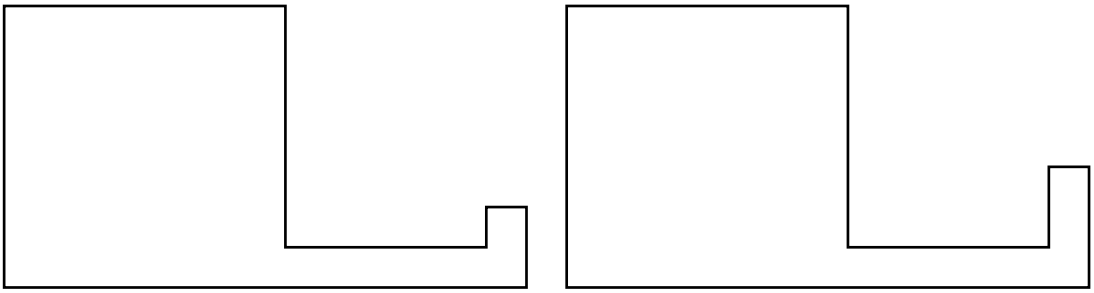

FIGURE 37. These two polygons only differ on a few short edges, so any distance based on normalized edge lengths with say these are close together. However, we want to define a distance that will place these about unit distance apart, recognizing that the "hooks" are significantly different shapes if we rescale them to unit size.

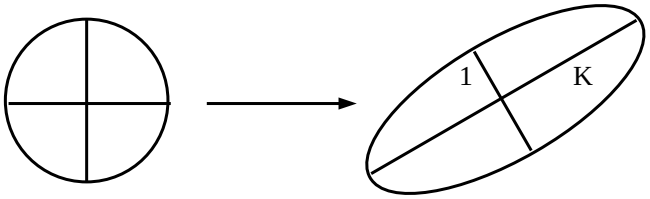

FIGURE 38. The derivative of a K-quasiconformal map sends circles to ellipses of eccentricy $\leq K$.

Suppose $f = (u, v)$ the derivative is given by

$$Df = \begin{pmatrix} u_x & u_y \\ v_x & v_y \end{pmatrix}.$$

The unit circle is mapped to an ellipse by this affine map and the eccentricity of the ellipse (the ratio of the length of major axis to the length of the minor axis) is $\sqrt{\lambda_1/\lambda_2}$ where λ_1, λ_2 are the eigenvalues of Df. The eigenvalues of this matrix are the roots of the equation

$$\det(DF - \lambda I) = \begin{pmatrix} u_x - \lambda & u_y \\ v_x & v_y - \lambda \end{pmatrix} = (u_x - \lambda)(v_y - \lambda) - u_y v_x = (u_x - \lambda)(v_y - \lambda) - u_y v_x.$$

We can use the quadratic formula to find the two roots $\lambda_1 \geq \lambda_2$ and then compute the eccentricy of the ellipse.

However, it is much more convenient to do this calculation in complex notation. Write

$$f_z = \frac{1}{2}(f_x - i f_y) = \frac{1}{2}(u_x + v_y) + \frac{i}{2}(v_x - u_y),$$

$$f_{\bar{z}} = \frac{1}{2}(f_x + if_y) = \frac{1}{2}(u_x - v_y) + \frac{i}{2}(v_x + u_y).$$

Then

$$df = f_z dz + f_{\bar{z}} d\bar{z},$$

i.e., the tangent map to f is given by

$$z \to f_z z + f_{\bar{z}} \bar{z}.$$

If $|z| = 1$ then the largest its image can be is $|f_z| + |f_{\bar{z}}|$ and this occurs when the two components have the same argument (so the absolute values add), i.e., when

$$\arg(f_z z) = \arg(f_{\bar{z}} \bar{z}),$$

$$\arg(f_z) + \arg(z) = \arg(f_{\bar{z}}) - \arg z),$$

$$\arg z = \frac{1}{2}(\arg(f_{\bar{z}}) - \arg(f_z)).$$

Similarly, the minimal length the image of z can have is $|f_z| - |f_{\bar{z}}|$ when $f_z z$ points in the opposite direction from $f_{\bar{z}} \bar{z}$, and this occurs when

$$\arg(f_z z) = \pi + \arg(f_{\bar{z}} \bar{z}),$$

$$\arg z = \frac{\pi}{2} + \frac{1}{2}(\arg(f_{\bar{z}}) - \arg(f_z)).$$

Thus the image of the unit circle has major axis length

$$|f_z| + |f_{\bar{z}}|,$$

and the minor axis of length

$$|f_z| - |f_{\bar{z}}|,$$

and

$$(|f_z| + |f_{\bar{z}}|)(|f_z| - |f_{\bar{z}}|) = |f_z|^2 - |f_{\bar{z}}|^2 = u_x v_y - u_y v_x,$$

is the Jacobian of f. It is often convenient to write

$$\mu = \frac{K-1}{K+1} = f_{\bar{z}}/f_z,$$

and call this the dilatation of the map. Note that $|\mu| < 1$ if K is finite.

LEMMA 15. *Suppose T_1, T_2 are triangles with vertices $\{z_1, z_2, z_3\}$ and $\{w_1, w_2, w_3\}$ respectively (in the same orientation). Then the affine map $f : T_1 \to T_2$ defined by mapping $z_k \to w_k$ for $k = 1, 2, 3$ has complex dilatation*

$$\mu = \frac{a-b}{b-\bar{a}},$$

where $a = (z_3 - z_1)/(z_2 - z_1)$ *and* $b = (w_3 - w - 1)/(w_2 - w_1)$.

PROOF. We can map T_1 to the triangle T_1' with vertices $\{0, 1, a\}$ by the conformal map $z \to (z - z_1)/(z_2 - z_1)$ and map T_2 to the triangle T_2' with vertices $\{0, 1, b\}$ by $z \to (z - w_1)/(w_2 - w_1)$. Since these are conformal, they have complex dilatation 0. We can map T_1' to T_2' by the map of the form

$$z \to \alpha z + \beta \bar{z},$$

where we need $\alpha + \beta = 1$ and $\alpha a + \beta \bar{a} = b$. Solving gives $\beta = (a - b)/(a - \bar{a})$ and $\alpha = 1 - \beta = (b - \bar{a})/(a - \bar{a})$. Thus $\mu = \beta/\alpha = (a - b)/(b - \bar{a})$. □

Consider the map that stretches in the horizontal direction $f : (x, y) \to (ax, y)$ with $a > 0$. Then in complex notation this is

$$f(z) = \frac{a}{2}(z + \bar{z}) + \frac{1}{2}(z - \bar{z}) = \frac{a+1}{2}z + \frac{a-1}{2}\bar{z},$$

which has derivatives $f_z = \frac{1}{2}(a + i)$ and $f_{\bar{z}} = \frac{1}{2}(a - i)$. Thus

$$K = (|a + 1| + |a - 1|)/(|a + 1| - |a - 1|),$$

which equals a if $a \geq 1$ and equals $1/a$ if $0 < a < 1$. Thus K measures the amount of stretching.

If f is a C^1 map we define $K_f(z)$ and $\mu_f(z)$ applying the definitions above to the tangent map of f. A C^1 mapping on Ω is called a K-quasiconformal mapping if

$$\sup_{z \in \Omega} |K_f(z)| \leq K.$$

If $K = 1$, then the mapping is conformal. The function $\mu = \mu_f$ is called the Beltrami coefficient of f and satisfies the following composition laws:

$$\mu_{f^{-1}} \circ f = -(f_z/\overline{f_z})^2 \mu_f,$$

$$\mu_{g \circ f}(z) = (f_z(z)/\bar{f}_z(z)) \frac{\mu_g(f(z)) - \mu_f(z)}{1 - \mu_g(f(z))\overline{\mu_f(z)}}.$$

We measure the distance between n-tuples, $\mathbf{z}, \mathbf{w} \in \mathbb{D}$, using the metric

$$d_{QC}(\mathbf{w}, \mathbf{z}) = \inf\{\log K : \exists\ K\text{-quasiconformal } h : \mathbb{D} \to \mathbb{D} \text{ such that } h(\mathbf{z}) = \mathbf{w}.\}$$

This metric is invariant under Möbius self-maps of the disk, which is natural, since we only expect to know the prevertices up to a Möbius transformation. Although the metric might seem a little awkward, we can often estimate this distance explicitly. In

particular, when n-tuples are sets of z-parameters associated to two polygons we can estimate the distance between the n-tuples by finding maps between the polygons.

LEMMA 16. *If there is a K-quasiconformal map $\varphi : P_1 \to P_2$ sending vertices to vertices, then there is a K-quasiconformal map of the disk sending the SC-parameters for P_1 to the SC-parameters for P_2.*

PROOF. Take $f_2^{-1} \circ \varphi \circ f_1$ where f_k is the conformal map $\mathbb{D} \to P_k$ for $k = 1, 2$. □

Note that the composition of a quasiconformal and conformal map is again quasiconformal and with the same constant. In particular, if $f_1 : \mathbb{D} \to \Omega_1$ and $f_2 : \mathbb{D} \to \Omega_2$ are conformal maps, and $g : \Omega_1 \to \Omega_2$ is quasiconformal, then $G = f_2^{-1} \circ g \circ f_1 : \mathbb{D} \to \mathbb{D}$ is quasiconformal with the same constant as g. Consider the case then Ω_1, Ω_2 are bounded by polygons. Then any map between them which sends vertices to vertices corresponds to a map of the disk whose boundary extension sends one set of prevertices to the other. One simple case when there is an "obvious" vertex preserving map between the polygons is when the two polygons have equivalent triangulations. This means that there are cyclic labellings of the vertices of each polygon's vertices and triangulations of the polygons so that exactly the same set of triples of vertices are used. See Figure 5. In general, two n-gons need not have any equivalent triangulations, but we are mostly interested in the case when both polygons have the same set of interior angles and are close in some sense, so that we hope this does occur. (If one allows triangulations with Steiner points, i.e., points in the interior of the polygon, and not just the original vertices then any two n-gons have equivalent triangulations with at most $O(n)$ extra vertices. Moreover, one can add $O(n^2)$ Steiner points and obtain a triangulation that is equivalent to a certain triangulation depending on n but not on the particular polygon. See []).

Given two polygons with compatible triangulations we can explicitly compute the quasiconformal constant of the piecewise affine map which maps one triangulation to the other and this gives an upper bound for the best quasiconformal map sending Ω_1 to Ω_2 and preserving the vertices, and hence for the quasiconformal distance between the two sets of prevertices.

If P_1, P_2 are two polygons that have equivalent triangulations, then we can compute the quasiconstant for mapping each triangle for P_1 to the corresponding triangle

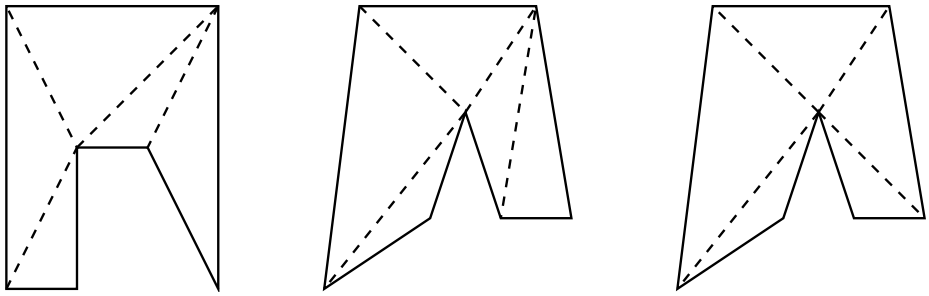

FIGURE 39. The left and center polygons have compatible triangulations but the one on the right is not compatible to either of these.

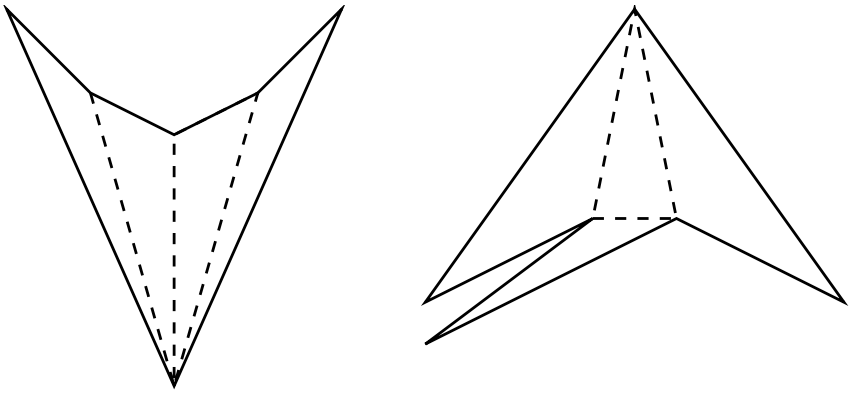

FIGURE 40. Each of these 8-gons has a single possible triangulation and they are not compatible. Thus general polygons need not have compatible triangulations if we do not allow Steiner points.

for P_2. These individual affine maps form a global quasiconformal map from the interior of P_1 to the interior of P_2 whose quasiconstant is the maximum constant over all the triangle maps. See Figure 41.

One example of estimating the QC distance for two polygons is illustrated in Figure 41. A more interesting example is to consider the three polygons shown in Figure 5. This shows a target polygon on the left and two Schwarz-Christoffel images using 1000 and 10000 random walks to estimate the z-parameters. The polygon on the right looks "better", i.e., closer to the target, and by considering affine maps between compatible triangulations we can make this more precise.

The idea of compatible triangulations is interesting in the context of conformal mappings in the following way. As noted above, two n-gons need not have compatible triangulations unless we allow Steiner points to be added. If we allow Steiner points,

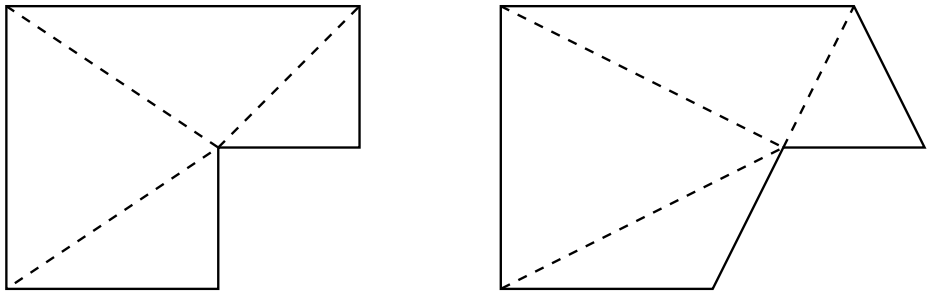

FIGURE 41. Two polygons with equivalent triangulations. The vertices for the first are $\{0, 3, 3+2i, 5+2i, 5+4i, 4i\}$, $\{0, 3, 4+2i, 6+2i, 5+4i, 4i\}$, and labeled counterclockwise starting at 0. The triangles (in terms of the vertex labels) are $\{1, 2, 3\}, \{1, 3, 6\}, \{3, 5, 6\}, \{3, 4, 5\}$. The distortion K for the four triangles is $1.64039, 1.33333, 1.64039, 1.64039$. The maximum of these is an upper bound for the QC-distance between the prevertices of the two polygons.

then any two n-gons have a compatible triangulations. Can we take corresponding triangles to be similarities, or close to similarities? For triangles which touch original vertices of the polygons, this is clearly impossible, but the Riemann mapping theorem implies that all triangles except those in an ϵ neighborhood of the original vertices can be taken to almost similar, i.e., corresponding triangles can be mapped to each other $1 + \epsilon$ quasiconformal affine maps. Conversely, shrinking ϵ to zero and taking the limit of such piecewise affine maps gives a conformal map in the limit and proves the Riemann mapping theorem.

A couple of examples will serve to show that the metrics based on side length vectors and on quasiconformal mappings can be very different. In Figure 42 we have shown domains that are far apart in the side length sense but are quasiconformally close. Each is a square with a long narrow corridor attached, the second one being exactly half the size in both dimensions. Because each side of the corridor is half as long in the second domain, the normalized side length vectors differ by about $1/12$ in two coordinates, and hence the distance will be large. However, these two domains are close in a quasiconforml sense. In each domain consider the half-annuli bounded by the dashed lines. We clam these can be mapped to each other by a quasiconformal map with small constant (at least if the inner and outer radii have large ratio). This is because the map

$$f_\alpha : z \to z|z|^{\alpha-1},$$

is quasiconformal on the plane with constant $K = \max(\alpha, \frac{1}{\alpha})$. This can be verified by a computation of its partial derivatives, but it is simpler to restrict to the upper half-plane, map the half-plane to an infinite horizontal strip by the (conformal) map $z \to \log z$ and note that our map is conjugated to $(x, y) \to (\alpha x, y)$ which is clearly K-quasiconformal. If we scale our first half-annuli so the outer radii is 1 and the inner is $r \ll 1$ then its image under f_α is a half-annuli with outer radius 1 and inner radius $R = r^\alpha = r/2$, if $\alpha = 1 - \frac{2}{\log r}$. We then extend out map to be conformal and linear on the remaining pieces of the domain, and obtain a K-quasiconformal map between the domain with K as close to 1 as we choose, depending only on the width of the corridor.

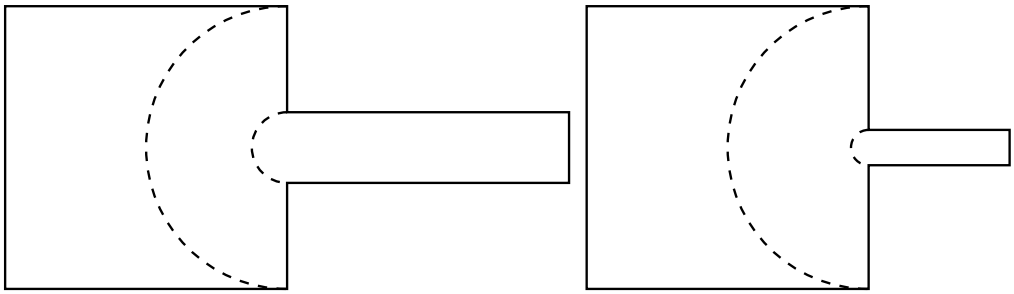

FIGURE 42. These two domain are close in the QC metric but far in the vector of side lengths metrics. The are far in the latter metric since the thin channels have significantly different lengths. They are close in the QC metric since the half-annulus regions between the dashed curves can be mapped to each other with small QC norm if the ratio between the inner and outer radius is large enough. Outside these regions we use linear conformal maps.

In Figure 43 we show two domains which are close in the vector sense but not in the QC sense. These domains are squares with two vertical slits removed, one attached to the top edge and the other to the bottom edge and each with length about 3/4's of the side length of the box and about ϵ apart. In the first domain the slit attached the top is to the left of the other slit and in the second it is to the right. In terms of side lengths, this only requires changes of about size ϵ in the segments along the top and bottom of the square, so these domain are close in this sense. However, any homeomorphism of the interiors must have large distortion. For example, we draw a dashed vertical line in the left picture; its image under such

a homeomorphism must look something like the dashed curve on the right, which requires a large QC constant.

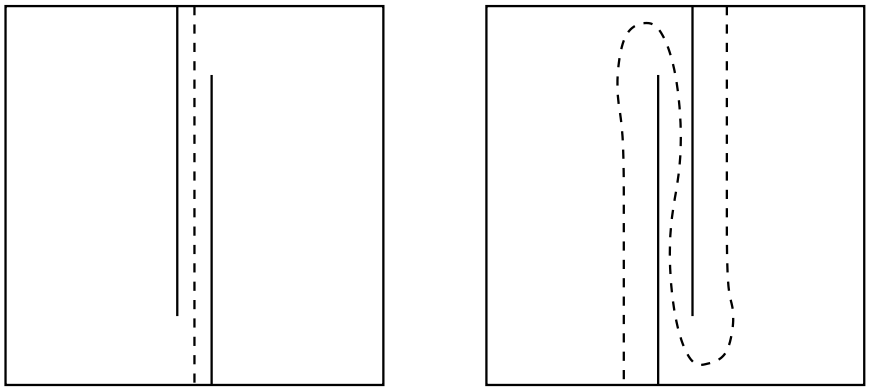

FIGURE 43. These are two domains which are close in the vector of side lengths sense, but not in the QC sense. Any homeomorphism of the interior which respects vertices must map the dashed vertical line on the left to something like the dashed curve on the right, which requires large distortion.

How can we bound the QC distance from below more explicitly? This can be done using conformal modulus, which will be discussed in a later chapter.

8. Schwarz-Christoffel iterations and Davis's method

Suppose Ω has polygonal boundary and $f : \mathbb{D} \to \Omega$ is conformal. The Schwarz-Christoffel formula (we abbreviate to "SC-formula" below) says

$$f(z) = A + C \int^z \prod_{k=1}^{n} (1 - \frac{w}{z_k})^{\alpha_k - 1} dw,$$

where $\alpha\pi = \{\alpha_1\pi, \ldots, \alpha_n\pi\}$, are the interior angles at the vertices $\mathbf{v} = \{v_1, \ldots, v_n\}$, and $\mathbf{z} = \{z_1, \ldots, z_n\} = f^{-1}(\mathbf{v})$ are the conformal preimages of the vertices (also know as the SC-parameters). For a fixed α, we can think of the formula as defining a map S from n-tuples in $\mathbb{T}$ to polygons (possibly self-overlapping). In fact, Möbius equivalent n-tuples give Euclidean similar polygons, so it is convenient to think of S as a map from $\mathbb{T}^n_*$ (n-tuples of distinct points on $\mathbb{T}$ modulo Möbius transformations) to P^n_* (complex n-tuples modulo similarities). We can identify $\mathbb{T}^n_* = \mathbb{R}^{n-3}$ as follows: fix a combinatorial triangulation of the n points, and for each pair of adjacent triangles let ρ_k be the cross ratio of the four vertices. This is a positive real number since

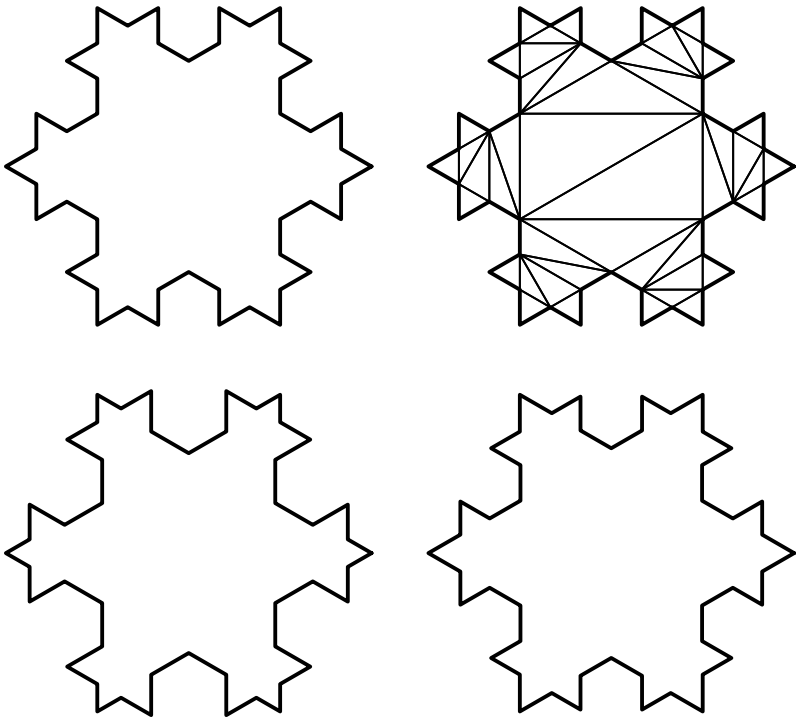

FIGURE 44. These polygons were drawn in Figure **??**. The top show the target polygon and a triangluation. The bottom shows two attemps to calculate the SC-parameters using random walks and symmetry. The QC distance in the first case is 1.63525 (100 walks) and in the second is 1.11956 (1000 walks), justifying the idea that the second picture looks "better" than the first.

the points lie on $\mathbb{T}$ (and if we take the correct ordering), so $\log \rho_k \in \mathbb{R}$. The original n-tuple (unique up to Möbius transformations) can easily be recovered from the $n-3$ values of $\log \rho_k$, so $\mathbb{T}^n_* = \mathbb{R}^{n-3}$.

Suppose we have a explicit way of guessing the SC-parameters for a given polygon, i.e., a map $G : P^n_* \to \mathbb{T}^n_* = \mathbb{R}^{n-g}$. Then $F = G \circ S$ gives a map $\mathbb{R}^{n-3} \to \mathbb{R}^{n-1}$. The desired SC-parameters for P, $\mathbf{z}_*$, are a solution of $F(\mathbf{z}) = \mathbf{z}_0 = G(P)$ and hence are a fixed point of the iteration

$$\mathbf{z}_{k+1} = \mathbf{z}_k - A^{-1}(F(\mathbf{z}_k) - \mathbf{z}_0). \tag{6}$$

We call this an SC-iteration. If A is the derivative DF of F, this iteration is Newton's method for $n-3$ real variables. If we don't know DF explicitly, can take a discrete

approximation using $n-3$ evaluations of F; we call this the "full iteration". If DF is close to the identity, then taking A to be the identity may also work and is much faster; this we call the "simple iteration". A compromise between these two extremes is to start A as the identity and to use Broyden updates at each step; this is called the "short-cut iteration" (A Broyden update multiplies A by a rank one matrix at each step, chosen to optimize the approximation to DF given the evaluations of F made so far. This method converges more slowly per iteration than the full iteration, but each iteration is faster to perform and it often beats full and simple iterations in practice).

One of the simplest such methods is due to Davis, which has the additional advantage of taking advantage of the geometry of the domain in a straightforward way. Suppose we are given points $\{z_1, \ldots, z_n\}$ on the unit circle. Compute an image polygon using the Schwarz-Christoffel formula with these parameters (and the known angles) and compare the side lengths of this polygon with the desired polygon. If a side is too short, the corresponding parameter values are moved apart in the next iteration and conversely. More precisely, if $\{z_1^k, \ldots, z_n^k\}$ is the current guess, and the image polygon has vertices $\{v_1^k, \ldots, v_n^k\}$ we define the next set of parameter guesses as

$$|z_k^{j+1} - z_{j-1}^{k+1}| = K|z_j^k - z_{j-1}^k| \frac{|v_j - v_{j-1}|}{|v_j^k - v_{j-1}^k|},$$

for $j = 0, \ldots, n$ where

$$K = 2\pi [\sum_j |z_j^k - z_{j-1}^k| \frac{|v_j - v_{j-1}|}{|v_j^k - v_{j-1}^k|}]^{-1},$$

is a normalizing constant (to make sure the new spacings add up to 2π) and $\mathbf{v} = \{v_0, \ldots, v_n\}$ are the vertices of the target polygon. An example of Davis' method is shown in Figure 45. Further details of the first ten steps of the iteration are given in Tables **??** and **??**.

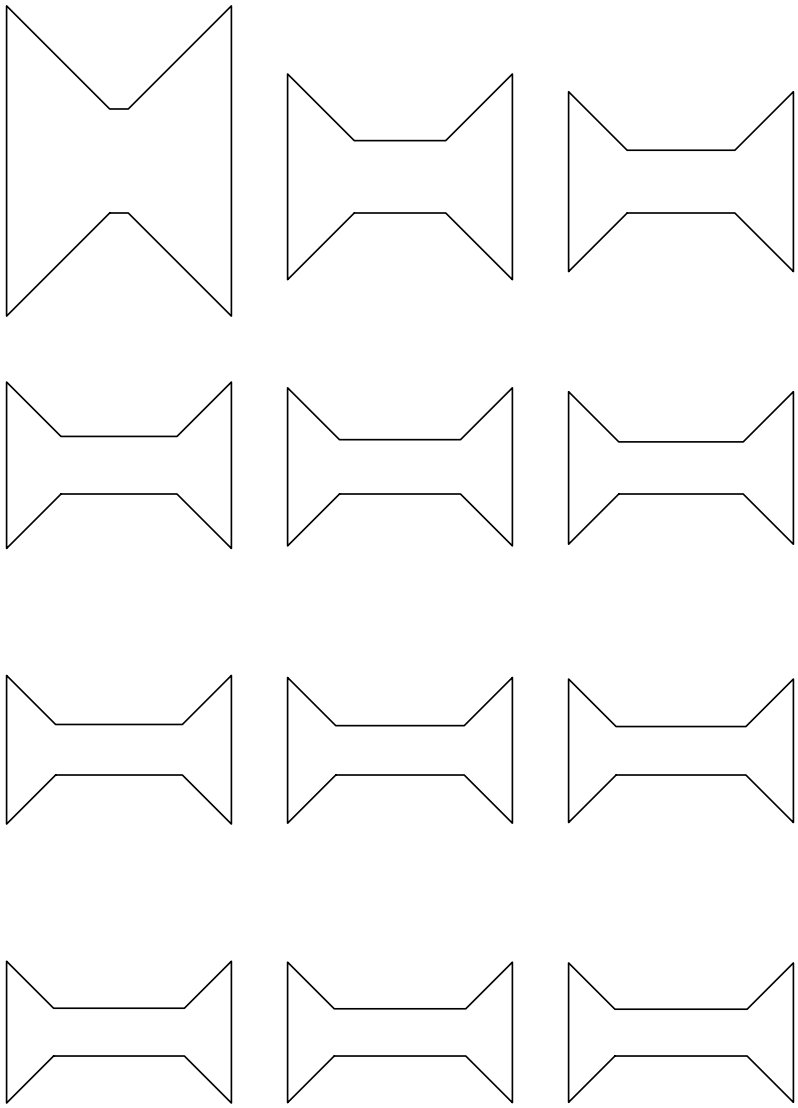

FIGURE 45. The first 12 iterations of Davis' method (including the first step where we assume equidistributed parameters). The upperbounds for the QC errors (for these iterations) obtained by triangulation are 16.7817, 2.37323, 1.74869, 1.4896, 1.34707, 1.25739, 1.19638, 1.15273, 1.1204, 1.09585, 1.07687, 1.06199

The method works in practice in many cases but is known to sometimes diverge even locally [**?**]. Davis' method assumes that increasing side length corresponds to increasing harmonic measure. However, in some examples, this is not case. See Figure 46. The edge on the far right makes angle $< \pi/2$ with both the adjacent edges. In this case, lengthening this side gives a polygon that strictly contains the first one, and the new right edge clearly has less harmonic measure. Thus we expect Davis' method to diverge in this case. However, when we do the experiment with this polygon and start iterating we get a kind of degeneration where all the z-parameters begin to cluster around one point of the unit circle. This corresponds to the origin being mapped to a point of the polygon which is tending towards the boundary. The behavior of the parameters under iteration is shown in Table 2.

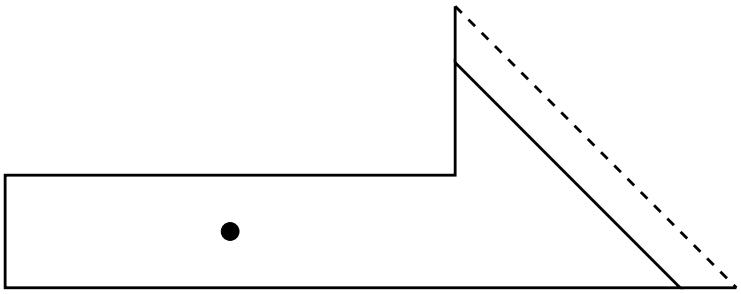

FIGURE 46. Lengthening the edge on the far right of the polygon decreases the harmonic measure of that edge from the given base point, and hence decreases the length of its conformal preimage on the circle (assuming the base point is mapped to the origin). Thus Davis' method will diverge from the correct answer given a starting point arbitrarily close to it. The example is taken from [**?**]. However, renormalizing seems to eliminate the divergence.

Davis' method is used in [**?**] by Banjai and Trefethen to give a $O(n)$ method for finding the prevertices that is practical for tens of thousands of vertices (the bound, however is an average case analysis, not a uniform estimate for all polygons).

The degeneration can be prevented by renormalizing the parameters each time we iterate. Choose two adjacent sides (say the first and second) and use a Möbius transformation of the disk to itself to map the corresponding three parameters to $1, i, -1$. Thus we are choosing a "center" for the polygon (i.e., the image of zero under the conformal map) from which these two sides each has harmonic measure

1.01811	0.412703	0.41663	4.06205	0.373695
0.721234	0.154016	0.181627	5.11414	0.112163
0.513933	0.0634117	0.0800658	5.58571	0.0400608
0.379569	0.0288556	0.0367562	5.82124	0.0167623
0.292544	0.0145189	0.0181267	5.95	0.00799366
0.234438	0.00801887	0.00971116	6.02679	0.00423033
0.193772	0.00479989	0.00563333	6.07655	0.00242752
0.163696	0.00306846	0.00350138	6.11144	0.00148175
0.140138	0.00206525	0.00230183	6.13773	0.000947121
0.120658	0.00144461	0.00157994	6.15888	0.000625846
0.103785	0.00103819	0.00111873	6.17682	0.000422947
0.0886404	0.000758795	0.000808338	6.19269	0.000289599
0.0747276	0.000558768	0.000590043	6.20711	0.000199199
0.0618022	0.000410843	0.00043094	6.2204	0.000136497
0.0497937	0.000298814	0.000311833	6.23269	0.0000923607
0.0387541	0.000212751	0.000221155	6.24394	0.0000610976
0.0288182	0.000146421	0.000151751	6.25403	0.0000390293
0.020169	0.0000958193	0.0000990789	6.2628	0.0000236892
0.0129987	0.0000582694	0.0000601445	6.27005	0.0000133538
0.00746055	0.0000318117	0.00003279	6.27565	0.000006755110

TABLE 2. The evolution of the SC parameters for Davis' method for the polygon in Figure 46. The iteration is started at equidistributed points, but seems to converge to a situation where all the parameters are clustered around a single point. This corresponds to the origin being mapped to a point in the image polygon which is closer and closer to the boundary. We can use Möbius transformations to renormalize the parameters by sending three of them to any three points we want. This is discussed below.

1/4. Such a point must remain in a compact region of the polygon (at least as long as the polygon itself stays in a compact set). This is because each of these two sides has harmonic measure 1/4 from this point and the complement has measure 1/2. There is a unique point of the domain at which this occurs and so the normalization prevents the kind of degeneration described above. I do not know if adding this normalization causes Davis' method to aways converge to the correct answer eventually.

The vertices of the polygon are

$$0, 2, 6, 4 + 2I, 4 + I, I$$

Note that we have placed a vertex of angle π on the bottom edge. We do this and normalize the edges $[0,2],[2,6]$ to have harmonic measure $1/3$ so that the center of the polygon is near the center of the long channel. This helps prevent the harmonic measure of any of the sides from getting two small. Fifty iterations of the normalized iteration gives harmonic measure (before renormalizing) of

$$0.333411, 0.335319, 0.000186381, 0.000180184, 0.328768, 0.00213578$$

relative sidelengths of

$$0.134715, 0.267896, 0.190897, 0.0674928, 0.271171, 0.0678286$$

whereas the true relative sidelengths are

$$0.134876, 0.269752, 0.190744, 0.067438, 0.269752, 0.067438$$

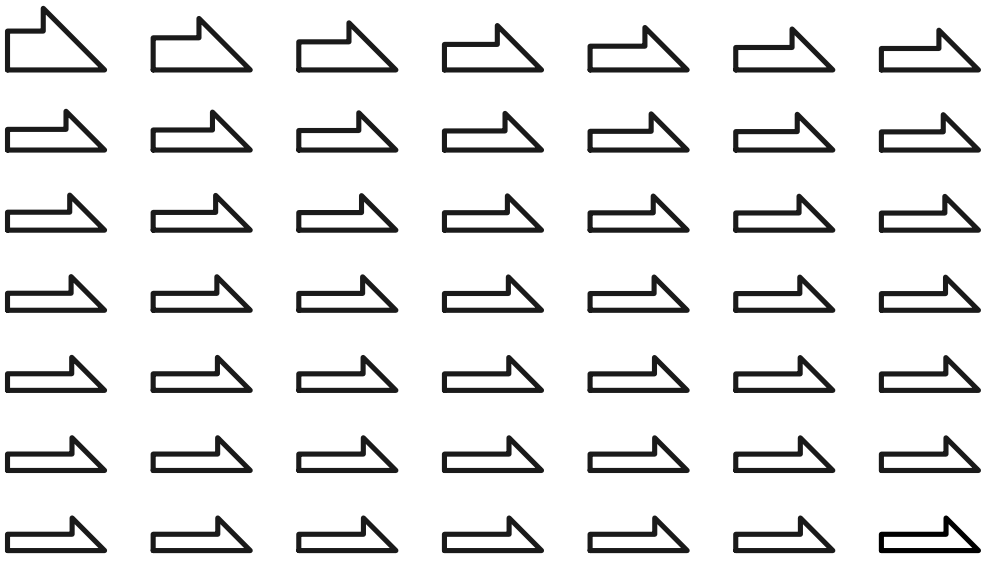

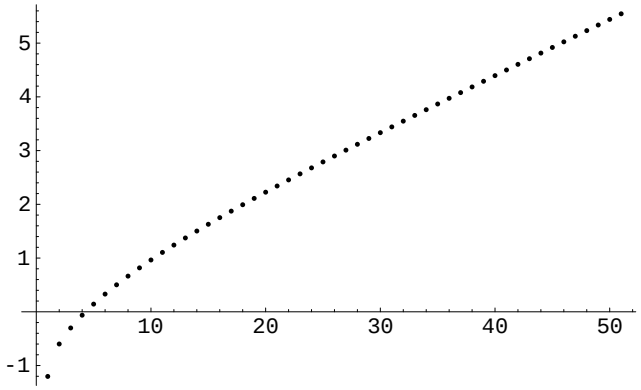

FIGURE 47. 49 iterations of Davis's method for the polygon in Figure 46 (with renormalizations) starting from equally spaced parameters. On the bottom is the graph of $-\log(K-1)$, which shows increasing accuracy.

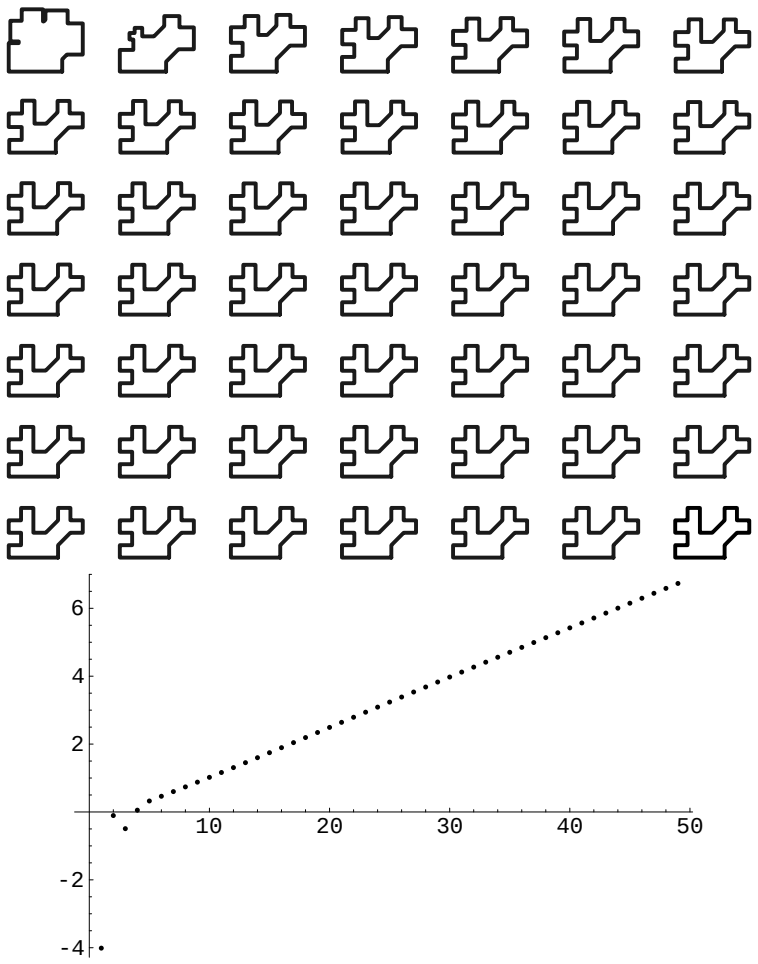

FIGURE 48. 49 iterations of Davis's method (with renormalizations) starting from equally spaced parameters. On the bottom is the graph of $-\log(K-1)$, which shows increasing accuracy.

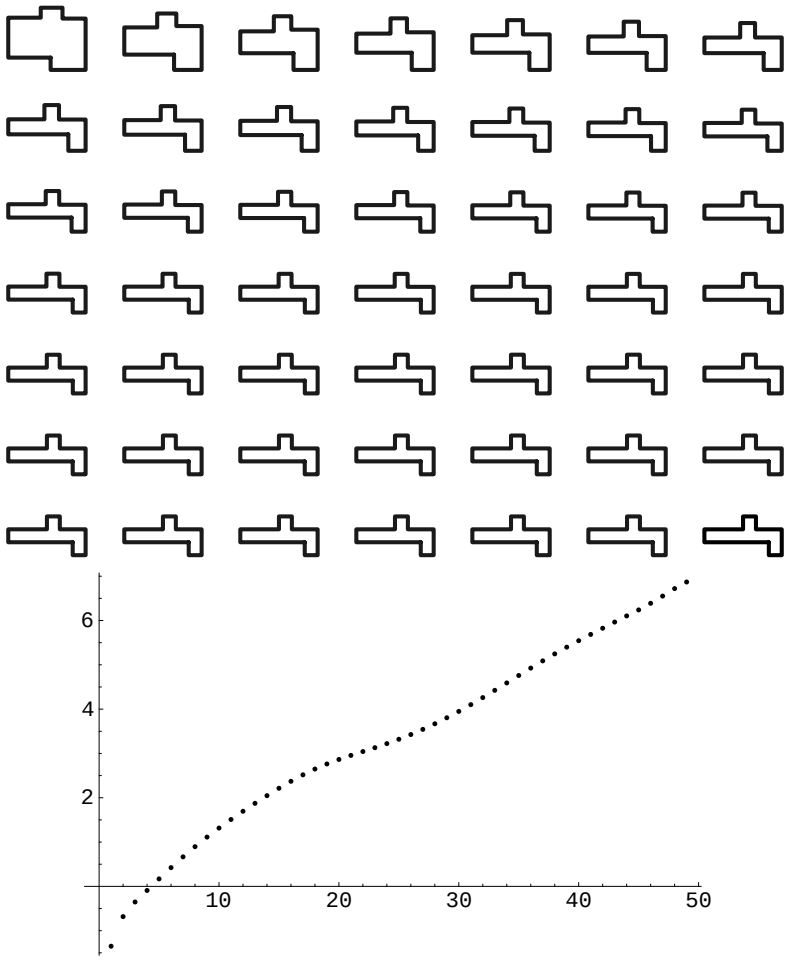

FIGURE 49. 49 iterations of Davis's method for another polygon.

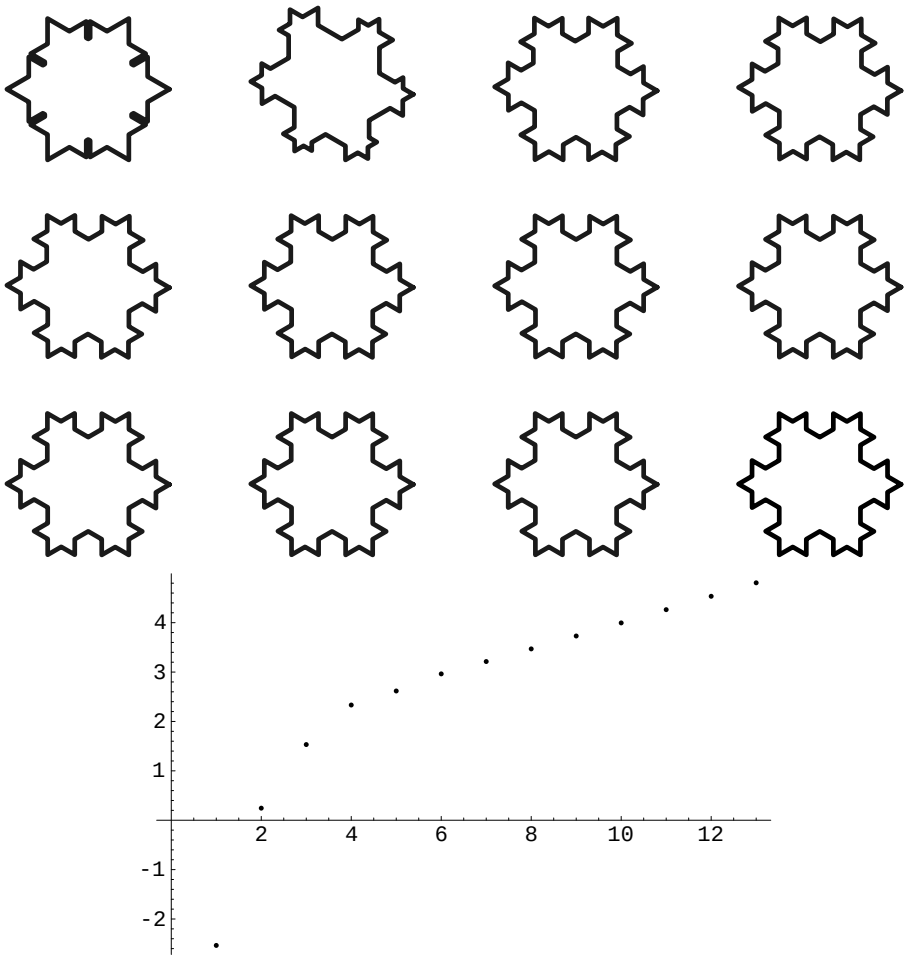

FIGURE 50. 12 iterations of Davis's method for the second generations von Koch snowflake.

CHAPTER 2

The Riemann mapping theorem

In this chapter we review basic results from one complex variable and potential theory and use them to give a proof of the Riemann mapping theorem (already quoted in the first chapter).

1. The hyperbolic metric

The hyperbolic metric on $\mathbb{D}$ is given by $d\rho_{\mathbb{D}} = 2|dz|/(1-|z|^2)$. Geodesics for this metric are circles orthogonal to the boundary. The orientation preserving isometries are exactly the Möbius transformations which preserve the disk, which all have the form $z \to e^{i\theta}(z-a)/(1-\bar{a}z)$, for some $\theta \in \mathbb{R}$ and $a \in \mathbb{D}$. The hyperbolic metric ρ_Ω on a simply connected domain Ω (or Riemann surface) is defined by transferring the metric on the disk to Ω by the Riemann map. We will sometimes write ρ for any hyperbolic metric when the domain is clear from context.

On the disk it is convenient to define the pseudo-hyperbolic metric

$$\rho(z,w) = |\frac{z-w}{1-\bar{w}z}|.$$

The hyperbolic metric between two points can then be expressed as

$$\psi(w,z) = \log \frac{1+\rho(w,z)}{1-\rho(w,z)}.$$

On the upper half-plane the corresponding function is

$$\rho(z,w) = |\frac{z-w}{w-\bar{z}}|,$$

and ψ is given as before. A hyperbolic ball in the disk is also a Euclidean ball, but the hyperbolic and Euclidean centers are different (unless they are both the origin).

The orientation preserving isometries of the hyperbolic disk are exactly the Möbius transformations that map the disk to itself. All of these have the form

$$e^{i\theta}\frac{z-a}{1-\bar{a}z},$$

where θ is real and $a \in \mathbb{D}$.

Simply connected, proper subdomains of the plane inherit a hyperbolic metric from the unit disk via the Riemann map. If $\varphi : \mathbb{D} \to \Omega$ is conformal and $w = \varphi(z)$ then $\rho_\Omega(w_1, w_2) = \rho_{\mathbb{D}}(z_1, z_2)$ defines the hyperbolic metric on Ω and is independent of the particular choice of φ. It is often convenient to estimate ρ_Ω in terms of the more geometric "quasi-hyperbolic" metric on Ω which is defined as

$$\tilde{\rho}(w_1, w_2) = \inf \int_{w_1}^{w_2} \frac{|dw|}{\operatorname{dist}(w, \partial\Omega)},$$

where the infimum is over all arcs in Ω joining w_1 to w_2.

Recall the sine and cosine rules for hyperbolic geometry (e.g., see page 148 of Beardon's book [**?**]). Let T denote a hyperbolic triangle with angles α, β, γ and opposite side lengths denoted by a, b, c. See Figure 1. Then we have the Sine Rule,

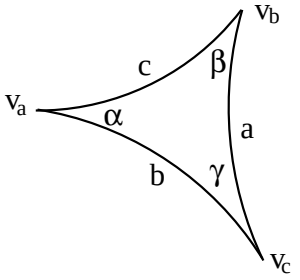

FIGURE 1. Definitions of a, b, c and α, β, γ

$$\frac{\sinh a}{\sin \alpha} = \frac{\sinh b}{\sin \beta} = \frac{\sinh c}{\sin \gamma} \tag{7}$$

the First Cosine Rule,

$$\cosh c = \cosh a \cosh b - \sinh a \sinh b \cos \gamma \tag{8}$$

and the Second Cosine Rule

$$\cosh c = \frac{\cos \alpha \cos \beta + \cos \gamma}{\sin \alpha \sin \beta} \tag{9}$$

LEMMA 17. *Möbius transformations of $\mathbb{D}$ to itself are isometries of the hyperbolic metric.*

PROOF. When f is a Möbius transformation of the disk we have

$$f(z) = \frac{z - a}{1 - \bar{a}z},$$

$$f(z) = \frac{1-|a|^2}{(1-\bar{a}z)^2}.$$

Thus

$$\begin{aligned}
|\nabla_H f(z)| &= \frac{1-|a|^2}{(1-\bar{a}z)^2}\frac{1-|z|^2}{1-|f(z)|^2} \\
&= \frac{1-|a|^2}{(1-\bar{a}z)^2}\frac{1-|z|^2}{1-|\frac{z-a}{1-\bar{a}z}|^2} \\
&= \frac{(1-|a|^2)(1-|z|^2)}{|1-\bar{a}z|^2-|z-a|^2} \\
&= \frac{(1-|a|^2)(1-|z|^2)}{(1-\bar{a}z)(1-a\bar{z})-(z-a)(\bar{z}-\bar{a})} \\
&= \frac{(1-|a|^2)(1-|z|^2)}{(1-\bar{a}z-a\bar{z}+|az|^2)-(|z|^2-a\bar{z}-z\bar{a}+|a|^2)} \\
&= \frac{(1-|a|^2)(1-|z|^2)}{(1+|az|^2-|z|^2-|a|^2)} \\
&= 1.
\end{aligned}$$

Thus Möbius transformations preserve hyperbolic length locally. Integrating along a path shows they do not increase hyperbolic distance. Since the inverse of a Möbius transformation also has this property, they do not decrease hyperbolic distance. Thus they are isometries. □

2. Schwarz's lemma

We start with the maximum prinicple:

LEMMA 18. *If f is holomorphic on the unit disk and $r < 1$, then*

$$\max_{|z|\leq r}|f(z)| \leq \max_{|z|=r}|f(z)|.$$

PROOF. By the Cauchy integral formula

$$|f(z)| = |\frac{1}{2\pi i}\int_\gamma \frac{f(w)}{w-z}dw| \leq \int_0^{2\pi}|f(re^{i\theta}))\frac{d\theta}{2\pi r} \leq \max_{|z|=r}|f(z)|.$$

□

As a consequence, we seen that if f is holomorphic on $\mathbb{D}$ and

$$\limsup_{|z|\nearrow 1}|f(z)| \leq M,$$

then $|f(z)| \leq M$ on all of $\mathbb{D}$. We use the "limsup" since we don't know if f has continuous boundary values. If it does then we can just write

$$\sup_{\mathbb{D}} |f(z)| \leq \sup_{\mathbb{T}} |f(z)|.$$

Perhaps the most important fact relating the hyperbolic metric and holomorphic functions is that a holomorphic map $f : \mathbb{D} \to \mathbb{D}$ is a contraction of the hyperbolic metric, with equality iff if is a Möbius transformation. This fact is usually presented as Schwarz's lemma:

LEMMA 19. *If $f : \mathbb{D} \to \mathbb{D}$ is holomorphic and $f(0) = 0$ then $|f'(0)| \leq 1$ with equality iff f is a rotation.*

PROOF. Simply to apply the maximum principle $f(z)/z$. □

The proof also show that $|f(z)| \leq |z|$ on the whole disk and thus

$$\psi(f(0), f(z)) = \psi(0, f(z)) \leq \psi(0, z),$$

which shows the hyperbolic distance from 0 to any point is non-increasing. For an arbitrary holomorphic self-map of the disk f and any point $w \in \mathbb{D}$ we can always choose Möbius transformations τ, σ so that $\tau(0) = w$ and $\sigma(f(w)) = 0$, so that $\sigma \circ f \circ \tau(0) = 0$. Since Möbius transformations are hyperbolic isometries, this shows $\psi(f(w), f(z)) \leq \psi(w, z)$ in general.

There are numerous generaliztions of Schwarz's lemma in the liturature.

In the proof of the Riemann mapping theorem, We will be particularly interested in the map $z \to z^2$. By Schwarz's lemma this is a strict contraction of the hyperbolic metric, although the hyperbolic derivative tends to 1 near the boundary as we can see from the explicit formula

$$\nabla_H(z^2) = \frac{2|z|}{1 + |z|^2}.$$

We will actually use the fact the the inverse map, $\sqrt{z}$ is an expansion of the hyperbolic metric in the following sense. Suppose W is a simply connected subdomain of $\mathbb{D}$ which does not contain the origin. Then there is a well defined branch of $\sqrt{z}$ on W and since z^2 is a contraction for the hyperbolic metric, we have

$$\psi(\sqrt{z}, \sqrt{w}) > \psi(z, w),$$

for any pair of points $z, w \in W$. We can actually be a little more precise and say

$$|\nabla_H \sqrt{z}| \geq \frac{1+|z|}{2\sqrt{z}}.$$

If $\sqrt{z} = 1 - \epsilon$ this becomes

$$|\nabla_H \sqrt{z}| \geq \frac{1+(1-\epsilon)^2}{2(1-\epsilon)} = 1 + \frac{\epsilon^2}{2(1-\epsilon)} = 1 + O(|1-z|^2).$$

Suppose (Y, d) is a metric space and let $\mathcal{F}$ be a subset of $C(X, Y)$, the continuous functions from X to Y. If $x_0 \in X$, we say the family is equicontinuous at x_0 if for any $\epsilon > 0$ there is a neighborhood U of x_0 so that $d(f(x), f(y)) < \epsilon$ for every $x, y \in U$. If the family is equicontinuous at every point we simply say it is equicontinuous.

A family of functions $\mathcal{F}$ is called pointwise bounded if for every x $\{f(x) : f \in \mathcal{F}\}$ is a bounded set (different bounds for different x are allowed). See, e.g., Exercise 5, page 279 of Munkres' *Topolygy* [].

THEOREM 20 (Arzela's theorem). *If X is compact and $\{f_n\} \subset C(X, \mathbb{R}^d)$ is pointwise bounded and equicontinuous, then $\{f_n\}$ has a uniformly convergent subsequence.*

COROLLARY 21. *Suppose Ω is a planar domain and $\{f_n\}$ is a sequence of holomorphic functions mapping Ω into $\mathbb{D}$. Then there is subsequence that converges uniformly on compact subsets.*

PROOF. Pointwise boundedness is obvious. To prove equicontinuity, fix a point $z_0 \in \Omega$ and $D = D(z_0, r)$ where $r = \text{dist}(z_0, \partial\Omega)$ and let $g(z) = z_0 + rz$ map the unit disk to D. Then $h_n = f_n \circ g$ is a holomorphic map of the unit disk to itself, hence is a contraction of the hyperbolic metric, hence

$$|z - z_0| \leq r\delta \quad \Rightarrow \quad \psi(,0,z) \leq \delta \quad \Rightarrow \quad |h_n(z) - h_n(z_0)| \leq \psi(h_n(z), h_n(z_0)) \leq \delta,$$

which is equicontinuity at z_0. Now Arsela's theorem applies. □

3. The Poisson integral formula

If f is holomorphic on $\mathbb{D}$ with continuous boundary values then the Cauchy integral formula implies

$$f(0) = \frac{1}{2\pi i} \int_\gamma \frac{f(w)}{w - z} dw = \int_0^{2\pi} f(e^{i\theta}) \frac{d\theta}{2\pi}.$$

If $\tau : \mathbb{D} \to \mathbb{D}$ is a Möbius transformation sending $z \to 0$ then $f \circ \tau$ is also holomorphic on $\mathbb{D}$ and

$$\begin{aligned} f(z) &= f \circ \tau(0) = \int_0^{2\pi} f \circ \tau(e^{i\theta}) \frac{d\theta}{2\pi} \\ &= \int_0^{2\pi} f(e^{i\theta}) |\tau'(e^{i\theta})| \frac{d\theta}{2\pi} \\ &= \int_0^{2\pi} f(e^{i\theta}) \frac{1-|z|^2}{|z-w|^2} \frac{d\theta}{2\pi} \\ &= \int_0^{2\pi} f(e^{i\theta}) P_z(\theta) d\theta \end{aligned}$$

where $P_z(\theta)$ is called the Poisson kernel. Since the kernel is real valued we also have

$$u(z) = \int_0^{2\pi} u(e^{i\theta}) P_z(\theta) d\theta,$$

if u is the real part of a holomorphic finction (i.e., if u is harmonic). The Poission kernel is also given by the formula

$$P_z(w) = \frac{1-r^2}{1-2r\cos(\theta-\psi)+r^2},$$

where $z = re^{i\psi} \in \mathbb{D}$ and $w = e^{i\theta} \in \mathbb{T}$. The minimum and maximum are attained for $\theta = \psi$ and $\theta = \psi + \pi$ and P_z satisfies estimates

$$\frac{1-r}{1+r} \leq P_z(w) \leq \frac{1+r}{1-r}.$$

If u is positive then replacing P_z by one of these bounds gives a bound for $u(z)$ in terms of its mean value, and since u is harmonic this means

$$\frac{1-|z|}{1+|z|} u(0) \leq u(z) \leq \frac{1+|z|}{1-|z|} u(0).$$

This is called Harnack's inequality. In particular, if u is a positive harmonic function on $D(z, 2r)$ then the minimum and maximum values of u on $D(z, r)$ are in a bounded ratio to each other.

The same holds for any compact connected set by covering by a finite number of such balls. In general, if K is a compact connected set in a domain Ω, we can cover K by a finite number N of disks $\{D_j\}$, so that the double of each disk is in Ω. Thus for any positive harmonic function on Ω, the minimum and maximum values of u on

any ball are within a factor 9 of each other. This implies the minimum and maximum values of u over K are with a factor of 9^N of each other. In other words,

LEMMA 22. *Suppose Ω is a domain and $K \subset \Omega$ is a compact set. Then there is a constant $C < \infty$ so that for any two points $z, w \in K$ and any positive harmonic function on Ω $u(z) \leq Cu(w)$. In particular, any sequence $\{u_n\}$ of positive harmonic functions on Ω has a subsequence which either tends to ∞ uniformly on every compact subset of Ω or is uniformly bounded on each compact subset of Ω.*

If f is holomorphic on Ω and $0 < |f(z)| < 1$, Then $-\log|f(z)| = \Re(-log(f(z))$ is harmonic and positive, so Harnack's inequality applies. Thus any sequence of such functions the limit is either non-vanishing or identically zero. This is Hurwitz's theorem:

THEOREM 23. *If $\{f_n\}$ is a sequence of non-vanshing holomorphic functions on a domain Ω, that converge uniformly on compact sets to a limiting function f, then f is either identially zero or nowhere zero.*

4. A proof of Riemann's theorem

We can now begin the proof of the Riemann mapping theorem. Fix a point $z_0 \in \Omega$ and let $\mathcal{F}_0$ be the class of 1-1 holomorphic functions from Ω into the unit disk so that $f(z_0) = 0$. This proof breaks up into three stages:

(1) Prove $\mathcal{F} \neq \emptyset$.
(2) Prove there is an element $f \in \mathcal{F}$ which maximizes $|f'(z_0)|$.
(3) Prove this element maps Ω onto $\mathbb{D}$.

Proof of (1): If Ω is bounded the first step is trivial; we can take a linear map which shrinks Ω enough and moves it to the origin. If Ω misses some disk, we can invert round the center of the disk and so map Ω to a bounded domain (and then we are done as before). In general, we use the fact that if $w \notin \Omega$ then $\sqrt{z-w}$ has a well defined branch on Ω and the image never contains both a point and its negative, from which we can deduce it omits a disk (since the image is open).

Proof of (2): We take a sequence so that $f_n'(z_0)$ approaches the supremum M and uses Montel's theorem to show there is a holomorphic limit. Clearly this function maps into the unit disk and has the desired derivative at z_0, so we only have to show

it is in $\mathcal{F}$, i.e., show it is 1-1. Choose any $w \in \Omega$ and note that $f_n(z) - f_n(w)$ is nowhere vanishing on $\Omega \setminus \{w\}$. By Hurwitz's theorem then $f(z) - f(w)$ is nowhere vanishing or identically 0 and the latter case does not happen since $|f'(z_0)| = M > 0$ ($M > 0$ since $\mathcal{F}$ is non-empty). Hence f never takes the same value twice, as desired.

Proof of (3): If $g \in \mathcal{F}$ omits a point of $\mathbb{D}$ from its image we will show how to construct another function in $\mathcal{F}$ with larger derivative at z_0. Thus the maximizing function must be onto.

Suppose $f \in \mathcal{F}$ omits the value w Let τ and σ be Möbius transformations of the disk to itself so that $\tau(w) = 0$ and $\sigma(\tau(f(z_0))) = 0$. Let $W = \tau(f(\Omega))$. Then W is a simply connected subdomain of the disk and omits 0 so there is a well defined branch of $z^{1/2}$ defined on Ω, call it S. Then $g = \sigma \circ S \circ \tau \circ f$ is holomorphic on Ω, 1-1, and maps z_0 to 0. Moreover, $\sigma \circ S \circ \tau$ fixes the origin and is the composition of two isometries and a strictly expanding map (all with respect to the hyperbolic metric), so its derivative at 0 is strictly greater than 1 in absolute value. Thus $|g'(z_0)| > |f'(z_0)|$, as claimed.

5. Koebe's method

The proof of Riemann's theorem in the previous section seems non-constructive at first glance: we use compactness to say a function maximizing a certain derivative exists and argue by contradiction to show this map is 1-1, onto the disk. However, it does describe a simple algorithm for mapping a bounded simply connected domain Ω conformally to the disk with a given point z_0 mapping to the origin:

(1) Find a linear map $f : \Omega \to \Omega_0 \subset \mathbb{D}$ with z_0 mapping to 0.
(2) Assuming Ω_n has been defined, find point w on $\partial\Omega_n$ closest to 0.
(3) Choose Möbius transformations τ, σ of the disk to itself so that $\tau(w) = 0$ and $\sigma(\tau(f(z_0))) = 0$.
(4) Let $\Omega_{n+1} = \sigma(\sqrt{\tau(\Omega_n)})$.
(5) Repeat steps until point w is within specified distance of unit circle.

In Step 3 of the proof of Riemann's theorem we merely stated that if f omitted a point of the disk then we could increase the derivative by composing with the map $\sigma \circ D \circ \tau$. However, it is easy to see that the multiplicative factor of this increase depends only on $|w|$, where w is the omitted point. Thus

LEMMA 24. *Suppose $\Omega \subset \mathbb{D}$ is simply connected and omits the point $w \in \mathbb{D}$. Let τ, σ be Möbius self-maps of the disk $\tau(w) = 0$ and $\sigma(\tau(f(z_0))) = 0$ and let $S(z)$ be a branch of $\sqrt{z}$ root function on $\tau(\Omega)$. Then*

$$|(\sigma \circ S \circ \tau)'(0)| \geq \frac{1+|w|}{2\sqrt{|w|}}.$$

COROLLARY 25. *Suppose $d_n = \text{dist}(\partial\Omega_n, 0)$ and $m = 4/(1-\sqrt{d_n})$. Then $d_{n+k} > \sqrt{d_n}$ for $k \geq m$. In particular, if $d_0 \geq 1/2$ then $1 - d_n = O(1/n)$.*

PROOF. Let $r = \sqrt{d_n}$. As long as $d_{n+k} < \sqrt{d_n} = r$ the derivative at 0 increases by a factor of $(1+r^2)/2r$ at each iteration. This is a contradiction if

$$(\frac{1+r^2}{2r})^k > r/d_n = 1/r,$$

or

$$k \geq \log\frac{1}{r} / \log\frac{1+r^2}{2r}.$$

A few simple estimates show

$$\log\frac{1}{r} / \log\frac{1+r^2}{2r} \leq 2(1-r)/\frac{1}{2}(\frac{1+r^2}{2r} - 1) \leq \frac{4r}{1-r} \leq 4/\sqrt{d_n},$$

so if k is larger than the right hand side, we get a contradiction. Thus $d_{n+k} > \sqrt{d_n}$ for $k \geq m$.

If $d_0 > 1/2$ we repeatedly take square roots of d_0 to get $s_n = d_0^{2^{-n}}$, these numbers approach 1 geometrically fast and the number of iterations where d_n is between s_k and s_{k+1} is at most $O(s_k^{-1})$, which grows exponentially in k. Thus the time to reach s_k is dominated by the time to cross between s_{k-1} and s_k. Thus $d_n > 1 - \epsilon$ after about $O(1/\epsilon)$ iterations. □

Note that we have only estimated the number of iterations needed to get Ω_n within an ϵ-neighborhood of the unit circle, not the amount of work needed to implement each iteration. If we are keeping track of N points this work should be around $O(N)$.

LEMMA 26. *Suppose Ω is simply connected and $\{0\} \in \Omega \subset \mathbb{D}$. Let $f : \Omega \to \mathbb{D}$ be 1-1, onto, holomorphic and $f(0) = 0$. If $w \in \mathbb{D} \setminus \Omega$, then $|f'(0)| \geq \frac{1}{2}(1+|w|)/\sqrt{w}$. If $\{|z| < r\} \subset \Omega$, then $|f'(0)| \leq 1/r$. Thus if $d = dist(\partial\Omega, 0)$, we have*

$$1 < \frac{1}{2}(1+R)/\sqrt{R} \leq |f'(0)| \leq 1/R.$$

PROOF. □

In Koebe's method we can easily renormalize the domain by a linear map or Möbius transformation to place any desired point at the origin. Thus we could use this iteration to simply find approximate preimages for vertices of a quadrilateral, as in Section 5 on domain decompositions, and combine these approximations as in that section. because of the slow convergence of Koebe's method, this will probably be faster in many cases than iterating at a single center, especially in examples where crowding is an issue.

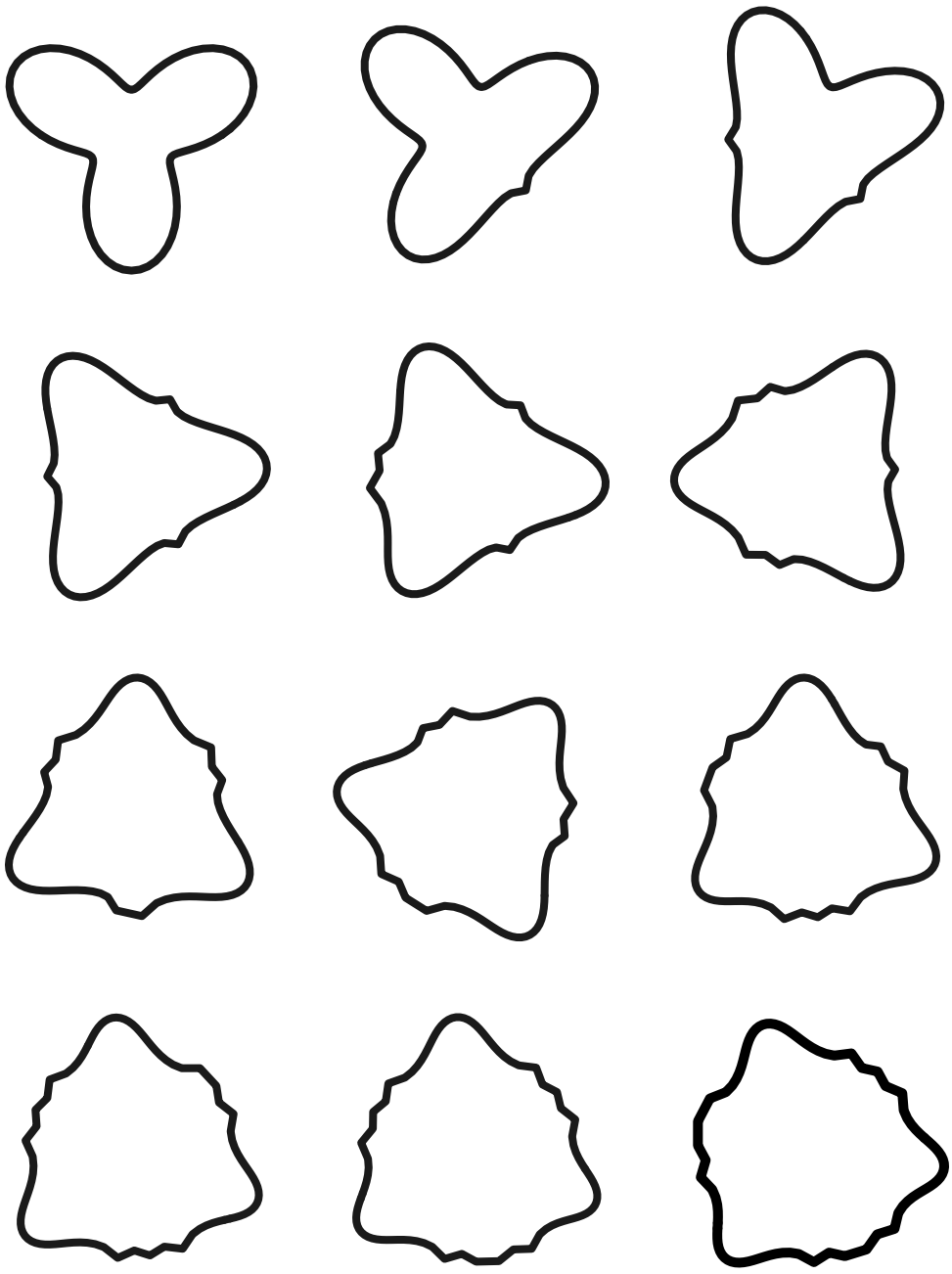

FIGURE 2. On the top left is a sudomain of the disk whose boundary is parameterized by $\gamma(t) = e^{it}\frac{1}{3}(3+\sin(t)))$. This is a polygon with 100 vertices defined by the points $t = k/100$, $k = 1, \ldots, 100$. The next 11 figures show the first 11 iterations of Koebe's method. The next figure show more iterations.

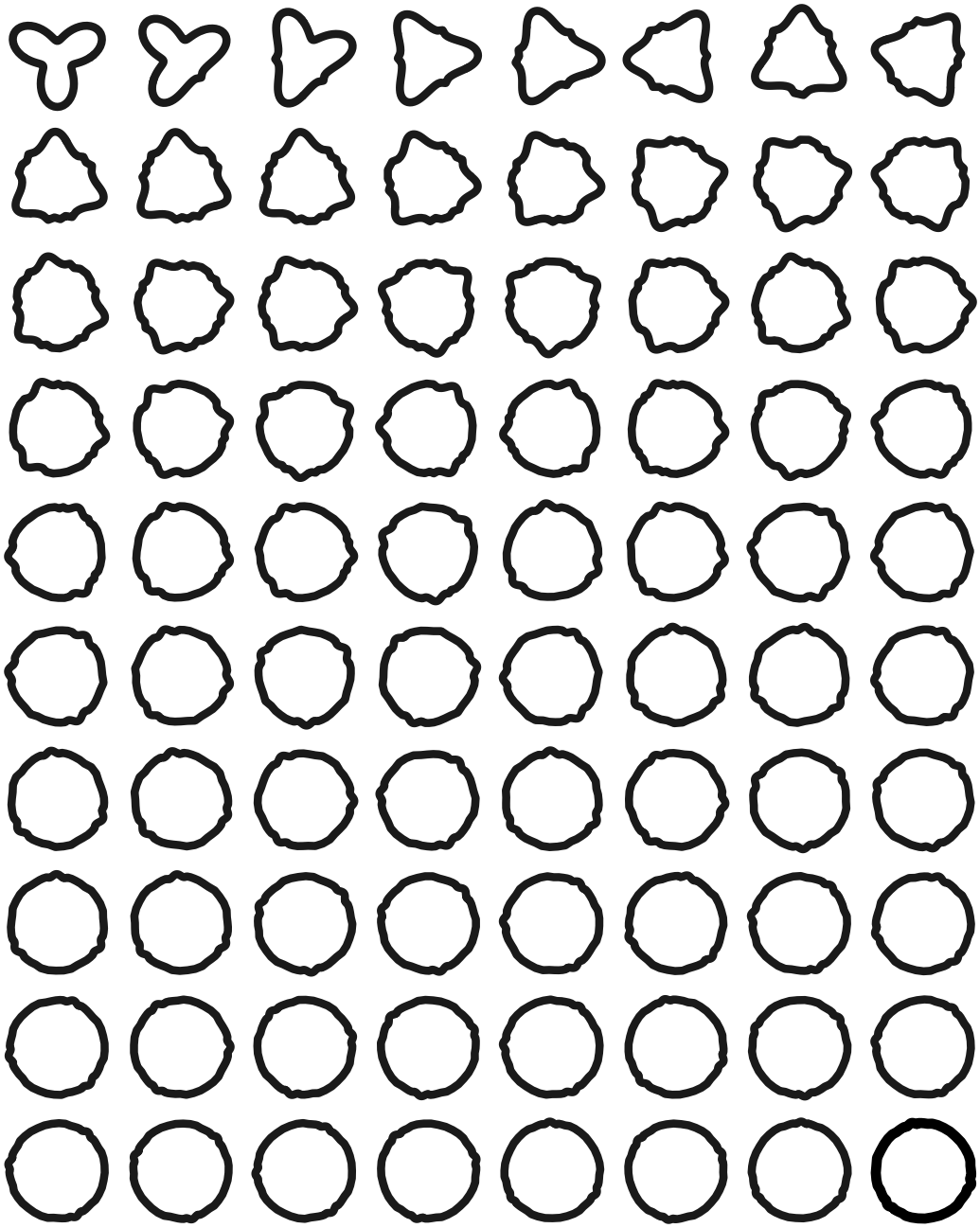

FIGURE 3. This shows the first 80 iterations of Koebe's method for the same domain as in Figure 2

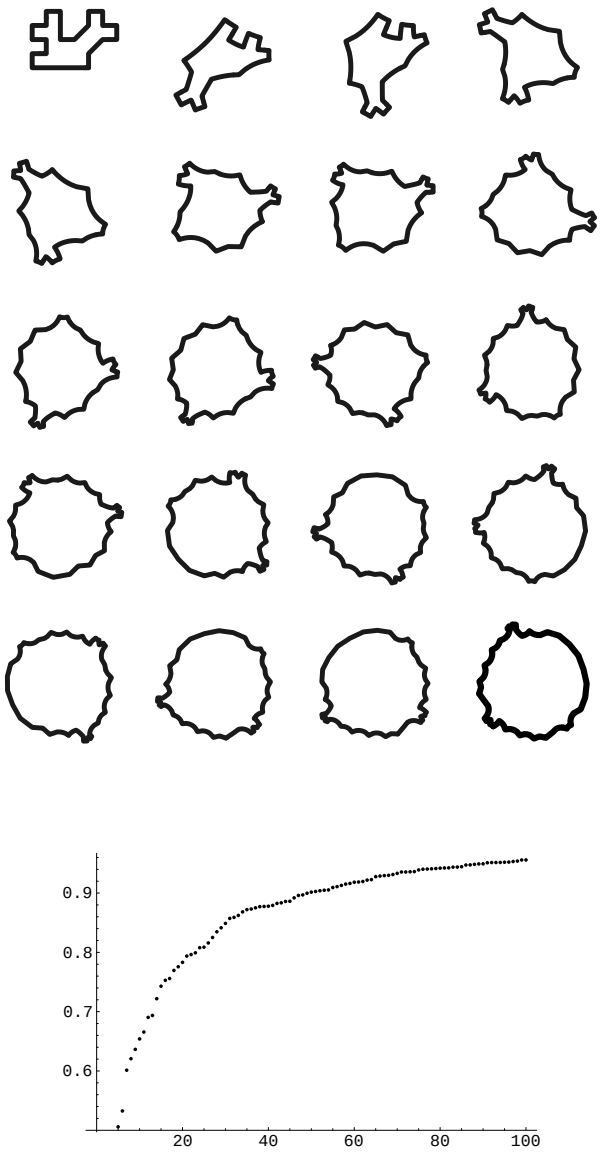

FIGURE 4. Koebe's method applied to a polygon. We have added 19 new, equally spaced vertices to the interior of each edge. On the bottom we have graphed the absolute value of the vertex closest to the origin at each iteration, up to 100 iterations.

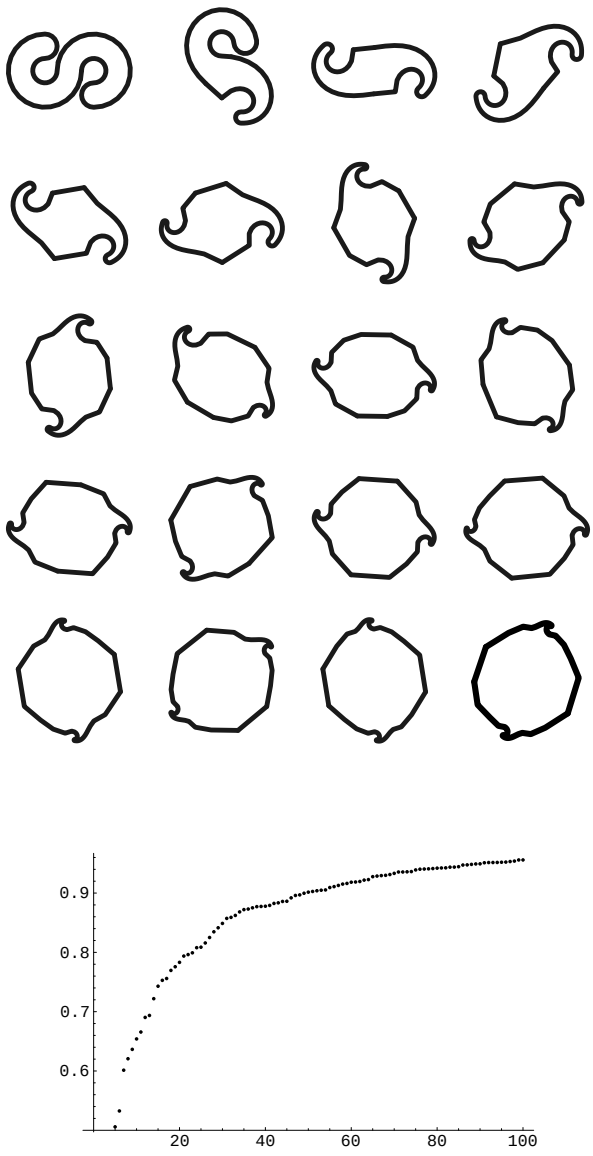

FIGURE 5. Koebe's method applied to a polygon and the absolute value of the vertex closest to the origin at each iteration, up to 100 iterations.

6. Caratheodory's Theorem

Next we want to give conditions when the Riemann mapping has a continuous extension to the boundary. This occurs iff the boundary is locally connected and the hardest part of the proof is topological arguments that show the usual definition of local connectedness is equivalent to a more useful version. We will simply accept the following.

THEOREM 27. *Suppose Ω is a bounded simply connected plane domain. The following are equivalent.*

(1) *If U is a relatively open subset of $\partial\Omega$ and $z \in U$, then there is a connected, relatively open subset V so that $z \in V \subset U$.*
(2) *$\partial\Omega$ is a continuous image of a circle.*
(3) *for any $\delta > 0$ there is an $\epsilon > 0$ such that the following holds: if γ is a Jordan arc in Ω with length $\leq$ epsilon, then at least one component of $\Omega \setminus \gamma$ has diameter $\leq \delta$.*

Part (1) is the usual definition of local connectedness and part (3) is the version we shall use (i.e. we will show that (3) implies the Riemann map has a continuous boundary extension). In the course of the proof we will also use a few well known results from real analysis that we explicitly state here:

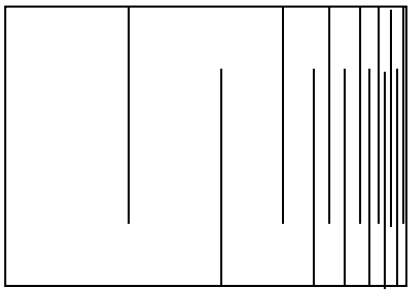

FIGURE 6. An example of a domain with a non-locally connected boundary. The Riemann map onto the interior of this domain fails to have a continuous boundary extension at one point. Examples can be constructed where it fails to have a continuous boundary extension at any point.

Fact 1: The Cauchy-Schwarz inequality

$$\int_I f(x)g(g)dx \leq (\int_I |f(x)|^2 dx)^{1/2} (\int_I |g(x)|^2 dx)^{1/2}.$$

Fact 2: If $\Omega_1 \supset \Omega_2 \supset \dots$ are nested open sets, $\text{area}(\Omega_1) < \infty$ and $\cap_n \Omega_n = \emptyset$, then $\text{area}(\Omega_n) \to 0$.

Fact 3: A continuous function on $\mathbb{D}$ has a continuous extension to the boundary iff it is uniformly continuous.

THEOREM 28 (Caratheodory). *Suppose $\Omega \subset \mathbb{C}$ is simply connected and condition (3) in Lemma 27 holds. Then the Riemann map $f : \mathbb{D} \to \Omega$ has a continuous extension to $f : \overline{\mathbb{D}} \to \overline{\Omega}$.*

PROOF. We assume $\partial\Omega$ satisfies (3) in Lemma **??** and will deduce that the Riemann map $f : \mathbb{D} \to \Omega$ is uniformly continuous, i.e., we have to show that given any ϵ, there is a $\delta > 0$ so that $z, w \in \mathbb{D}$, $|z - w| \leq \delta$ implies $|f(z) - f(w)| < \epsilon$.

Next we would like to assume $\text{area}(f(\{z : \frac{1}{2} < |z| < 1\})) < \infty$. If Ω is bounded, this is obvious since then $f(\mathbb{D}) = \Omega$ has finite area. If Ω is unbounded, consider $\tau(z) = 1/(z - f(0))$. This maps Ω to a domain containing ∞ and $\tau \circ f$ maps $D(0, \frac{1}{2})$ to a neighbohood of ∞. The remainder of the disk is mapped to a bounded region, hence has finite area. Rather than introduce a new symbol, we will let f denote the composed map and Ω the new image.

Fix $\eta > 0$ and choose δ_0 so small that $\text{area}(f(\{z : 1 - \delta_0 < |z| < 1\})) \leq \eta$. Suppose $\delta < \delta_0$ and fix $w \in \mathbb{T}$. Let D be the disk of radius δ around D. Note that $\text{area}(f(D \cap \mathbb{D})) \leq \text{area}(f(\{z : 1 - \delta_0 < |z| < 1\})) \leq \eta$.

Let γ_r be the circular arc in $\mathbb{D}$ centered at w or radius r. Then

$$\ell(f(\gamma_r)) \leq \int_{\gamma_r} |f'(w + re^{i\theta})| r d\theta \leq (r\pi \int_{\gamma_r} |f'(w + re^{i\theta})|^2 r d\theta)^{1/2}.$$

Now square and integrate with respect to $s \in (\delta/2, \delta)$,

$$\begin{aligned} \int_{\delta/2}^{\delta} \ell(f(\gamma_s))^2 ds &\leq \pi \int_{\delta/2}^{\delta} \int_{\gamma_s} |f'(re^{i\theta})|^2 r^2 dr d\theta \\ &\leq \delta \iint_{D \cap \mathbb{D}} |f'(re^{i\theta})|^2 r dr d\theta \\ &\leq \delta \text{area}(f(D \cap \mathbb{D})). \end{aligned}$$

Thus the average value of $\ell(f(\gamma_r))^2$ is at most 2η, so there is at least one value $r \in (\frac{\delta}{2}, \delta)$ with length less than this.

Since D does not contain 0, $W = f(D \cap \mathbb{D})$ does not contain z_0 and hence if $\delta < \delta_1$ is small enough, W must have diameter less than *epsilon*. Thus if $1 - |z| < \delta_1/2$ or $1 - |w| < \delta_1/2$ and $|z - w| < \delta_1/2$, then both points lie in a δ_1-ball around some boundary point. Thus $|f(w) - f(w)| \leq \epsilon$ by the argument above. If both $1 - |z| \geq \delta_1/2$ and $1 - |w| \geq \delta_1/2$ then both points lie in a compact subset of $\mathbb{D}$ and f is uniformly continuous on $D(0, 1 - \delta_1/2)$ by compactness. Thus there is a δ_2 so that for any two points in this disk $|z - w| \leq \delta_2$ implies $|f(w) - f(z)| \leq \epsilon$. Taking $\delta = \min(\delta_1, \delta_2)$ proves the result. □

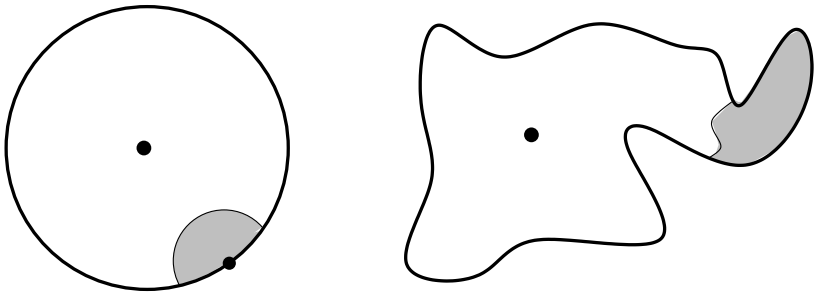

FIGURE 7. By assumption, if a circular crosscut of the disk maps to a curve of short length, it cuts off a subdomain with small diameter.

If the Riemann mapping $f : \mathbb{D} \to \Omega$ has a continuous extension, then $\partial\Omega$ is obviously a continuous image of a circle. Thus using Lemma **??**, we see that the Riemann map has a continuous extension to the whole boundary iff $\partial\Omega$ is locally connected. It is not to hard to deduce (3) of Lemma **??** directly; we will do this later when we have Beurling's lemma at our disposal (this says that the conformal image of a set of small diameter in Ω also has small diameter in $\mathbb{D}$). See Lemma **??**.

The proof also shows the Riemann map extends continuously to a single point $w \in \mathbb{T}$ if there is sequence of circular crosscuts γ_n centered at w so that $f(\gamma_n)$ divides Ω into two subdomains, and the one not containing $f(0)$ has diameter tending to zero. Such a sequence of crosscuts is closely related to the idea of compactifying a domain using prime ends, but we will not discuss thus further here.

7. The Schwarz reflection principle

If $\partial\Omega$ is a polygon then Caratheodory's theorem implies the conformal map $f\mathbb{D} \to \Omega$ has a continuous extension to the boundary, but much more is true: f has a holomorphic extension at every boundary point except the preimages of the vertices. This follows from the well known:

THEOREM 29 (Schwarz Reflection principle). *Suppose f is holomorphic on $\mathbb{H}$, has a continuous extension to an arc $I \subset \mathbb{R}$ and $f(I) \subset \mathbb{R}$. Extend f to $\mathbb{L} = \{\bar{z} \in \mathbb{H}\}$ by setting*

$$f(z) = \overline{f}(\bar{z}).$$

Then the extended function is holomorphic on $\Omega = \mathbb{H} \cup I \cup \mathbb{L}$.

First we nned to prove:

THEOREM 30 (Morera's theorem). *If f is defined on a disk $D = D(0, r)$ and the integral $\int_T f(z)dz = 0$ for every triangle in D, then f is holomorphic in D.*

PROOF. Define $F(z) = \int_0^z f(\zeta)d\zeta$, where the integral is over the line segment from 0 to z. Consider the triangle with vertices $0, z, w$ with w close to z. Since the integral of f around this triangle is zero,

$$F(z) - F(w) = \int_0^z f(\zeta)d\zeta - \int_0^w f(\zeta)d\zeta = \int_w^z f(\zeta)d\zeta.$$

Since f is continuous, for any $\epsilon > 0$ we can choose $\delta >$ so that $|z - \zeta| \leq \delta$ implies $|f(z) - f(\zeta)| < \epsilon$ and hence

$$|F(z) - F(w) - f(z)(z - w)| \leq \epsilon|z - w|.$$

This means $F'(z)$ exists and equals f. Thus F is holomorphic and hence is $F' = f$, as desired. □

SCHWARZ REFLECTION. Clearly f is holomorphic on $\mathbb{H}$ and $\mathbb{L}$, so we really need only check f is holomorphic in small balls centered in I. Let T be a triangle in the ball. If such T does not intersect I, the integral is clearly 0. Similarly if T hits I at one vertex of along one edge, for then we can write the integral as a limit of integrals over curves that do not hit I and hence are zero.

Otherwise I divides T into two polygons whose interiors are contained in $\mathbb{H}$ and $\mathbb{L}$ respectively. The integrals over the boundaries of these two pieces add up to the

integrals over T (since the sum differs from the integral over T by two integrals over I in opposite directions). Moreover each piece has integral zero, for the same reasons as above. □

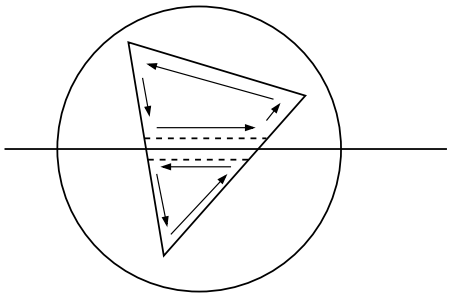

FIGURE 8. The integral around a triangle is zero becuase we can write the integral as the limit of the sum of two integrals inside the half-planes.

The Schwarz reflection principle readily extends to reflections across boundary arcs which are circular arcs (simply map then to real axis by a Möbius transformation).

8. Existence of parameters

In the first chapter we introduced the Schwarz-Christoffel formula and showed that it always defines a holomorphic map of the disk whose bounadry is a polygon with given angles (but it may be self-intersecting). We left open the question of whether the conformal map onto every polygon can be represented in this way. Now that we have the Riemann mapping theorem at our disposal, we can prove this.

LEMMA 31. *Suppose f is a holomorphic function on $\mathbb{D}$ and f' never vanishes on $\mathbb{D}$. Suppose f has a continuous extension to the boundary and is 1-1 on the boundary. Then f is 1-1 on $\mathbb{D}$, i.e., is a conformal map.*

Using these results we can prove:

COROLLARY 32. *The conformal map from the half-plane to a polygon satisfies the Schwarz-Christoffel formula for some choice of A and C. Similarly for the map from the unit disk to a polygon.*

PROOF. Let $F : \mathbb{D} \to \Omega$ be the conformal map of the disk to the interior of the polygon, let $\{z_k\}$ be the preimages of the vertices and let G be the locally 1-1 holomorphic maps given by the Schwarz-Christoffel maps with these parameters (and the correct α_k's). Then we can choose C with $|C| = 1$ so that $\arg(CG') = \arg(F')$ on the interior of every parameter interval (but these arguments are not defined at the prevertices). Assume for the moment that this implies $\arg(CG'(z)) = \arg(F'(z))$ on the interior of the half-plane. Since these are the imaginary parts of $\log(CG')$ and $\log F'$ we deduce the real parts of $\log(CG')$ and $\log F'$ differ by a real additive constant and hence CG' an F differ by a real multiplicative constant. By putting this factor into C we may assume $CG' = F'$ thus CG and F differ by an additive constant, which we call A and we are done, except to verify the claim, which follows from the following lemma. □

LEMMA 33. *Suppose u, v are bounded harmonic functions on a bounded domain Ω which each have continuous boundary values everywhere on $\partial\Omega$, except fora finite set E. If the boundary values of u, v agree except on E, then $u = v$ on Ω.*

PROOF. Suppose $E = \{z_1, \ldots, z_n$ and let

$$g(z) = \log(\text{diam}(\Omega)) - \frac{1}{n}\sum_{k=1}^{n} \log|z - z_k|.$$

Then g is positive and harmonic on Ω and tends to $+\infty$ on the set E. Thus for any $\epsilon > 0$,

$$\limsup_{z\to\partial\Omega} \epsilon g(z) + v(z) - u(z) \geq 0,$$

so by the maximum principle for harmonic functions,

$$v(z) \geq u(z) - \epsilon g(z),$$

on Ω. Taking $\epsilon \to 0$ gives $v \geq u$. Reversing the roles of v and u gives $v = u$, as desired. □

9. Maps to a rectangle

Now that we have the Schwarz reflection theorem at our disposal, we can go back and verify formula (14) in Chapter 5. First we need a famous result about holomorphic functions.

THEOREM 34 (Liouville's Theorem). *If f is bounded and holomorphic on the whole plane then f is constant.*

PROOF. By Cauchy's formula

$$|f'(z)| = |\int_0^{2\pi} f(z + Re^{i\theta}) \frac{iRe^{i\theta}d\theta}{(Re^{i\theta})^2}| \leq \max_{\mathbb{C}} |f| \frac{2\pi}{R} \to 0,$$

as $R \to \infty$. Thus $f' = 0$ everywhere. □

Now for the promised formula.

LEMMA 35. *Suppose Ω is a $1 \times R$ rectangle, let $f : \Omega \to \mathbb{D}$ be conformal and let P be the cross ratio of the four images of the vertices of Ω. Then*

$$P = \exp(-\pi/R) \frac{1}{16} \prod_{n=1}^{\infty} (\frac{1 + \exp(-2n\pi/R)}{1 + \exp((-2n-1)\pi/R)})^8.$$

PROOF. Since cross ratio is invariant under Möbius transformations we may assume f maps Ω to the upper half-plane, $\mathbb{H}$. To be even more specific, assume the vertices of Ω are $\{0, R, R+i, i\}$ and that these are mapped to $\{1, \infty, 0, P\}$ respectively. See Figure 9

Applying Schwarz reflection to each of the sides, we can extend f to be conformal on each of the adjacent, similar rectangles, and mapping these rectangles to the lower half-plane. In fact, we can continue reflecting until the map is defined on the whole plane, as illustrated in the bottom of Figure 9. The gray squares are mapped to the upper half-plane and the white squares are mapped to the lower half-plane. When there is more than one way to reach a rectangle in the grid by reflections, it is easy to check that the alternate definitions of the extension agree. Moreover, since angles are doubled at the corners of the rectangles we see that the values $\{0, \infty, 1, P\}$ are taken on with multiplicity 2.

In other words, f is holomorphic function on the plane, except for poles of order 2 at the points $\mathcal{L}_1 = (2\mathbb{Z} + 1)R + 2i\mathbb{Z}$ and it has zeros of order two at the points $\mathcal{L}_2 = 2R\mathbb{Z} + i(2\mathbb{Z} + 1)$. Another function with this same property is

$$F(z) = (\prod_{n=-\infty}^{\infty} (\frac{1 - \exp(\frac{\pi i}{R}(2ni + (R+i) - z))}{1 - \exp(\frac{\pi i}{R}(2ni + i - z)}))^2.$$

It is easy to check that the infinite product converges in both directions and defines a function with periods $2R$ and $2i$. The numerators vanish exactly iff $z \in \mathcal{L}_1$

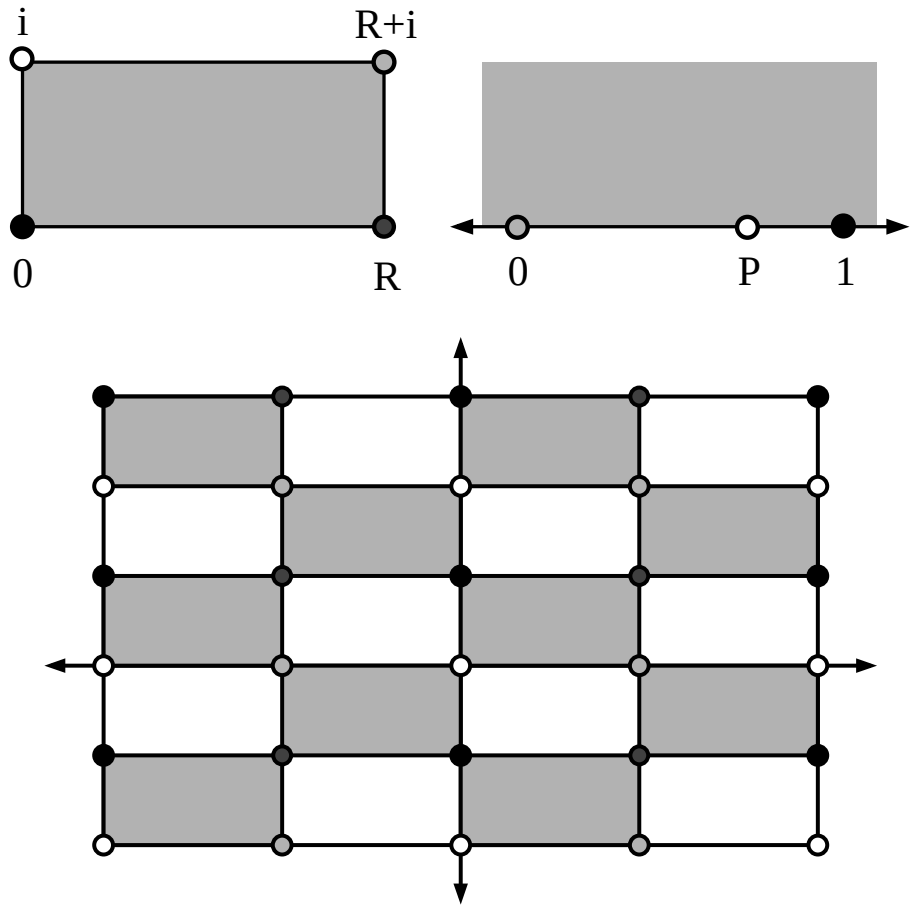

FIGURE 9. We assume f maps a rectangle to the upper half-plane with the vertics mapped as shown. After repeated reflection, this extends to a map of the plane to the Riemann sphere, with poles at the dark gray points, zeros at the light gray, value 1 at the black points and value $P \in (0,1)$ at the white points.

and the denominators vanish exactly on $\mathcal{L}_2$. Thus f/F is holomorphic off $\mathcal{L}_2$. In fact, on $\mathcal{L}_2$ the poles cancel, so that f/F is actually holomorphic and periodic on the whole plane and hence bounded. By Liouville's theorem, f/F is constant. Since $f(0) = 1$, this means $f(z) = F(z)/F(0)$. In particular, $f(i) = F(i)/F(0)$, and the right hand side is computable.

First rewrite the product by reindexing some of the terms

$$F(z) = (\prod_{n=-\infty}^{\infty} \frac{(1-\exp(\frac{\pi i}{R}(2ni+(R+i)-z)))(1-\exp(\frac{\pi i}{R}(2ni-(R+i)-z)))}{(1-\exp(\frac{\pi i}{R}(2ni+R-z)))(1-\exp(\frac{\pi i}{R}(2ni-R-z)))}.$$

Now separate the $n = 0$ terms and combine n and $-n$, and let $q = e^{-\pi R}$, $p = e^{-i\pi z/R}$,

$$\begin{aligned}
F(z) &= \frac{(1-\exp(\frac{\pi i}{R}((R+i)-z)))(1-\exp(\frac{\pi i}{R}(-(R+i)-z)))}{(1-\exp(\frac{\pi i}{R}(R-z)))(1-\exp(\frac{\pi i}{R}(-R-z)))} \\
&\quad \cdot \prod_{n=1}^{\infty} \frac{(1-\exp(\frac{\pi i}{R}(2ni+(R+i)-z)))(1-\exp(\frac{\pi i}{R}(-2ni+(R+i)-z)))}{(1-\exp(\frac{\pi i}{R}(2ni+R-z)))(1-\exp(\frac{\pi i}{R}(-2ni+R-z)))} \\
&\quad \cdot \frac{(1-\exp(\frac{\pi i}{R}(2ni-(R+i)-z)))(1-\exp(\frac{\pi i}{R}(-2ni-(R+i)-z)))}{(1-\exp(\frac{\pi i}{R}(2ni-R-z)))(1-\exp(\frac{\pi i}{R}(-2ni-R-z)))} \\
&= \frac{(1+qp)(1+q^{-1}p)}{(1+p)(1+p)} \prod_{n=1}^{\infty} \frac{(1+q^{2n+1}p)(1+q^{-2n+1}p)(1+q^{2n-1}p)(1+q^{-2n-1}p)}{(1+q^{2n}p)^2(1+q^{-2n}p)^2} \\
&= \frac{(1+qp)(1+q^{-1}p)}{(1+p)(1+p)} \prod_{n=1}^{\infty} \frac{(1+q^{2n+1}p)(p+q^{-2n+1})(1+q^{2n-1}p)(p+q^{-2n-1})q^{-4n}}{(1+q^{2n}p)^2(p+q^{-2n})^2q^{-4n}} \\
&= \frac{(1+qp)(1+q^{-1}p)}{(1+p)(1+p)} \prod_{n=1}^{\infty} \frac{(1+q^{2n+1}p)(p+q^{2n-1})(1+q^{2n-1}p)(p+q^{2n+1})}{(1+q^{2n}p)^2(p+q^{-2n})^2}
\end{aligned}$$

First take $z = 0$ (i.e., $p = 1$) and this becomes

$$\begin{aligned}
F(0) &= \frac{(1+q)(1+q^{-1})}{4} \prod_{n=1}^{\infty} \frac{(1+q^{2n+1})^2(1+q^{2n-1})^2}{(1+q^{2n})^4} \\
&= \frac{(1+q)(1+q^{-1})}{4(1+q)^2} \frac{(1+q^{2n-1})^4}{(1+q^{2n}p)^4} \\
&= \frac{1}{4q} \frac{(1+q^{2n-1})^4}{(1+q^{2n}p)^4}
\end{aligned}$$

Next set $z = i$ or $p = \exp(-\pi iz/R) = \exp(\pi/R) = 1/q$. We get

$$\begin{aligned}
F(i) &= \frac{(1+1)(1+q^{-2})}{(1+q^{-1})^2}\prod_{n=1}^{\infty}\frac{(1+q^{2n})(q^{-1}+q^{2n-1})(1+q^{2n-2}p)(q^{-1}+q^{2n+1})}{(1+q^{2n-1}p)^2(q^{-1}+q^{2n})^2} \\
&= \frac{2(1+q^{-2})}{(1+q^{-1})^2}\prod_{n=1}^{\infty}\frac{(1+q^{2n})(1+q^{2n})(1+q^{2n-2})(1+q^{2n+2})q^{-2}}{(1+q^{2n-1})^2(1+q^{2n+1})^2q^{-2}} \\
&= \frac{2(1+q^{-2})}{(1+q^{-1})^2}\prod_{n=1}^{\infty}\frac{(1+q^{2n})^2(1+q^{2n-2})(1+q^{2n+2})}{(1+q^{2n-1})^2(1+q^{2n+1})^2} \\
&= \frac{4(1+q)^2(1+q^{-2})}{(1+q^2)(1+q^{-1})^2}\prod_{n=1}^{\infty}\frac{(1+q^{2n})^4}{(1+q^{2n-1})^4} \\
&= 4\prod_{n=1}^{\infty}\frac{(1+q^{2n})^4}{(1+q^{2n-1})^4}
\end{aligned}$$

Thus

$$P = f(i) = F(i)/F(0) = 16q\prod_{n=1}^{\infty}(\frac{1+q^{2n}}{1+q^{2n+1}})^8 = 16e^{-\pi/R}\prod_{n=1}^{\infty}(\frac{1+e^{-2n\pi/R}}{1+e^{-(2n+1)\pi/R}})^8$$

□

Thus we have explicit (if somewhat involved) parameters for the Schwarz-Christoffel map onto any rectangle. A similar proof shows

$$Q(R) = \prod_{n=1}^{\infty}(\frac{1-q^{2n-1}}{1+q^{2n-1}})^8.$$

CHAPTER 3

Representing conformal maps

We saw in the previous chapter that a conformal map from the disk onto a polygon is determined by the numbers $A, C, \{z_k\}, \{\alpha_k\}$, i.e., if we record these numbers then we "know" what the map is via the Schwarz-Christoffel formula. But what is the most convenient way to plug the parameters into the formula and compute an image point? We saw in the first Chapter than we can compute the power series expansion of the map at the origin, but that this converges slowly and that even for some simple polygons, very many terms are needed to give a good appoximation. In this chapter we will dicuss to way to get around this problem: using multiple power series in disks that cover the unit disk or using numerical integration to directly evaluate the Schwarz-Christoffel formula.

1. The Carleson decomposition

Figures **??** and **??** indicate that using power series to evaluate conformal maps will be slow and inaccurate in general. This is because the accuracy of the power series decreases as we approach the radius of convergence (which is the just the distance from the center of the series to the closest singularity). However, if a power series has radius of convergence r and we only evaluate it within distance λr of the center (with $\lambda < 1$, then the accuracy is $O(\lambda^n)$. So we want to compute several power series expansions for $\int \prod (1 - \frac{w}{z_k})^{\alpha_k - 1}$ with different centers, so that for any $z \in \mathbb{D}$ we can find one of these expansions whose center is close enough to z to give a good approximation. The tool we use for this is the Carleson decomposition of the disk associated to the set of singularities $S = \{z_k\} \subset \mathbb{T}$.

Given an interval $I \subset \mathbb{T}$, the corresponding Carleson box Q is the region in the disk of the form $\{z = x + iy : z/|z| \in I, 0 < 1 - |z| < |I|\}$. The "top-half" of Q is $T(Q) = \{z \in Q : 1 - |z| > |I|/2\}$. This will be called a Whitney box, and its Euclidean diameter is comparable to its Euclidean distance from $\mathbb{T}$ (abusing notation we may

also call them Whitney "squares"). When I ranges over all dyadic intervals (i.e., all intervals of the form $[j2^{-n}, (j+1)2^{-n}]$), the corresponding Whitney boxes partition the disk into pieces with approximately unit hyperbolic size. Carleson squares are named after Lennart Carleson who used them in his solution of the corona problem and they are now ubiquitous in function theory [**?**], [**?**].

Dyadic Carleson squares form a tree under intersection of the interiors. Each square has a unique parent and two children. The parent of a dyadic Carleson square Q will be denoted Q^*. This obviously also induces a tree structure on Whitney boxes. We will say two dyadic Whitney boxes are neighbors if they are the same size and adjacent; each box therefore has a "left" and a "right" neighbor. One of these is a "sibling" in the sense that it shares a parent, while the other does not.

The decomposition will always begin with a root disk, which we take to be the disk of radius 1/2 around the origin. We will call this the unique type 1 piece. We break the unit circle into 16 intervals using equally spaced points starting at 1 (we could use other values than 16, but this will give decomposition pieces that are "roundish"). Let this list be denoted $\mathcal{L}$. For each interval, compute three numbers: the length, $|I|$, of the interval, the distance, $d(I, S)$, to the closest point of S (which is zero if the interval contains this point) and the distance $d_f(I, S)$ to the second closest point. The f stands for "feature" since this distance is sometimes called the feature distance in the computer science literature.

(1) If $d_f(I, S) \leq 4|I|$ then we say I is type 2 and we add the Whitney box with base I to the decomposition. The interval I is divided into two disjoint, equal length subintervals and each of these is added to the list $\mathcal{L}$ of intervals for testing. The interval I is removed from $\mathcal{L}$. For these intervals there are at least two points of S that are fairly close to I (when compared to $|I|$).
(2) If $d_f(I, S) > 4|I|$ and $d(I, s) > |I|$ then call I type 3 and let the Carleson square with base I be added to the decomposition. No new intervals are added to $\mathcal{L}$. These intervals are "far" from all points of S in the sense that tripling the interval misses all points of S.
(3) If $d_f(I, S) > 4|I|$ and $d(I, s) < |I|$ then call I type 3 and let the Carleson square with base I be added to the decomposition. No new intervals are

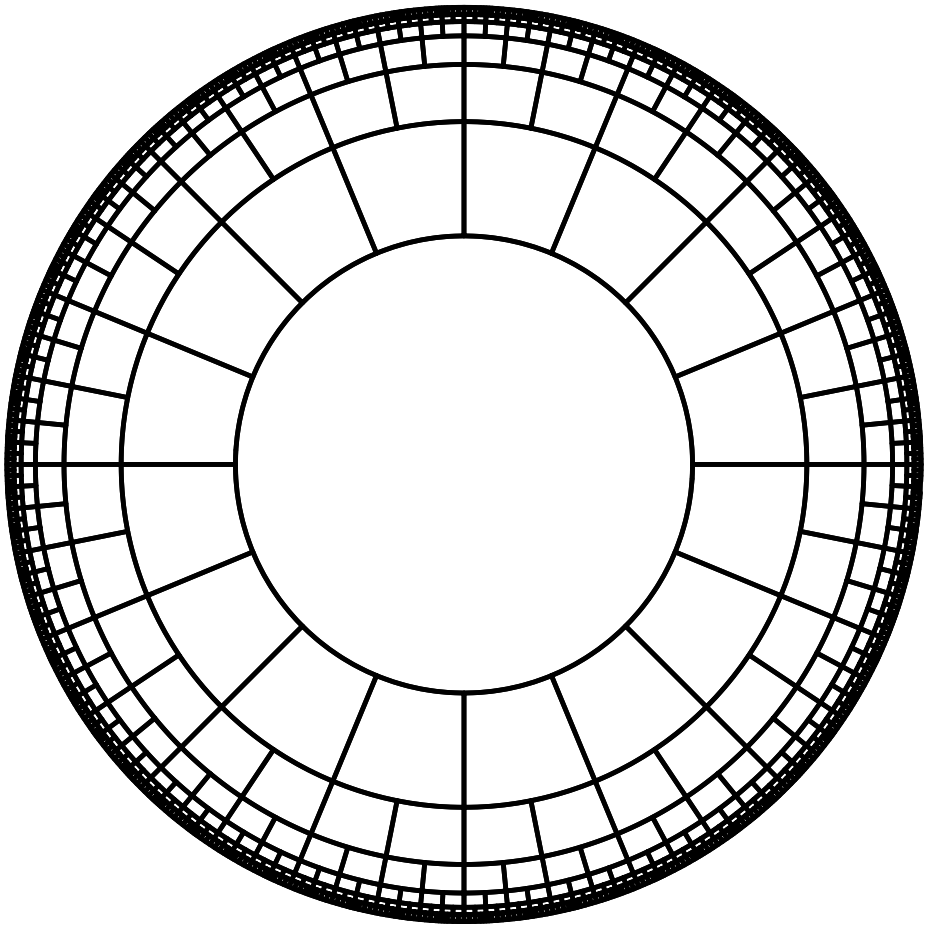

FIGURE 1. A decomposition of the disk into Whitney squares. There is a central disk which has 16 children, each of which has 2 children, and so on towards the boundary. The choice of 16 and 2 is arbitrary, but made here so that the Whitney boxes are "roundish" and so that each box is contained in a disk whose double is still in the unit disk. This means that any holomorphic function on the unit disk has a power series expansion around the center of each Whitney box which converges geometrically fast on the box.

added to $\mathcal{L}$. These intervals are close to some point of S (there is one contained in its triple) but far from all other points of S.

No interval created in this way can be shorter than $\frac{1}{10}$ the distance ϵ between the two closest points of S, and the created intervals are all disjoint, so the number of created intervals is at most $O(n \log \frac{1}{\epsilon})$. This upper bound is attained if we take $2n$

points with two points in each ϵ-neighborhood of a different nth root of unity. If the points of S are more evenly spaced then the number of decomposition pieces is more like $O(n)$.

Note that crowding of the z-parameters leads to more pieces in our decomposition. We shall see later that the extra effort needed to deal with crowding of the prevertices in S is roughly the same as N, the number of distinct pieces in the Carleson decomposition for S.

By adding a fifth type of decomposition piece, called an "arch", it is possible to guarantee that there are at most $O(n)$ pieces with a constant that is independent of n and the geometry of S. However, on the arches, the representation of the function is not with a power series, but with a Laurent series. While the arches provide a fast method if we assume infinite precision computations, if we stick to finite precision calculations then the extra space needed to deal with the Laurent series in the arches is about the same as the number of Whitney boxes that would be needed to fill in the arch and convert "the arched decomposition" into a "regular decomposition". Moreover, constructing the arched decomposition requires some more sophisticated ideas from computational geometry (namely the medial axis of the set S). For all these reasons, will leave the discussion of arches until later.

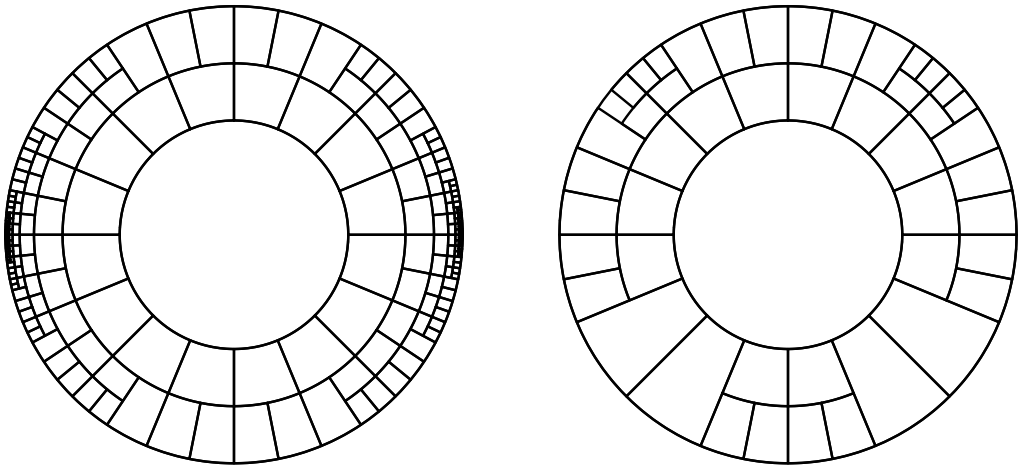

FIGURE 2. Two Carleson decompositions associated to different finite sets on the boundary. On the left is the set $\{0, 0.000628319, 3.14159, 3.14222\}$. On the right is the set $\{0, 1.5708, 3.14159\}$.

On each of the type 1, 2 and 3 pieces, we can compute a power series for $\int \prod_{k=1}^{n}(1-\frac{w}{z_k})^{\alpha_k-1}$. The center of the series is the "center" of the box. The radius of convergence is the distance to the nearest point of S (or more precisely the nearest point where $\alpha_k \neq 1$). By construction, each decomposition piece lies inside a compact subdisk of the disk of convergence and the ratio of these disk is bounded away from 1 uniformly. Thus the power series associated to a piece converges geometrically fast on that piece.

The power series for adjacent pieces may not agree, so we have to make them consistent. We take the power series for the root piece as is. We then compute the images of the 16 points on the boundary of the root piece which are the endpoints of the top edges of its children. Then for each child of the root we choose a, b so that $a + bf$ agrees at these two points with the values compute for the root. In general, if we have a series for a type 2 piece we compute the images of the two endpoints of its bottom edge and for the midpoint of the bottom edge. The maps for each of its children are then normalized by a linear map to agree with the parent map at the two endpoints of its top edge. Continuing is this way we can define a map from the union of type 1, 2 and 3 edges.

The type 3 boxes are clustered into groups, one corresponding to each of the components of $\mathbb{T} \setminus S$. By computing the images of two points on each of these components we can compute the line that the image boundary segment lies on. Doing this for the two components on either side of a point of S and computing their intersecting, we can find that vertex of the image polygon that corresponds to that parameter value. Thus we can compute all the vertices of the image polygon, using only the expansions on type 1, 2 and 3 pieces. For purposes of iteratively finding the parameters, this is all that is needed.

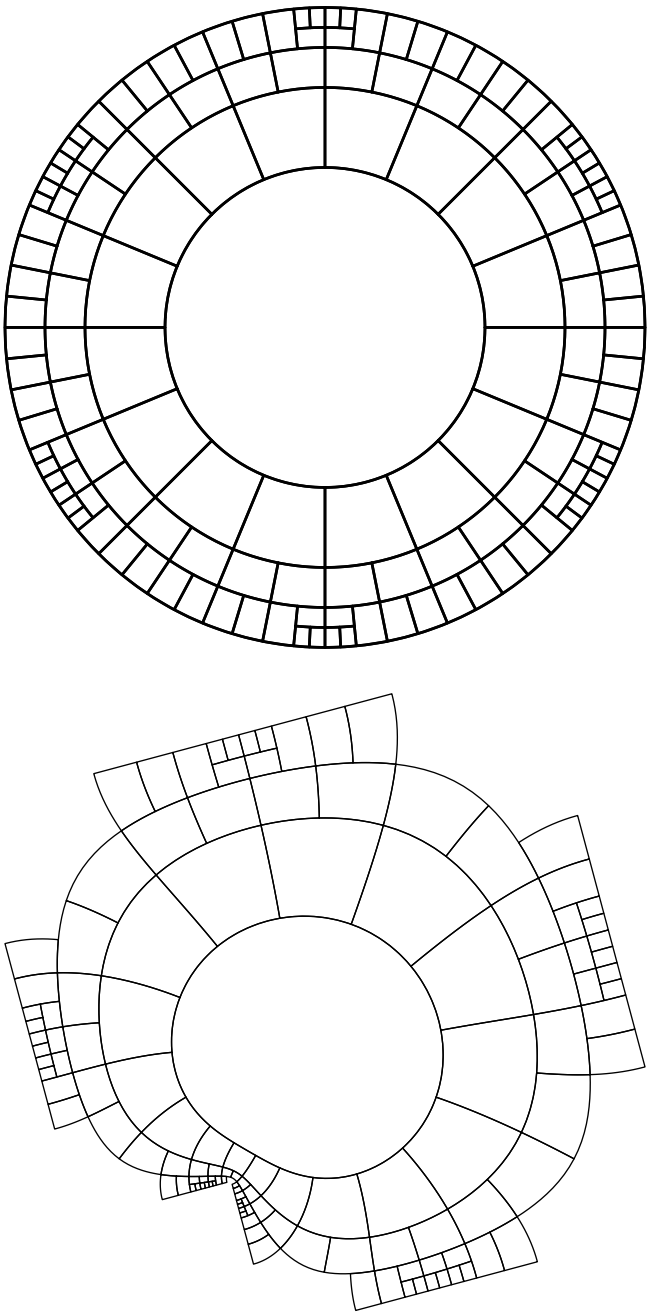

FIGURE 3. The top shows the Whitney-Carleson decomposition of the disk corresponding to six equidistributed points. The bottom shows the image of each box of type 1, 2 and 3 under a degree 10 polynomial, as derived in the text. The figure is rotated compared with the target because we have not yet normalized to find the A and C in the Schwarz-Christoffel formula. However, given the image above we can compute the lines containing the edges of the type 3 boxes and find the intersection points for adjacent edges. Once we know these vertices, we can rotate the figure to match the desired polygon. The result of this normalizing step is shown in Figure 5

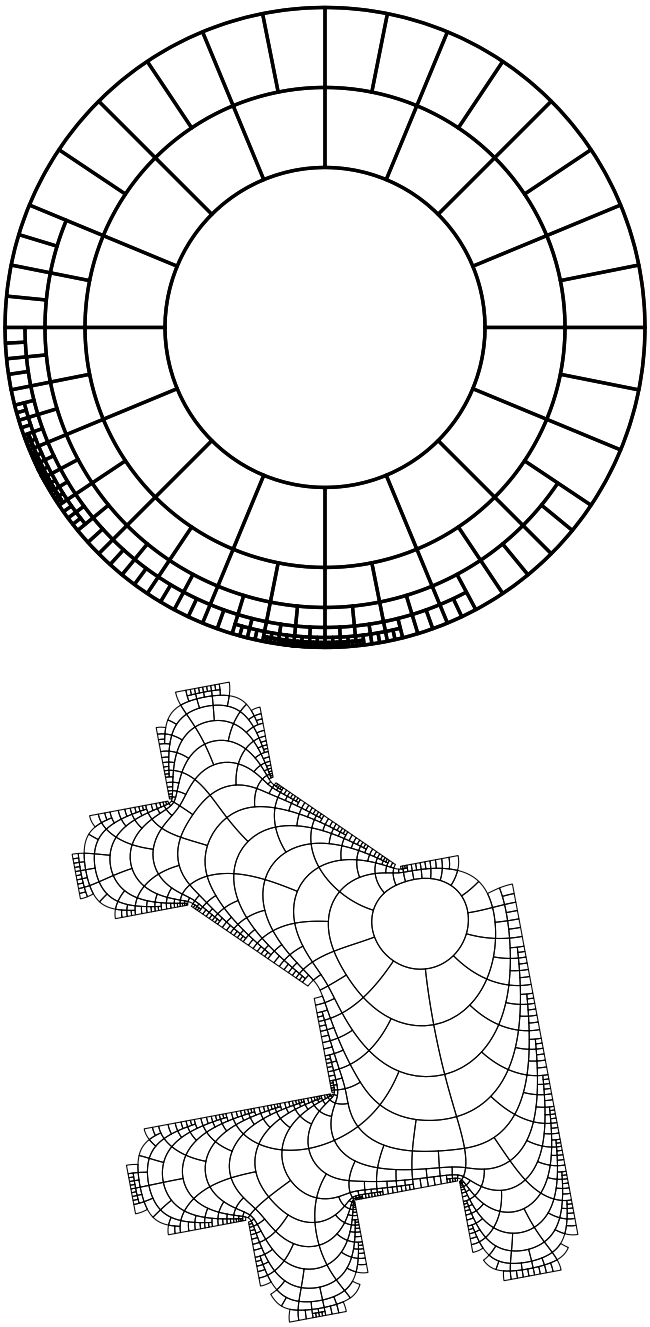

FIGURE 4. Same as for Figure 7 but for a more complicated 20-gon. By counting boxes in the image we can estimate the harmonic measure of any side. For example, the horizontal edge at the top left has measure about 2^{-15}

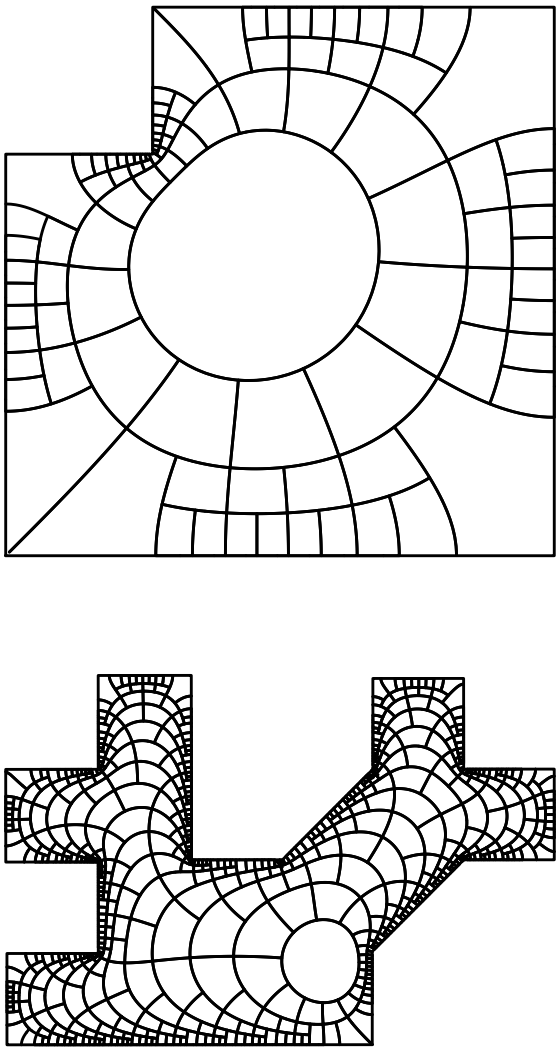

FIGURE 5. These are the normalized versions of Figures 7 and 8. We have computed the lines containing each edge and their intersection points and drawn the corresponding polygon (we have not cheated by using the given vertices except to normalize our figures to have the same first edge, thus setting A and C in the Schwarz-Christoffel formula). Note that the images of the type 4 boxes are not shown. We will see how to draw them in the next section. However, this final step is not needed if all we want is to compute the location of the vertices for use in a iterative solver.

2. An expansion around the singularities

We have already seen how to compute quick convergent power series expansions for the Schwarz-Christoffel map on the boxes of type 1, 2 and 3. This map need not have such an expansion on a type four box if that box contains a singularity, or it map not converge well, if the singularity is outside the box but nearby in an adjacent box. Suppose Q is a type 4 box, $z_k \in \mathbb{T}$ is the nearby parameter and v_k is the vertex of the image polygon corresponding to this parameter (recall that we can compute v_k using our computation on the type 3 boxes). Let θ_k be the interior angle of the polygon at this vertex. Suppose $f : \mathbb{D} \to \Omega$ is our conformal map. Let τ be a Möbius transformation that maps the upper half-plane to the unit disk with $z_k \to 0$, $-z_k \to \infty$ and $0 \to i$, i.e.,

$$\tau(z) = -i\frac{z - z_k}{z + z_k}, \qquad \tau^{-1}(z) = z_k\frac{1 + iw}{1 - iw}.$$

Choose $r_1 > r_2 > 0$ so that the disks $D(0, r_j)$, $j = 1, 2$ are mapped by τ^{-1} to disks $D_2 \subset D_1$, so that D_2 contains all the type 4 boxes associated to z_k and $\partial D_1 \cap \mathbb{D}$ is contained in the union of boxes of type 1, 2 and 3. Then

$$g(z) = \lambda_1(f(\tau^{-1}(r_1 z)) - v_k)^{\pi/\theta_k}, \tag{10}$$

maps $\mathbb{D} \cap \mathbb{H}$ to a neighborhood of 0 in some half-plane whose boundary contains 0 and by choosing a constant λ_1 with $|\lambda_1| = 1$ correctly, we may assume $g(z)$ maps the upper half-plane to itself. Thus by the Schwarz Refection Principle g has an holomorphic extension across the real line (at least in a neighborhood of 0 an so we can write

$$g(z) =,$$

(we can drop the zero term since $g(0) = 0$ by definition). Moreover,

$$f(z) = v_k + [\lambda_2 \sum_{k=1}^{\infty} a_k(\tau(z)/r_1)^k]^{\theta_k/\pi},$$

where λ_2 is chosen so the left hand side map into a cone of angle θ_k with the correct direction.

So this gives us a nice, compact representation for f, if we can compute power series for g. This can be done using a discrete Fourier transforms. Fix a positive integer N and consider the Nth roots of unity $R_N = \{w_k\} = \{e^{i2\pi k/N}\}$. Let V^N be

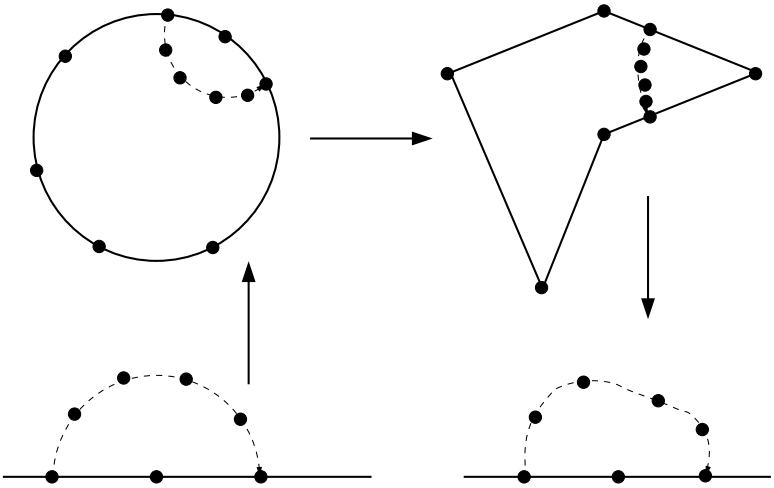

FIGURE 6. This illustrates how (10) is derived. We map the upper half-plane to the disk with 0 going to one of the Schwarz-Christoffel parameters (up arrow). Then we map to the polygon by f (across) and then open the vertex to 180 degrees by a power map (the down arrow). The resulting composition has a holomorphic extension to a neighborhood of 0 by the Schwarz reflection principle. We can compute the power series for this extension by sampling roots-of-unity on the half-circle as shown, mapping them forward as shown and defining the map on the corresponding roots-of-unity in the lower half-plane by reflection. Then apply an FFT to the data to get the coefficients of the power series.

the N-dimensional complex vector space of functions from R_N to $\mathbb{C}$. The functions $e_k(z) = z^k$, $k = 0, \ldots N-1$ form an orthonormal basis with respect to the inner product

$$\langle f, g \rangle = \frac{1}{N} \sum_{k=0}^{N-1} f(w_k)\overline{g(z_k)},$$

as can easily be seen by verifying

$$\|e_n\|^2 = \frac{1}{\sqrt{N}} \sum_{k=0}^{N-1} f(w_k^n)\overline{w_k^n} = \frac{1}{N} \sum_{k=0}^{N-1} 1 = 1,$$

$$\begin{aligned}\langle e_m, e_n\rangle &= \frac{1}{N}\sum_{k=0}^{N-1} w_k^m w_k^{-n} \\ &= \frac{1}{N}\sum_{k=0}^{N-1}(w_1^{m-n})^k \\ &= \frac{1}{N}\frac{1-(w_1^{m-n})^N}{1-w_1^{m-n}} = 0,\end{aligned}$$

where we have used the geometric formula $\sum_{k=0}^{N} z^k = \frac{1-z^N}{1-z}$ and the fact that $w_1^{m-n})^N (w_1^N)^{m-1} = 1$ since w_1 is an Nth root of unity. Therefore any function in V_N can be written

$$f(z) = \sum_{k=0}^{N-1} e_k \langle f, e_k\rangle = \sum_{k=0}^{N-1} a_k z^k,$$

for $z \in R_N$. Using the definition, each coefficient of f can be computed as a sum of N terms, so the whole expansion can be computed in time $O(N^2)$. However, the Fast Fourier Transform gives a $O(n \log n)$ algorithm for computing the same coefficients and will be discussed in Section 5.

The function g defined above maps the upper half-plane to itself and we can define g at the roots of unity that lie in the upper half-plane using (10) because we only need to evaluate f at points that lie in type 1, 2 or 3 boxes. We then define g at the roots of unity in the lower half-plane using $\overline{g(z)} = g(\bar{z})$. Then use the discrete Fourier transform to define a polynomial of degree $N-1$ g_0 which agrees with g at all the Nth roots of unity.

Unfortunately, this does not necessarily mean that g and g_0 are close anywhere else. If we start with $g(z) = z^N$ then the restriction to the Nth roots of unity gives the constant 1 functions and the resulting g_0 is also the constant 1. Fortunately, the maps we want to approximate are conformal and so we can do better than this.

Later on we will prove distortion estimates for conformal maps that say that if g is 1-1 and holomorphic on $D(0,2)$ then $|g'(z)| \le 3|g'(0)|$ on $D(0,1)$. Lets assume for the moment that $g'(0) = 1$. Let

$$g(z) = \sum_{k=0}^{\infty} b_k z_k,$$

be the power series for the function g and let

$$g_0(z) = \sum_{k=0}^{N-1} a_k z_k,$$

be the function derived using the discrete Fourier transform from the restriction of g to the Nth roots of unity. The coefficients $\{b_k\}$ can be obtained from the Cauchy integral formula as

$$b_k = \frac{1}{2\pi i} \int_{\mathbb{T}} \frac{g(z)}{z^{k+1}} dz = \int_0^{2\pi} g(e^{it}) e^{-ik} \frac{dt}{2\pi}.$$

Now break the unit circle into N arcs each of length $2\pi/N$ and centered at the Nth roots of unity. Then on each arc, the product $g(z)z^{-k}$ has second derivative bounded by $O(k^2)$ and therefore differs from a linear function by at most $O(k^2/N)$ on each arc. Therefore

$$|\int_{I_j} g(e^{it}) e^{-ik} \frac{dt}{2\pi} - g(w_j) w_j^k| = O(k^2/N^2).$$

Hence

$$|b_k - a_k| \leq O(k^2/N).$$

The coefficients $\{b_k\}$ satisfy $|b_k| = O(2^{-k})$, and therefore $|a_k| = O(\max(k^2/N, 2^{-k})$. Let $M = \lfloor \log_2 N \rfloor$ and

$$g_1(z) = \sum_{k=0}^{M} a_k z_k.$$

So if $r < 1$ and $|z| \leq r$, then

$$\begin{aligned} |g(z) - g_0(z)| &\leq \sum_{k=0}^{M} |a_k - b_k| r^k \sum_{k=M+1}^{\infty} |b_k| r^k + \sum_{k=M+1}^{N-1} |a_k| r^k \\ &= O(\frac{M^3}{N} + O(2^{-M}) + O(r^{-M}) \\ &= O(\frac{1}{N}(\log N + \frac{1}{1-r})). \end{aligned}$$

This tends to zero for any fixed $r < 1$ and $N \to \infty$. This the series we have constructed will uniformly approximate the conformal map.

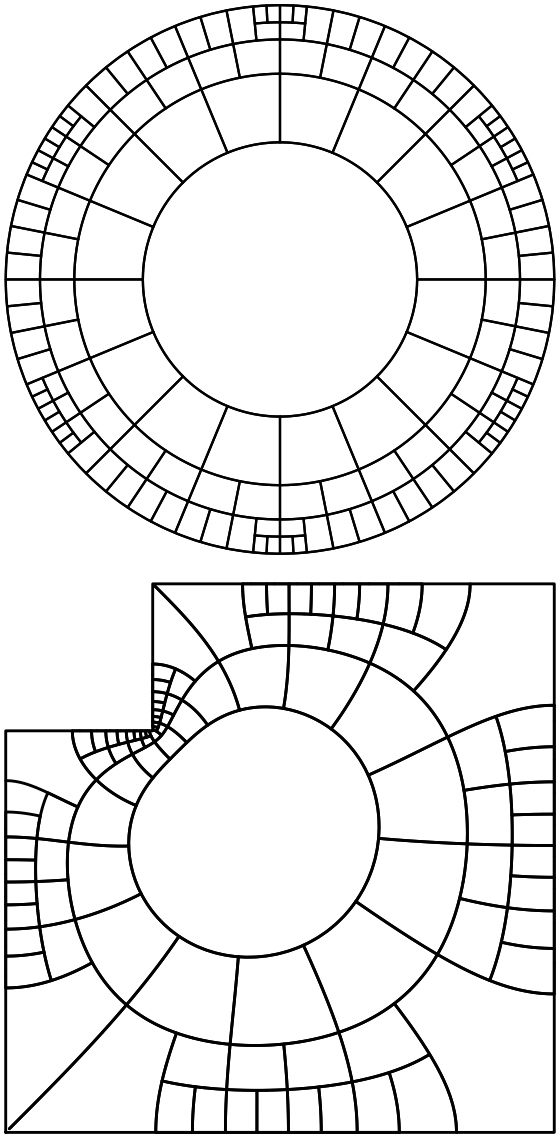

FIGURE 7. The top shows the Whitney-Carleson decomposition of the disk corresponding to six equidistributed points. The bottom shows the image of each box under a degree 10 polynomial, as derived in the text. The vertices of the polygon are found by computing two points on each edge using the type 3 boxes and then finding the intersection points of the corresponding lines.

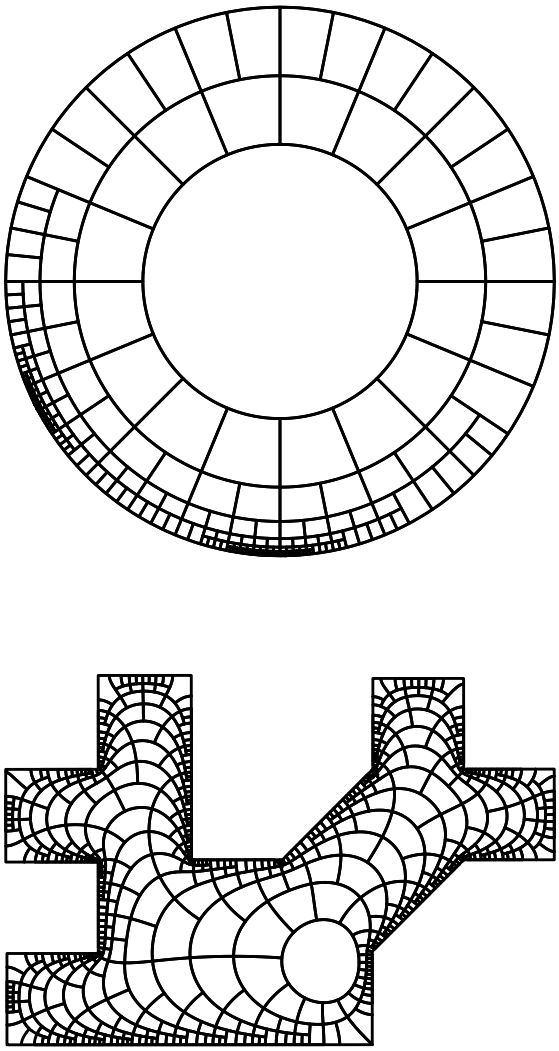

FIGURE 8. Same as for Figure 7 but for a more complicated 20-gon. By counting boxes in the image we can estimate the harmonic measure of any side. For example, the horizontal edge at the top left has measure about 2^{-15}

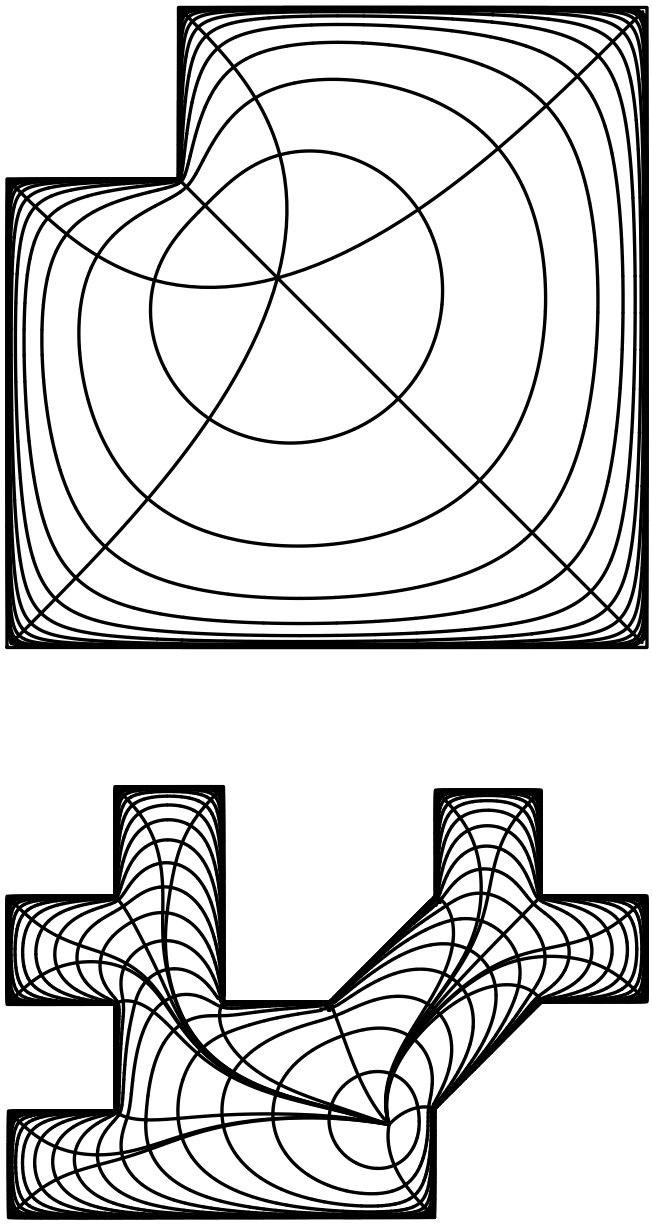

FIGURE 9. For the polygons in Figure 7 and 8 we have used the multiple power series representation to plot the images of the circles of radius $1 - 2^{-n}$ and the radial segments that end at the vertices. As before, polynomials of degree 10 are used for all approximations.

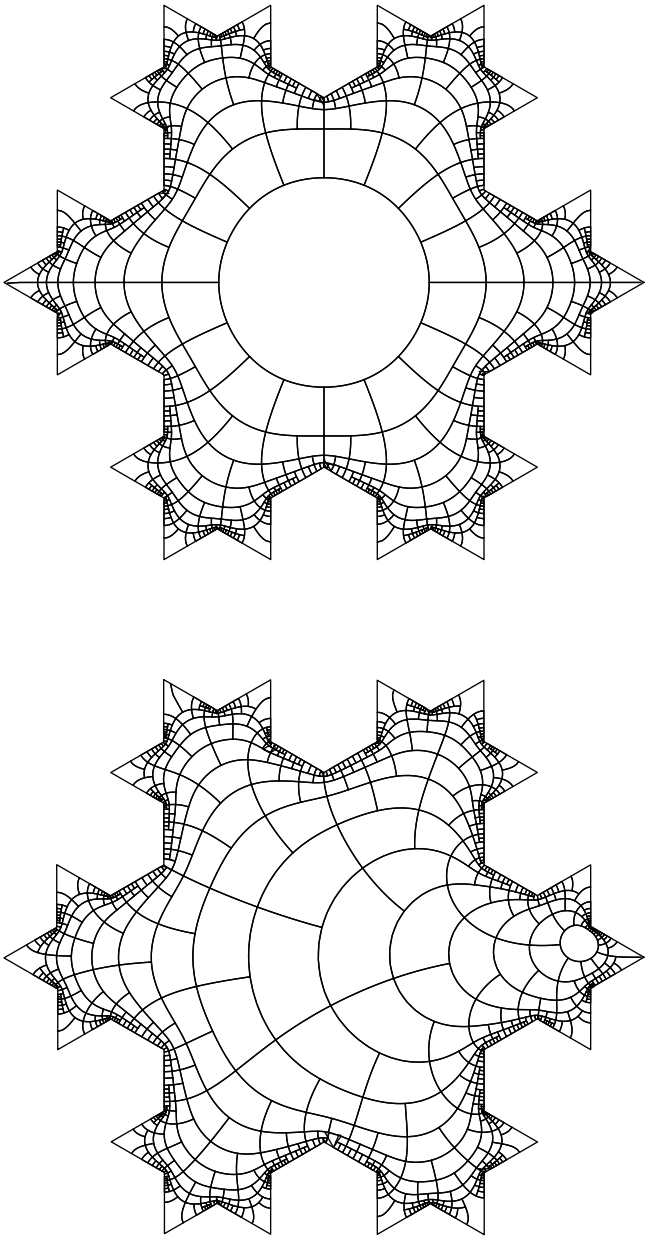

FIGURE 10. Images of the Whitney boxes for the second generation von Koch snowflake.

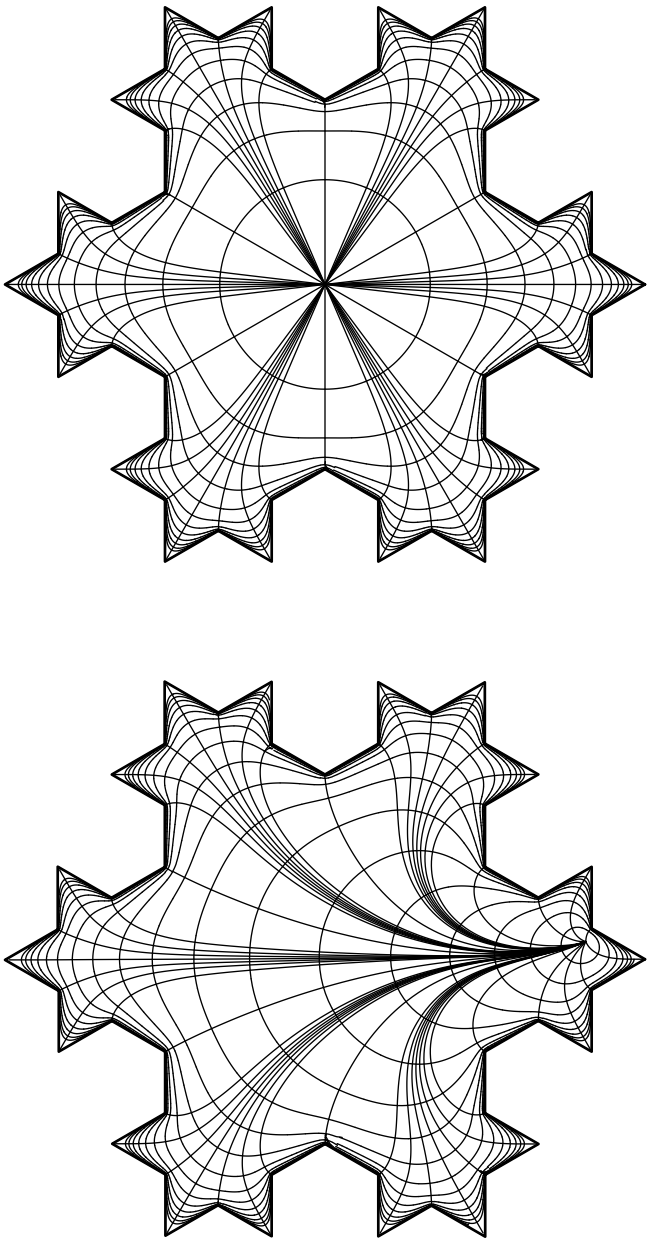

FIGURE 11. Level lines and radial images for the second generation von Koch snowflake. In the top picture the origin is mapped to the center of the snowflake and in the bottom the origin is mapped close to the boundary.

3. Gauss-Jacobi quadrature

The multiple power series described above have the advantage of covering the whole unit disk, so that to evaluate the conformal map at any point we merely have to decide which decomposition box contains the point and sum the corresponding power series. However, if we only want to evaluate the map at a few points, it may not be worth building the map everywhere. For example, in order to use certain iterative methods to estimate the unknown z-parameters, we only need to compute the vertices of the image polygons. In this case, it may be faster simply to numerically evaluate the integral in the Schwarz-Christoffel integral.

There are at least two choices: integrate f' on a ray from the origin to each parameter value (to find the position of the corresponding vertex relative to 0) or integrate $|f'|$ along the boundary arc between two parameters (to get the length of the corresponding polygonal side, which, with the known angles, is enough to determine the polygon). The boundary integral has the advantage of being real valued, whereas the interior integral in complex valued.

Simpson's rule for evaluating an integral $\int_a^b f(t)dt$ gives the correct answer with error of about $O(n^{-4})$ (with a constant that depends on f, in particular, it depends on the size of the fourth derivative of f). If f has a power series centered at $(a+b)/2$ with radius of convergence $\frac{\lambda}{2}|a-b| > |a-b|/2$, then evaluating n terms of the power series and integrating term by terms will give the integral to accuracy $O(\lambda^{-n})$ which is much better for large λ or large n. However, we can do much better than Simpson's rule for evaluating integrals.

Suppose w is defined and integrable on $[a, b]$ and we want to evaluate

$$\int_a^b p(t)w(t)dt,$$

for $p \in \mathcal{P}_n$ (the polynomials of degree n). Think of $w = 1$ or $w(t) = (t-a)^\alpha$ as the main examples. If we are given any $n+1$ distinct points $\{x_k\}_0^n \subset [a, b]$ then p is determined by its values at these points, i.e., the map

$$p \to \{p(x_0), \ldots p(x_n)\}$$

is an invertible map $\mathcal{P}_n \to \mathbb{R}^n$. Thus there must be real numbers w_k so that

$$\int_a^b p(t)e(t)dt = \sum_{k=0}^{n} w_k p(x_k), \tag{11}$$

holds for all $p \in \mathcal{P}_n$.

What are these weights more explicitly? Given the point set $\{x_k\}$ define the Lagrange polynomials

$$L_k(x) = \prod_{1\le j\le n, j\neq k} \frac{x - x_j}{x_k - x_j}.$$

This is equal to 1 at x_k and equal to 0 at the other x_j's. Since any degree $n-1$ polynomial p is determined by its values at n points we must have

$$p(x) = \sum_{k=1}^{n} p(x_k)L_k(x),$$

since both sides are degree $n-1$ that agree at n points. Thus

$$\int_a^b p(x)w(x)dx = \int_a^b \sum_{k=1}^{n} p(x_k)L_k(x)w(x)dx = \sum_{k=1}^{n} p(x_k)[\int_a^b L_k(x)w(x)dx].$$

Thus (11) holds with $w_k = \int_a^b L_k(x)w(x)dx$.

We can simplify this a bit farther by noting that

$$L_k(x) = \prod_{1\le j\le n, j\neq k} \frac{x - x_j}{x_k - x_j} = \frac{p_n(x)}{(x - x_k)p_n'(x_k)},$$

since both sides are degree $n-1$ polynomials that are 1 at x_k and 0 at x_j, $j \neq k$. Thus

$$w_k = \int_a^b \frac{p_n(x)}{(x - x_k)p_n'(x_k)} w(x)dx. \tag{12}$$

In fact, we can do better and choose $n+1$ points $\{x_k\}$ so that (11) holds for all polynomials of degree $\le 2n+1$. The secret is to choose a polynomial p of degree $n+1$ which is orthogonal to every polynomial q of lesser degree, i.e., so that

$$\langle p, q\rangle = \int_a^b p(t)q(t)w(t)dt = 0,$$

for all $q \in \mathcal{P}_n$. Now let $\{x_k\}$ be the zeros of p and let $\{w_k\}$ be the weights which make (11) true for polynomials of degree $\le n$. If f is a polynomial of degree $\le 2n+1$,

then long division of polynomials shows that we can write $f = a + bp$ where a, b are polynomials of degree $\leq n$. Thus

$$\begin{aligned}\int_a^b f(t)w(t)dt &= \int_a^b a(t)w(t)dt + \int_a^b b(t)p(t)w(t)dt \\ &= \sum_k w_k a(x_k) + 0 \\ &= \sum_k w_k f(x_k),\end{aligned}$$

where the last line holds since $f = a$ on the zeros of p. To see that it is not possible to increase the degree of f to $2n+2$, consider the function $\prod_{k=0}^n (t - x_k)^2$. It vanishes at the points $\{x_k\}$ so $\sum_k w_k f(x_k) = 0$, but $\int_a^b f(t)w(t)dt > 0$, at least if $w > 0$ since $f > 0$ except at $n+1$ points.

For orthonormal polynomials we have

$$w_k = \frac{k_n}{k_{n-1}} \frac{\langle p_{n-1}, p_{n-1}\rangle}{p_{n-1}(x_k)p_n'(x_k)},$$

where k_n is the leading coefficient of p_n (i.e., the coefficient of x^n. To prove this we need two preliminary results

LEMMA 36. *Let*

$$K_n(x, y) = \sum_{k=0}^n p_k(x)p_k(y).$$

Suppose $K(x, y)$ is a polynomial of degree n in both x and y. Then

$$\langle p(x), K(x, y)\rangle_{w(x)} = p(y),$$

holds for every polynomial p of degree n iff $K = K_n$.

)

PROOF. If p is polynomial of degree $\leq n$ then it has a n expansion in terms of the basis $p(x) = \sum a_m p_m(x)$, so

$$\begin{aligned}\langle p(x), K_n(x)\rangle_w &= \langle \sum a_m p_m(x), \sum p_k(x)p_k(y)\rangle_w \\ &= \sum_{m,k} a_m p_k(y)\langle p_m(x), p_k(x)\rangle_w \\ &= \sum_k a_k p_k(y) \\ &= p(y),\end{aligned}$$

so the equality holds when $K = K_n$. Conversely, some equality holds for K and all p. Fix w and choose $p(x) = K_n(x, w)$. Then

$$\langle K_n(x,w), K(x,y)\rangle_w K_n(y,w).$$

But by our earlier calculation k_n has the reproducing property so

$$\langle K(x,w), K_n(x,y)\rangle_w K(y,w).$$

Since the two left hand sides equal the same integral, we deduce $K(y,w) = K_n(y,w)$ for any y, w, which proves the lemma. □

THEOREM 37 (Christoffel-Darboux). *With notation as above,*

$$K_n(x,y) = \frac{k_n}{k_{n+1}} \frac{p_{n+1}(x)p_n(y) - p_n(x)p_{n+1}(y)}{x-y}$$

PROOF. Let $K(x,y)$ denote the right hand side above. The numerator is a polynomial in x of degree $\leq n+1$ and vanishes when $x = y$, so $K(x,y)$ is actually a polynomial in x of degree $\leq n$. Similary for y. Thus to show $K = K_n$ we only have to show it has the reproducing property of the previous lemma.

A bit of expanding and using $\langle p_n, p_{n+1}\rangle_w = 0$ shows

$$\begin{aligned}\langle p(x)m, K(x,y)\rangle_w &= \frac{k_k}{k_{n+1}}\langle (p_{n+1}(x)p_n(y) - p_n(x)p_{n+1}(y)), \frac{p(x)-p(y)}{x-y}\rangle_w \\ &+ \frac{k_k}{k_{n+1}} p(y)\langle p_{n+1}(x), \frac{p_n(y)-p_n(x)}{x-y}\rangle_w \\ &+ \frac{k_k}{k_{n+1}} p(y)\langle p_n(x), \frac{p_{n+1}(x)-p_{n+1}(y)}{x-y}\rangle_w\end{aligned}$$

Note that $(p(x)-p(y))/(x-y)$ has degree $\leq n-1$ as a polynomial in x and hence is orthogonal to p_n. Thus the first inner product is 0. Similarly for the second inner product. To compute the third inner product, write

$$\begin{aligned}\frac{k_k}{k_{n+1}} p(y) \frac{p_{n+1}(x)-p_{n+1}(y)}{x-y} &= k_n[\frac{y^{n+1}-x^{n+1}}{y-x} + \dots] \\ &= k_n x^n + \dots \\ &= p_n(x) + q(x,y),\end{aligned}$$

where q is a polynomial of degree $\leq n-1$ and hence orthogonal to p_n. Thus the thrid inner product equals $\langle p_n, p_n\rangle_w = k_{n+1}/k_n$, and hence

$$\langle p(x)m, K(x,y)\rangle_w = p(y).$$

By the previous lemma this implies $K = K_n$, as desired. □

LEMMA 38. *For orthonormal polynomials $\{p_k\}$ the weights in the Gauss quadrature formular satisfy*

$$w_k = \frac{k_n}{k_{n-1}} \frac{1}{p_{n-1}(x_k)p_n'(x_k)},$$

where k_n is the leading coefficient of p_n (i.e., the coefficient of x^n.

PROOF. We already know from (12) that

$$w_k = \frac{1}{p_n'(x_k)} \int_a^b \frac{p_n(x)}{x - x_k} w(x)dx$$

Since $p_n(x_k) = 0$,

$$\begin{aligned}
\int_a^b \frac{p_n(x)}{x - x_k} w(x)dx &= \frac{1}{p_{n-1}(x_k)} \int \frac{p_n(x)p_{n-1}(x_k)}{x - x_k} w(x)dx \\
&= \frac{1}{p_{n-1}(x_k)} \int \frac{p_n(x)p_{n-1}(x_k) - p_{n-1}(x)p_n(x_k)}{x - x_k} w(x)dx \\
&= \frac{1}{p_{n-1}(x_k)} \frac{k_{n+1}}{k_n} \int K_n(x, x_k)w(x)dx \\
&= \frac{k_{n+1}}{k_n p_{n-1}(x_k)}.
\end{aligned}$$

□

For more general functions, the difference between out discrete estimate and the actual integral can be bounded as follows:

$$E_n(f) = \int_a^b f(t)w(t)dt - \sum_k w_k f(x_k) = \frac{f^{(2n)}(\zeta)}{(2n)!k_n^2},$$

where ζ is some point in (a, b) and k_n is the coefficient of the power t^n in $p(t)$. For Schwarz-Christoffel integrals, the most relevant case is when w is a Jacobi weight

$$w(t) = (1 - x)^\alpha (1 + x)^\beta,$$

when this estimate becomes

$$E_n(f) = f^{(2n)}(\zeta) \frac{2^{2n+\alpha+\beta+1}\Gamma(n + \alpha + 1)\Gamma(n + \beta + 1)\Gamma(n + \alpha + \beta + 1)n!}{\Gamma(2n + \alpha + \beta + 1)\Gamma(2n + \alpha + \beta + 2)(2n)!}.$$

If $\alpha = \beta = 0$ then $w = 1$ and p is a Legendre polynomial. Then the error bound simplifies to

$$E_n(f) = f^{(2n)}(\zeta) \frac{2^{2n+1}(n!)^4}{(2n + 1)((2n)!)^3}.$$

Consider a simple case like $f(t) = e^t$. Then all the derivatives of f are bounded on $[-1, 1]$ and using Stirling's formula

$$n! \sim n^n e^{-n} \sqrt{2\pi n},$$

we see that

$$E_n(e^t) = O(n^{-2n}).$$

On the other hand, the nth order Taylor series for e^t only approximates it to within $1/n! \gg n^{-n}$ on $[-1, 1]$. Thus the numerical integration using n points should give about twice as many correct digits as term-by-term integration of the nth order power series. Of course, we can just double the number of terms in the power series to obtain the same accuracy.

Even for fairly small n, both error estimates will be less than machine precision, so a practical comparison would have to estimate the work to produce the approximations. Very roughly, if $f(t) = \prod_{j=1}^{N} (1 - \frac{t}{z_j})^{\alpha_k - 1}$ is the sort of function that arises in the Schwarz-Christoffel formula, then naively, it takes N multiplications to evaluate f at one point and so takes $O(nN)$ operations to compute the Gauss-Jacobi approximation to the integral. To compute the power series expansion, we have to multiply N individual power series each of length n. Naively multiplication of two of these takes $O(n^2)$, but the fast Fourier transform allows this to be done in $O(n \log n)$. Thus about $o(Nn \log n)$ work is needed to compute the integral via power series, which is only slightly worse. This does not seem to be a decisive win for either method (especially since we probably only need $n \leq 20$ to attain machine precision), so any practical comparison boils down to estimating the size of the multiplicative constants implicit in the big-O estimates. This depends on the particular implementations, and we will not address it further.

So efficient numerical integration is possible if we can

(1) find $p_{n+1} \in \mathcal{P}_{n+1}$ so that $p_{n+1} \perp \mathcal{P}_n$ and $\|p_{n+1}\|_w \langle p_{n+1} p_{n+1} \rangle_w = 1$,
(2) find the zeros $\{x_k\}$ of p_{n+1}
(3) find the weights $\{w_k\}$.

The first step is the main difficulty. Once we have the polynomial p, we can use Newton's method to find the roots of p_{n+1} and the weights are given by

$$w_k = -\frac{k_{n+1}}{k_n} \frac{1}{p_{n+1}(x_k) p_n'(x_k)}.$$

Suppose $\{p_k\}_0^n$ are orthonormal polynomials of degree k and the coefficient of x^k in p_k is c_k. We can find a polynomial (orthogonal to $\mathcal{P}_n$, but not necessarily of unit norm) p_{n+1} by taking any $(n+1)$st degree polynomial p and subtracting aways its orthogonal projection onto each of the 1-dimensional subspaces corresponding to these vectors, i.e.,

$$p_{n+1}(x) = p(x) - \sum_{k=0}^{n} p_k(x)\langle p, p_k\rangle_w.$$

Since we get to choose p, we take $p = xp_n$, so that

$$\begin{aligned}
p_{n+1}(x) &= xp_n(x) - \sum_{k=0}^{n} p_k(x)\langle xp_n, p_k\rangle_w \\
&= xp_n(x) - p_n(x)\langle xp_n, p_n\rangle_w - p_{n-1}(x)\langle xp_n, p_{n-1}\rangle_w - \sum_{k=0}^{n-2} p_k(x)\langle p_n, xp_k\rangle_w \\
&= xp_n(x) - p_n(x)\langle xp_n, p_n\rangle_w - p_{n-1}(x)\langle xp_n, p_{n-1}\rangle_w \\
&= p_n(x)(x - \langle xp_n, p_n\rangle_w) - p_{n-1}(x)\langle xp_n, p_{n-1}\rangle_w \\
&= p_n(x)(x - a_n) - p_{n-1}(x)b_n
\end{aligned}$$

We have used the facts that $\langle xf, g\rangle_w = \langle f, xg\rangle_w$ and that p_n is perpendicular to xp_k if $k < n-1$. The polynomial constructed is not necessarily of unit norm, but we can fix this by replacing p_{n+1} by

$$\frac{p_{n+1}}{\|p_{n+1}\|_w}.$$

To implement the method we have to be able to compute the recursion coefficients

$$\begin{aligned}
a_n &= \langle xp_n, p_n\rangle_w \\
b_n &= \langle xp_n, p_{n-1}\rangle_w \\
c_n &= \|p_{n+1}\|_w = \|p_n(x - a_n) - p_{n-1}b_n\|_w.
\end{aligned}$$

Recall that each of these inner products is an integral of the form

$$\int_a^b f(t)w(t)dt.$$

We already know p_n (by induction) so we could find its roots and use these to exactly evaluate such integrals for polynomials of degree $\leq 2n-1$. However, the inner products above involve polynomials of degree up to $2n+1$, and using the roots of p_n

will definitely give a wrong answer for $\int_a^b tp_n^2(t)w(t)dt$. Therefore these coefficients should be computed by other means.

For evaluating Schwarz-Christoffel integrals, we will only need to consider the case of Jacobi weights with a singularity at one endpoint (or possibly neither endpoint), i.e., weights of the form $w(x) = (x-a)^\alpha$ on the interval $[a,b]$. However, we can compute an integral of the form

$$\int_a^b (\sum_{k=0}^n a_k x^k)(x-a)^\alpha dx,$$

using the following observation. A polynomial $p(x) = \sum_{k=0}^n a_k x^k$ has a Taylor expansion around any point, including the point a. This Taylor expansion, must also be a polynomial of degree n. Thus we can write

$$\sum_{k=0}^n b_k (x-a)^k = p(x) = \sum_{k=0}^n a_k x^k.$$

Then

$$\begin{aligned}
\int_a^b (\sum_{k=0}^n a_k x^k)(x-a)^\alpha dx &= \int_a^b \sum_{k=0}^n b_k (x-a)^k (x-a)^\alpha \\
&= \sum_{k=0}^n b_k \int_a^b (x-a)^{k+\alpha} dx \\
&= \sum_{k=0}^n b_k \frac{(b-a)^{k+\alpha+1}}{k+\alpha+1}.
\end{aligned}$$

So now we have to compute the $\{b_k\}$ from the $\{a_k\}$. Note that

$$\begin{aligned}
\sum_{k=0}^n a_k x^k &= \sum_{k=0}^n a_k (x-a+a)^k \\
&= \sum_{k=0}^n a_k [\sum_{j=0}^k (x-a)^j a^{k-j} \binom{k}{j},
\end{aligned}$$

so be get $\mathbf{b} = (b_0, \ldots, b_n)$ we just have to apply the matrix

$$M = (m_{jk}) = (a^{k-j} \binom{k}{j},$$

to the vector $\mathbf{a} = (a_0, \ldots, a_n)$. This can be done naively in $O(n^2)$, but we will show in Section 5 how to apply this $n \times n$ matrix to a vector in time only $O(n \log n)$.

If $w(t) = 1$, the Gauss-Jacobi polynomials specialize to the Legendre polynomials. Here are the first ten Legendre polynomials for the interval $[a, b] = [-1, 1]$.

$$
\begin{aligned}
P_1(x) &= x, \\
P_2(x) &= -\left(\frac{1}{2}\right) + \frac{3\,x^2}{2} \\
P_3(x) &= \frac{-3\,x}{2} + \frac{5\,x^3}{2} \\
P_4(x) &= \frac{3}{8} - \frac{15\,x^2}{4} + \frac{35\,x^4}{8} \\
P_5(x) &= \frac{15\,x}{8} - \frac{35\,x^3}{4} + \frac{63\,x^5}{8} \\
P_6(x) &= -\left(\frac{5}{16}\right) + \frac{105\,x^2}{16} - \frac{315\,x^4}{16} + \frac{231\,x^6}{16} \\
P_7(x) &= \frac{-35\,x}{16} + \frac{315\,x^3}{16} - \frac{693\,x^5}{16} + \frac{429\,x^7}{16} \\
P_8(x) &= \frac{35}{128} - \frac{315\,x^2}{32} + \frac{3465\,x^4}{64} - \frac{3003\,x^6}{32} + \frac{6435\,x^8}{128} \\
P_9(x) &= \frac{315\,x}{128} - \frac{1155\,x^3}{32} + \frac{9009\,x^5}{64} - \frac{6435\,x^7}{32} + \frac{12155\,x^9}{128} \\
P_{10}(x) &= -\left(\frac{63}{256}\right) + \frac{3465\,x^2}{256} - \frac{15015\,x^4}{128} + \frac{45045\,x^6}{128} - \frac{109395\,x^8}{256} + \frac{46189\,x^{10}}{256}
\end{aligned}
$$

4	1.999984228457721944767532072144696487557194483115
5	2.000000110284471879766230094981509385528232424409
6	1.999999994772707155704064026794080767157032702 62
7	2.000000000017904713988979522802725396882589551 6
8	1.999999999999953604266189667719853555573370158 2
9	2.000000000000000094136064072597719396414294942
10	1.999999999999999999846379297653491184960575953
11	2.000000000000000000000206013457173278936238709
12	1.999999999999999999999997689286574808910213 3
13	2.000000000000000000000000002199828811945538 7
14	1.999999999999999999999999999999820014656592 10
15	2.000000000000000000000000000000001279196248
16	1.999999999999999999999999999999999999202885
17	2.000000000000000000000000000000000000000439
18	2.000000000000000000000000000000000000000000

TABLE 1. Approximating $\frac{\pi}{2}\int_{-1}^{1}\cos(\frac{\pi}{2}t)dt$ using the roots of the nth Legendre polynomial.

4	1.0985703536493604213694507148231753197893152746 43
5	1.0986092418124719605204127411395244504262000897 26
6	1.0986120681169406437641500147652327985037897430 85
7	1.0986122727383456082370423301475424478891767017 7
8	1.0986122875191782529458652680660122250343151602 4
9	1.0986122885853231560758415201023000760438081814
10	1.0986122886621485872861135030048483168226650251
11	1.0986122886676806754603956463038864607321813301
12	1.0986122886680788273422876748043133557118525407
13	1.0986122886681074716527849715264721291023344 49
14	1.0986122886681095317892196695313251920927242 42
15	1.0986122886681096799212936635863512799859204 4
16	1.0986122886681096905705207364007642199981394 3
17	1.0986122886681096913359733724191428226330298 5
18	1.0986122886681096913909859076206421219228913
19	1.0986122886681096913949391857585049768764517
20	1.0986122886681096913952232475480128000949082
21	1.0986122886681096913952436571211548679735 54
22	1.0986122886681096913952451234301287602618 56
23	1.0986122886681096913952452287696849626202 0
24	1.0986122886681096913952452363368843107935 1
25	1.0986122886681096913952452368804590989262 2
26	1.0986122886681096913952452369195041669804
27	1.0986122886681096913952452369223086820056
28	1.0986122886681096913952452369225101173798
29	1.0986122886681096913952452369225245851 48
30	1.0986122886681096913952452369225256246 245

TABLE 2. Approximating $\log(3) = \int_{-1}^{1} \frac{1}{2+t} dt$ using the roots of the nth Legendre polynomial. *Mathematica* gives the first 50 digits of $\log 3$ as 1.0986122886681096913952452369225257046474905578227

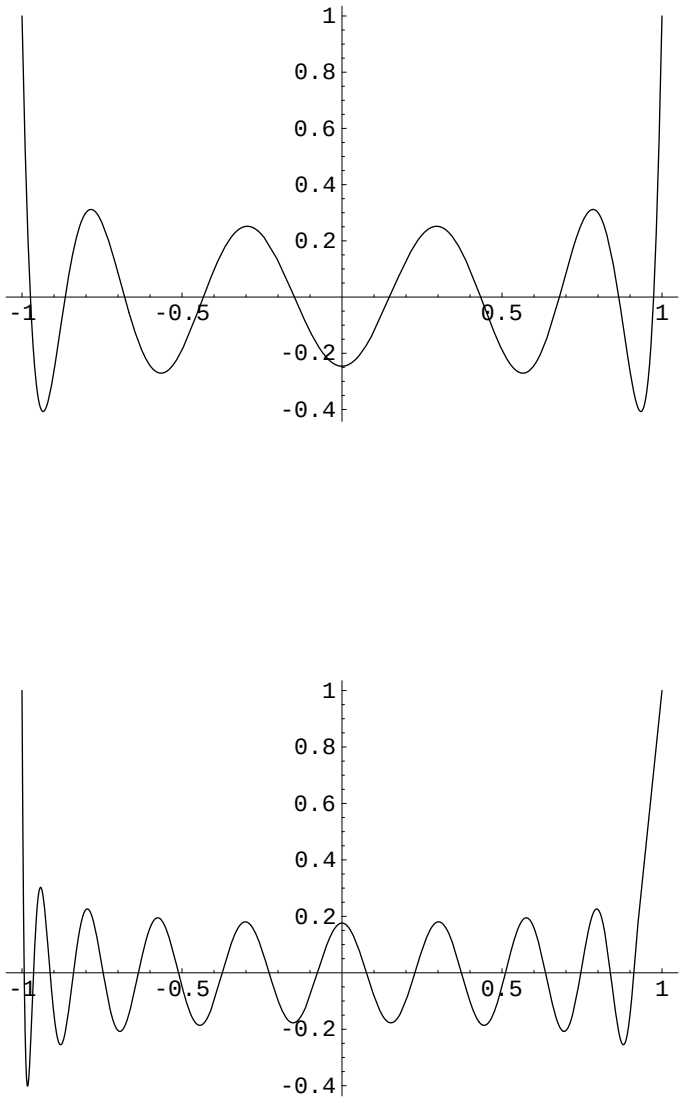

FIGURE 12. Some example of Legendre polynomials. The roots of P_n are the optimal n points to sample to compute an integral of the form $\int_{-1}^{1} f(t)dt$ in the sense that they will give the correct answer if f if a polynomial of degree at most $2n+1$. Shown are $n = 10, 20$.

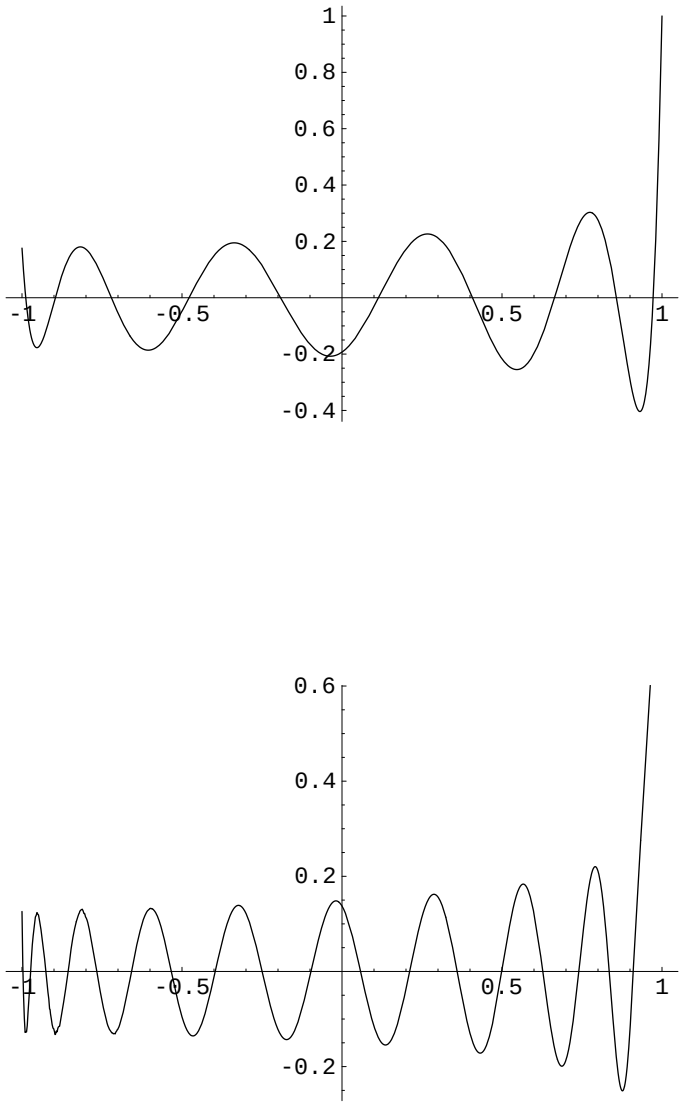

FIGURE 13. Some examples of Jacobi polynomials. This is P_{10} and P_{20} for the weight $(1+x)^{-1/2}$ (so there is only a singularity at the left end of the interval).

4. The fast Fourier transform

As we saw earlier in this chapter, efficient computation of the Schwarz-Christoffel formula requires efficient manipulation of power series (either to compute the power series of the map locally on each piece of our Carleson decomposition or to find the orthogonal polynomials used in the numerical integration). Most of these manipulations can be easily interpreted as applying a matrix to a vector and in this section we will review known results about applying structured matrices to vectors quickly. This summary is taken mostly from [**?**] and [**?**].

An n term power series centered at 0 has the form

$$p(z) = \sum_{k=0}^{n-1} a_n z^k,$$

and is polynomial of order $n-1$. Thus p is also determined by its values at any n distinct points $\{w_k\}_{k=1}^n$ and as we saw earlier can be recovered from these values using the Lagrange polynomials as

$$p(z) = \sum_{k=1}^{n} p(w_k) L_k(z),$$

where

$$L_k(z) = \prod_{1 \le j \le n, j \ne k} \frac{z - w_j}{w_k - w_j}.$$

Given the values $\{p(w_k)\}$, this formulation takes about $O(n^2)$ additions and multiplications to evaluate the coefficients of p. Similarly, given the coefficients of p it takes about $O(n^2)$ steps to evaluate it at the n points $\{w_k\}$. Can we do these conversions between the two representations of p faster. The answer is yes, at least if we assume the $\{w_k\}$ are special points, namely the nth roots of unity.

In this case, the problem of evaluating a polynomial or recovering its coefficients from its values is the same as computing a discrete Fourier transform. As before, fix a positive integer N and consider the Nth roots of unity $R_N = \{w_k\} = \{e^{i2\pi k/N}\}$. Let V^N be the N-dimensional complex vector space of functions from R_N to $\mathbb{C}$. The functions $e_k(z) = z^k$, $k = 0, \ldots N-1$ form an orthonormal basis with respect to the inner product

$$\langle f, g \rangle = \frac{1}{N} \sum_{k=0}^{N-1} f(w_k) \overline{g(z_k)}.$$

Therefore any function in V_N can be written

$$f(z) = \sum_{k=0}^{N-1} e_k \langle f, e_k \rangle = \sum_{k=0}^{N-1} a_k z^k,$$

for $z \in R_N$. Let $\mathrm{FFT}(N)$ denote the number of complex additions and multiplications to compute all N of the numbers $\{a_k\}$ given the N numbers $\{f(w_k\}$. Suppose that $N = 2M$. We claim that

$$\mathrm{FFT}(N) \leq 2\mathrm{FFT}(M) + O(N).$$

To prove this suppose $\{w_j\}_0^{N-1}$ are the Nth roots of unity and $\{v_j\}_0^{M-1}$ are the Mth roots of unity. Then write down the definition of the coefficients and split the sum into the sums over the even and odd terms:

$$\begin{aligned}
a_k &= \frac{1}{N} \sum_{j=0}^{N-1} f(w_j) w_j^k \\
&= \frac{1}{2M} \sum_{j=0}^{2M-1} f(w_j) w_j^k \\
&= \frac{1}{2M} \sum_{j=0}^{M-1} f(w_(2j) w_{2j}^k + \frac{1}{2M} \sum_{j=0}^{M-1} f(w_{2j+1}) w_{2j+1}^k \\
&= \frac{1}{2M} \sum_{j=0}^{M-1} f(v_(j) v_j^k + \frac{1}{2M} \sum_{j=0}^{M-1} f(v_j w_1) v_j^k w_1^k \\
&= \frac{1}{2}(b_k + w_i^k c_k),
\end{aligned}$$

where $\{b_k\}$ is the discrete Fourier transform on R_M of the function $g(z) = f(z)$ and $\{c_k\}$ is the discrete Fourier transform of the function $h(z) = f(w_1 z)$. Both $\{b_k\}$ and $\{c_k\}$ can be computed with $\mathrm{FFT}(M)$ operations and it clearly takes only $O(N)$ operations to combine them to get $\{a_k\}$. Thus the claim is proved. If $N = 2^n$ is a power of 2, then

$$\begin{aligned}
\mathrm{FFT}(N) &= 2\mathrm{FFT}(N/2) + O(N) \\
&= 4\mathrm{FFT}(N/4) + 2O(N/2) + O(N) \\
\ldots &= 2^n \mathrm{FFT}(2) + O(N) + O(N) + \cdots + O(N) \\
&= O(N \log N).
\end{aligned}$$

There are $O(N \log N)$ FFT algorithms for every N, but we shall shall only present the one above, for powers of 2.

Computing a discrete Fourier transform is the same as applying the Fourier matrix to a vector, where the Fourier matrix is given by

$$F_n = \begin{pmatrix} 1 & 1 & 1 & \dots & 1 \\ 1 & \omega & \omega^2 & \dots & \omega^{n-1} \\ 1 & \omega^2 & \omega^4 & \dots & \omega^{2(n-1)} \\ \vdots & \vdots & \vdots & \ddots & \vdots \\ 1 & \omega^{n-1} & \omega^{2(n-1)} & \dots & \omega^{(n-1)(n-2)} \end{pmatrix}$$

where ω is an nth root of unity. The fast Fourier transform (FFT) applies F_n to an n-vector in time $O(n \log n)$ [**?**]. F_n is unitary and its conjugate transpose, F^*, can also be applied in $O(n \log n)$ time. The discrete Fourier transform (DFT) takes a n-long sequence of complex numbers $\{a_k\}_0^{n-1}$ and a n-root of unity ω and returns the values of the polynomial $p(z) = a_0 + a_1 x + \dots a_{n-1} z^{n-1}$ at the points $z = \{1, \omega, \omega^2, \dots, \omega^{n-1}\}$. Composing DFT with itself returns the original sequence times n. It turns our that being able to apply this matrix to a vector quickly is the key to many other fast computations.

5. Fast power series mainulations

Suppose $f(z) = \sum_{k=0}^{n} a_k z^k$ and $g(z) = \sum_{k=0}^{n} b_k z^k$. How fast can we multiply, divide or compose these series? Let $M(n)$ denote the number of field operations it takes to multiply two power series of length n. The usual process of convolving the coefficients shows $M(n) = O(n^2)$. A divide and conquer method of Karatsuba and Ofman [**?**] improves this to $O(n^\alpha)$ with $\alpha = \log 3 / \log 2$, but the fastest known method uses the Fast Fourier Transform [**?**], which shows $M(n) = O(n \log n)$ (two power series of length n can be multiplied by taking the DFT of each, multiplying the results term-by-term, taking the DFT of the result and finally dividing by n).

Other operations on power series are generally estimated in terms of $M(n)$. For example, inversion (finding the reciprocal power series, $1/f$, given the series for f) is $O(M(n))$. Like several other operations on power series, this is most easily proven using Newton's method (applied to series rather than numbers). For example, $1/f$ is the solution of the equation $\frac{1}{g} - f = 0$. If g is an approximate solution with $n > 0$

terms correct, then

$$g = g - \frac{\frac{1}{g} - f}{-1/g^2} = g - \frac{fg - 1}{z^n} g z^n,$$

has $2n$ correct terms. The right side requires two multiplications and so the work to compute inversions is $O(M(n)) + O(M(n/2)) + \cdots + O(1) = O(M(n))$.

Given inversion, one can divide power series (multiply f by $1/g$) compute $\log f$ (integrate f'/f term-by-term) or $\exp(f)$ (solve $\log g = f$ by Newton's method) all in time $O(M(n))$.

Composition of power series is a little harder. Brent and Kung showed that given power series f, g of order n and $g_0 = 0$, the composition $f \circ g$ can be computed in time $\mathrm{Comp}(n) = O(\sqrt{n \log n} M(n))$. Using FFT multiplication, this gives $O(n^{3/2} \log^{3/2} n \log\log n)$. They also showed that reversion (i.e., given f find g so $f \circ g(z) = z$) can be solved using Newton's method with the iteration

$$g \to g - \frac{f \circ g}{f' \circ g},$$

which doubles the number of correct terms in g with every step. Thus $\mathrm{Rev}(n) = O(\mathrm{Comp}(n)) = O(\sqrt{n \log n} M(n))$.

Fortunately, there are some special cases when composition is faster. For example, if we want to post-compose with a linear fractional transformation $\sigma(z) = (az + b)/(cz + d)$, this is the same as adding and dividing series, so is only $O(M(n))$.

Pre-composing by σ is more complicated. A function f is called algebraic if it satisfies

$$P_d(z) f(z)^d + \cdots + P_0(z) = 0,$$

for some polynomials $P_0, \cdots P_d$. Clearly every rational function is algebraic with $d = 1$. The power series of such functions satisfy linear recursions and n terms of the series can be computed in $O(n)$. Moreover, pre-composition by algebraic functions is fast; if f has p terms, g has q terms and is algebraic of degree d then the first n terms of $f \circ g$ can be computed in time $O(qd^2 \frac{p(q-v)}{n} M(n + pv) \log n)$ where v is the valuation of P_d (the largest power of z which divides $P_d(z)$) and q is the maximum of the degrees of P_i, plus 1. For linear fractional transformations $v = 0$ and $q = 2$ so the time to pre-compose by such a map is $O(M(n) \log n) = O(n \log^2 n)$. (There is an extensive generalization of the algebraic case to fast manipulations of holonomic

functions, as developed by van der Hoeven [**?**], although we do not need to use it here.)

This is too slow for our purposes. Fortunately, the only times we will have to pre-compose with a Möbius transformation correspond to various manipulations of power and Laurent series in the fast multipole method and all of these can be accomplished in $O(n \log n)$ by fast application of Toeplitz, Hankel and Pascal matrices as shown by Tang in [**?**]. A matrix is called circulant if each column is a down-shift of the previous one, is called Toeplitz if it is constant on diagonals and called Hankel if it is constant on antidiagonals. The general forms of these three types are:

$$C(x) = \begin{pmatrix} x_1 & x_n & x_{n-1} & \dots & x_2 \\ x_2 & x_1 & x_n & \dots & x_3 \\ x_3 & x_2 & x_1 & \dots & x_4 \\ \vdots & \vdots & \vdots & \ddots & \vdots \\ x_n & x_{n-1} & x_{n-2} & \dots & x_1 \end{pmatrix},$$

$$T_(x) = \begin{pmatrix} x_0 & x_1 & x_2 & \dots & x_{n-1} \\ x_{-1} & x_0 & x_1 & \dots & x_{n-2} \\ x_{-2} & x_n & x_0 & \dots & x_{n-3} \\ \vdots & \vdots & \vdots & \ddots & \vdots \\ x_{-n+1} & x_{-n+2} & x_{-n+3} & \dots & x_0 \end{pmatrix},$$

$$H(x) = \begin{pmatrix} x_{-n+1} & x_{-n+2} & x_{-n+3} & \dots & x_0 \\ x_{-n+2} & x_{-n+3} & x_{-n+4} & \dots & x_1 \\ x_{-n+3} & x_{-n+4} & x_{-n+5} & \dots & x_2 \\ \vdots & \vdots & \vdots & \ddots & \vdots \\ x_0 & x_1 & x_2 & \dots & x_{n-1} \end{pmatrix}$$

A circulant matrix can be applied to a vector using three applications of FFT, i.e., because $C_n(x)$ applied to a vector y is the same as $\mathrm{IFFT}(\mathrm{FFT}(x) \cdot \mathrm{FFT}(y))$. A Toeplitz matrix can be embedded in a circulant matrix of the form

$$C_{2n} = \begin{pmatrix} T_n & S_n \\ S_n & T_n \end{pmatrix}$$

where

$$S_n = \begin{pmatrix} 0 & x_{-n+1} & x_{-n+2} & \dots & x_{-1} \\ x_{n-1} & 0 & x_{-n+1} & \dots & x_{-2} \\ x_{n-2} & & 0 & \dots & x_{-3} \\ \vdots & \vdots & \vdots & \ddots & \vdots \\ x_1 & x_2 & x_3 & \dots & 0 \end{pmatrix}$$

To apply T to an n-vector y, append n zeros to y to get a $2n$-vector, apply C_n and take the first n coordinates of the result. This takes $O(n \log n)$ time. If H is a Hankel matrix then $R \cdot H$ is a Toeplitz matrix where R is the permutation matrix which is 1's on the main anti-diagonal and 0 elsewhere, i.e., it reverses the order of the coordinates of a vector. Thus $H = R \cdot (R \cdot H)$, is a Toeplitz matrix followed by a permutation and can clearly be applied in time $O(n \log n)$ as well.

The Pascal matrix is lower triangular with its (j,k)th entry being the binomial coefficient $C_i^j = \binom{i}{j}$.

$$\begin{pmatrix} 1 & 0 & 0 & \dots & 0 \\ 1 & 1 & 0 & \dots & 0 \\ 1 & 2 & 1 & \dots & 0 \\ \vdots & \vdots & \vdots & \ddots & \vdots \\ C_{n-1}^0 & C_{n-1}^1 & C_{n-1}^2 & \dots & C_{n-1}^{n-1} \end{pmatrix}$$

This matrix can be written as $P = \mathrm{diag}(v_1) \cdot T \cdot \mathrm{diag}(v_2)$ where

$$v_1 = (1, 1, 2!, 3!, \dots, (n-1)!),$$

$v_2 = \frac{1}{v_1}$ (term-wise) and T is the Toeplitz matrix

$$T = \begin{pmatrix} 1 & 0 & 0 & \dots & 0 \\ 1 & 1 & 0 & \dots & 0 \\ \frac{1}{2!} & 1 & 1 & \dots & 0 \\ \vdots & \vdots & \vdots & \ddots & \vdots \\ \frac{1}{(n-1)!} & \frac{1}{(n-2)!} & \frac{1}{(n-3)!} & \dots & 1 \end{pmatrix}$$

The diagonal matrices can be applied in $O(n)$ and the Toeplitz in $O(n \log n)$ and hence so can P. Similarly for the transpose of P.

Now for the applications to fast multipole translation operators. There are three types of conversions to consider. First, local to local translation

$$\sum_{k=0}^{n-1} a_k (z-a)^k \quad \to \quad \sum_{k=0}^{n-1} b_k (z-b)^k,$$

then multipole to local

$$\sum_{k=0}^{n} a_n (z-a)^{-k} \quad \to \quad \sum_{k=0}^{n} b_n (z-b)^k,$$

and finally, multipole to multipole,

$$\sum_{k=0}^{n} a_n(z-a)^{-k} \quad \rightarrow \quad \sum_{k=0}^{n} b_n(z-b)^{-k}.$$

Let $c = b - a$ and consider the local-to-local translation. We have

$$\sum_{k=0}^{n-1} a_k(w-c)^k = \sum_{k=0}^{n-1} a_k \sum_{j=0}^{k} w^j(-c)^{k-j}\binom{k}{j},$$

so the matrix corresponding to local translation has kth column

$$((-c)^k, (-c)^{k-1}\binom{k}{1}, \ldots, (-c)^0\binom{k}{k}, 0, \ldots, 0)^t$$

or

$$LL = \begin{pmatrix} 1 & -c & c^2 & \ldots & (-c)^{n-1} \\ 0 & 1 & -2c & \ldots & (-c)^{n-2}C_{n-1}^1 \\ 0 & 0 & 1 & \ldots & (-c)^{n-3}C_{n-1}^2 \\ \vdots & \vdots & \vdots & \ddots & \vdots \\ 0 & 0 & 0 & \ldots & 1 \end{pmatrix}$$

This matrix is equal to

$$\mathrm{diag}(1, -\mathrm{z}, \ldots, (-\mathrm{z})^{\mathrm{n}-1}) \cdot \mathrm{P}' \cdot \mathrm{diag}(1, -\mathrm{z}^{-1}, \ldots (-\mathrm{z})^{-\mathrm{n}+1}),$$

where P' is the transpose of P. The diagonal matrices can be applied in $O(n)$ time and P' can be applied in $O(n \log n)$. Thus local-to-local translations can be done this fast.

Similarly, the multipole-to-multipole and multipole-to-local transformations correspond to applying the matrices

$$MM = \begin{pmatrix} 1 & 0 & 0 & \ldots & 0 \\ \binom{1}{1}c & 1 & 0 & \ldots & 0 \\ \binom{2}{2}c^2 & \binom{2}{1}c & 1 & \ldots & \\ \vdots & \vdots & \vdots & \ddots & \vdots \\ \binom{n-1}{n-1}c^{n-1} & \binom{n-1}{n-2}c^{n-2} & \binom{n-1}{n-3}c^{n-3} & \ldots & 1 \end{pmatrix}$$

$$ML = \begin{pmatrix} -c^{-1} & c^{-2} & c^{-3} & \ldots & c^{-n+1} \\ -c^{-2} & 2c^{-3} & -3c^{-4} & \ldots & \\ -c^{-3} & 3c^{-4} & -6c^{-5} & \ldots & \\ \vdots & \vdots & \vdots & \ddots & \vdots \\ -c^{-n+1} & (n-1)c^{-n} & -\binom{n}{2}c^{-n-1} & \ldots & (-1^{n-1}\binom{2p-2,p-1}{c})^{-2n-1} \end{pmatrix}.$$

We can rewrite these matrices as

$$MM = \mathrm{diag}(1, \mathrm{z}, \ldots, \mathrm{z}^{\mathrm{n}-1}) \cdot \mathrm{P} \cdot \mathrm{diag}(1, \mathrm{z}^{-1}, \ldots \mathrm{z}^{-\mathrm{n}+1}),$$

$$ML = \mathrm{diag}(1, \mathrm{z}^{-1}, \ldots, \mathrm{z}^{1-\mathrm{n}}) \cdot \mathrm{P} \cdot \mathrm{P}' \cdot \mathrm{diag}(-\mathrm{z}^{-1}, \mathrm{z}^{-2} \ldots (-\mathrm{z})^{-\mathrm{n}}),$$

where P' is the transpose of P. As with local translations, these are compositions of diagonal matrices (which can be applied in $O(n)$) and matrices that can be applied in $O(n \log n)$ time.

We will also use structured matrices to compute expansions around ∞ of functions of the form $\int \frac{d\mu(z)}{(z-w)^k}$, $k = 1, 2, 3$. We will only consider the Cauchy transform ($k = 1$) since the others can be obtained by term-by-term differentiation of that one. Suppose $f(z) = \sum_{k=0}^{n} a_k z^k$ is a power series for an analytic function, bounded by one and defined on $\mathbb{D}$ and $\varphi(x, y)$ is a polynomial in x and y of uniformly bounded degree. Then the Cauchy transform

$$F(w) = \int_S \frac{f(z)\varphi(x, y)dxdy}{z - w},$$

is analytic in w outside $S = [-\frac{1}{2}, \frac{1}{2}]^2$, so has an expansion $F(w) = \sum_{k=1}^{\infty} b_n w^{-n}$. Given $\{a_k\}_0^p$, thinking of φ as fixed, we want to compute $\{b_k\}_1^n$. For each monomial of the form $z^k x^a y^b$ we can precompute the expansion using explicit formulas ($O(n)$ for each of $O(n)$ monomials) and then we simply apply the resulting matrix to the vector $\{a_k\}$. Naively, we can do this in time $O(n^2)$.

Actually we can compute the expansion in only $O(n \log n)$. Let $d\mu = x^a y^b dxdy$ restricted to $Q = [0, 1]^2$. We want to compute the expansion at ∞ of

$$\begin{aligned} F(w) = \iint \frac{z^n}{w - z} d\mu(z) &= \iint z^n \frac{1}{w}(1 + \frac{z}{w} + (\frac{z}{w})^2 + \ldots)d\mu(z) \\ &= \sum_{k=0}^{\infty} w^{-k-1} \iint z^{n+k} d\mu(z) \\ &= \sum_{k=1}^{\infty} a_{k,n} w^{-k}, \end{aligned}$$

where

$$a_{k,n} = c(n + k + 1, a, b) = \iint_Q (x + iy)^{n+k-1} x^a y^b dxdy.$$

Since $a_{k,n}$ only depends on $k + n$, A is a Hankel matrix. As noted above, a $n \times n$ Hankel matrix can be applied to a n-vector using FFT in time $O(n \log n)$.

The individual coefficients have explicit formulas involving Euler's Beta function. Evaluations for a few small values of a, b (as given by *Mathematica* are)

$$c(n,0,0) = \frac{i - i^{n+1} + 2(1+i)^n}{2+3n+n^2},$$

$$c(n,1,0) = \frac{2i - i^n + in + 2(1+I)^n((2-i)+n)}{(1+n)(2+n)(3+n)},$$

$$c(n,2,0) = \frac{i(6+2i^n+5n+n^2) + 2(1+i)^n((4-4i)+n((5-2i)+n))}{(1+n)(2+n)(3+n)(4+n)}$$

$$c(n,1,1) = -\frac{1+i^n-2(1+i)^n(2+n)}{(1+n)(2+n)(4+n)},$$

$$c(n,2,1) = \frac{-3(2i)i^n - n + 2(1+i)^n(1+n)((4-i)+n)}{(1+n)(2+n)(3+n)(5+n)},$$

$$c(n,0,1) = \frac{-1 - i^{n+1}(2+n) + 2(1+i)^n((2+i)+n)}{(1+n)(2+n)(3+n)}.$$

Thus n-term Laurent expansions for Beurling transforms of the appropriate degree n polynomials can can be computed in time $O(n \log n)$.